Crystal-chemical studies of cation-exchanged zeolite A

Dissertation

zur Erlangung des Doktorgrades der Naturwissenschaften (Dr. rer. nat.)
am Fachbereich Geowissenschaften
der Universität Bremen

vorgelegt von
Li Wang

Bremen, July 2016

Reviewer:

Prof. Dr. Reinhard X. Fischer

Prof. Dr. Josef-Christian Buhl

Date of public colloquium:

06 September 2016

Versicherung an Eides Statt

Ich, _____

(Vorname, Name, Anschrift, Matr.-Nr.)

versichere an Eides Statt durch meine Unterschrift, dass ich die vorstehende Arbeit selbständig und ohne fremde Hilfe angefertigt und alle Stellen, die ich wörtlich dem Sinne nach aus Veröffentlichungen entnommen habe, als solche kenntlich gemacht habe, mich auch keiner anderen als der angegeben Literatur oder sonstiger Hilfsmittel bedient habe.

Ich versichere an Eides Statt, dass ich die vorgenannten Angaben nach bestem Wissen und Gewissen gemacht habe und dass die Angaben der Wahrheit entsprechen und ich nichts verschwiegen habe.

Die Strafbarkeit einer falschen eidesstattlichen Versicherung ist mir bekannt, namentlich die Strafandrohung gemäß § 156 StGB bis zu drei Jahren Freiheitsstrafe oder Geldstrafe bei vorsätzlicher Begehung der Tat bzw. gemäß § 161 Abs. 1 StGB bis zu einem Jahr Freiheitsstrafe oder Geldstrafe bei fahrlässiger Begehung.

_____ _____

Ort, Datum Unterschrift

Contents

Abstract

Zeolite A is one of the most important synthetic zeolites as a commercial product especially as an additive to household detergents for the softening of water. Zeolite A has high ion exchange ability due to its low Si/Al ratio. Most previous work studied the crystal structure of different cation exchanged zeolite A in space group $Pm\bar{3}m$. Therefore, investigation of the thermal stability and crystal structure of hydrated zeolite A in subgroup $Fm\bar{3}c$ become the key aspects of this thesis.

Powder and single crystals of K^+ and NH_4^+ exchanged zeolite A were prepared by static exchange methods. The crystal structure of hydrated zeolite K,Na-A (a = 24.5714(8) Å) was investigated by X-ray diffraction methods (space group $Fm\bar{3}c$) at ambient temperature. The refinement results indicated that all cations and large proportion of water molecules (forming sodalite-cage-shaped clusters) were located in the big *grc* units (α cages). The residual water molecules (forming cubic-shaped clusters) resided on the 6-fold axes in the *toc* units (β cages). The thermal behavior of zeolite K-A was studied by means of in situ X-ray powder diffraction combined with thermal gravimetric analyses from ambient temperature up to 1000°C. The lattice parameter a of zeolite K-A under vacuum conditions reveals a weak negative thermal expansion upon heating. Rietveld refinements of powder X-ray diffraction patterns showed that no changes occur in the Si-O bond distances and Si-O-Si angles. The negative thermal expansion was ascribed to the rotation of the rigid SiO_4 tetrahedra upon heating.

The crystal structure of fully hydrated NH_4^+ exchanged zeolite A was studied based on single-crystal X-ray diffraction methods (space group $Fm\bar{3}c$) at ambient temperature. Two crystallographic distinct positions for NH_4^+ and three for water molecules were found. The lattice parameter a of zeolite NH_4-A decreased from 24.5996(3) Å to 24.3378(3) Å when it is exposed to the atmosphere, which could be a sign for the ongoing dealumination process. Difference Fourier maps revealed the position (0, 0, 0) possessing a high electron density of approximately 20 e/Å^3. This position was assigned to extraframework Al^{3+} due to the close distance to water molecules (1.9 Å). In addition,

a series of zeolite A with different K^+/NH_4^+ ratio were prepared by controlling the concentration of exchanged NH_4NO_3 solution. Their thermal behaviors were studied by means of in situ X-ray diffraction in air and under vacuum conditions combined with in situ TG-FTIR. The result showed that when the K/NH_4^+ ratio is less than 4.5, the zeolite structure is unstable upon heating under both atmospheric and vacuum conditions.

Heavy atoms (Ba^{2+} and Sr^{2+}) exchanged zeolite A were prepared. The results showed that the low X-ray intensity compared with zeolite Na-A was due to the high absorption coefficient of heavy atoms for X-rays.

Kurzfassung

Zeolith A ist einer der wichtigsten synthetischen Zeolithe bezüglich der Verwendung in kommerziellen Produkten und wird vor allem als Additiv in Haushaltsprodukten zur Wasserenthärtung genutzt. Dank seines niedrigen Si/Al Verhältnisses besitzt der Zeolith A eine sehr hohe Ionenaustauschkapazität. Die meisten der vorangegangenen Forschungen beschäftigten sich mit dem Kationentausch an Zeolith A und den resultierenden Kristallstrukturen in der Raumgruppe $Pm\bar{3}m$. Darauf aufbauend liegt der Fokus der folgenden Arbeit auf der thermischen Stabilität und der Kristallstruktur des hydratisierten Zeolith A in der Untergruppe $Fm\bar{3}c$.

Mittels statischer Austauschmethoden konnten Pulverproben sowie Einkristalle von K^+ und NH_4^+ substituiertem Zeolith A dargestellt werden. Die Kristallstruktur des hydratisierten Zeolith K,Na-A (a = 24.5714(8) Å) wurde mit röntgenographischen Methoden bei Raumtemperatur (Raumgruppe $Fm\bar{3}c$) untersucht. Die Ergebnisse der Verfeinerungen deuteten darauf hin dass die gesamten Kationen, sowie ein Großteil der Wassermoleküle (welche Sodalith-Käfig-artige Agglomerate formen), in den großen *grc* Einheiten (α Käfige) lokalisiert sind. Die verbleibenden Wassermoleküle (kubisch agglomeriert) befanden sich auf den 6-zähligen Achsen in den *toc* Einheiten (β Käfige). Das thermische Verhalten von Zeolith K-A wurde mittels in-situ Pulver-Röntgendiffraktometrie in Kombination mit thermogravimetrischen Analysen von Raumtemperatur bis 1000°C untersucht. Unter Vakuumbedingungen zeigt der Gitterparameter a des Zeolith K-A eine schwach negative thermische Ausdehnung. Rietveld-Verfeinerungen an Pulver-Röntgendiffraktogrammen konnten zeigen dass keine Änderungen an Si-O Bindungslängen sowie Si-O-Si Bindungswinkeln auftreten. Die negative thermische Expansion wurde der Rotation der starren SiO_4-Tetraeder zugeschrieben.

Die Kristallstruktur des vollständig hydratisierten NH_4^+ substituierten Zeolith A wurde mittels Methoden der Röntgenbeugung am Einkristall (Raumgruppe $Fm\bar{3}c$) bei Raumtemperatur untersucht. Es wurden zwei kristallographisch unabhängige Positionen für NH_4^+ sowie drei für Wassermoleküle gefunden. Der Gitterparameter a des Zeolith NH_4-A verringerte sich von 24.5996(3) Å auf 24.3378(3) Å bei Exposition mit der

Atmosphäre, was ein Zeichen für den fortlaufenden Prozess der Dealuminierung sein könnte. Differenz-Fourier-Karten konnten eine hohe Restelektronendichte von etwa 20 $e/Å^3$ auf der Position (0, 0, 0) aufzeigen. Selbige Position wurde den Extra-Gerüstaluminiumkationen aufgrund ihrer kurzen Distanz (1.9 Å) zu Wassermolekülen zugeschrieben. Zusätzlich konnte eine Reihe von Zeolith A mit verschiedenen K^+/NH_4^+-Verhältnissen durch Änderung der Konzentration der ausgetauschten NH_4NO_3-Lösung dargestellt werden. Ihr thermisches Verhalten wurde mittels in-situ Röntgendiffraktometrie an Luft und unter Vakuum-Bedingungen, in Kombination mit in-situ TG-FTIR untersucht. Die Ergebnisse konnten zeigen, dass bei einem K/NH_4^+-Verhältnis unter 4.5 die Zeolith-Struktur beim Aufheizen instabil wird, sowohl unter atmosphärischen als auch Vakuum-Bedingungen.

Ebenfalls wurde Zeolith A mit substituierten Schweratomen (Ba^{2+} and Sr^{2+}) dargestellt. Die resultierenden Röntgendiffraktogramme zeigten, verglichen mit denen von Zeolith Na-A, deutlich niedrigere Intensitäten, was auf die hohen Absorptionskoeffizienten der Schweratome zurückzuführen ist.

Chapter 1 Introduction

Zeolites are a large class of microporous crystalline aluminosilicate materials that consist of a three-dimensional framework of SiO_4 and AlO_4 tetrahedra (Fig. 1.1). Generally, the majority of the research work on zeolites focused on synthetic zeolites. The natural zeolites usually have variations in chemical composition because they are formed in various environments. The synthetic zeolites are used more widely because of their purity, degree of crystallinity, and pore-size uniformity. The evolution trends of synthetic zeolite are shown in Table 1.1 (Flanigen *et al.*, 2012).

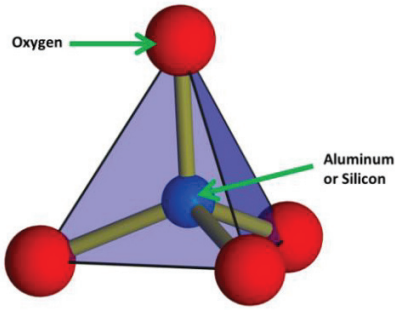

Fig. 1.1 Tetrahedra of zeolite structure.

Table 1.1 Evolution trends of synthetic zeolites.

Time of discovery	Composition
Late 1940s to early 1950s	Low Si/Al ratio zeolites
Mid-1950s to late 1960s	High Si/Al ratio zeolites
Early 1970s	SiO_2 molecular sieves
Late 1970s	$ALPO_4$ molecular sieves
Late 1970s to early 1980s	SAPO and MeAPO molecular sieves
Later 1970s	Metallo-silicates, aluminosilicates
Early to mid-1980s	$ALPO_4$ based molecular sieves
Early to mid-1990s	Metallophosphates
	Mesoporous molecular sieves
	Octahedral-tetrahedral frameworks
Late 1990s	Metal organic frameworks
2000s to present	UZM aluminosilicate zeolite, Si/Al = 2-30
	Germanosilicate zeolites
	SiO_2 molecular sieves in fluoride media

The simplified chemical composition of zeolite is $M_{x/n}[(AlO_2)_x(SiO_2)_y]\cdot wH_2O$, where M represents the exchangeable cations for balancing the charge of the aluminosilicate framework, n is the valency of the cation M, w is the number of water molecules per unit cell, x and y are the total numbers of tetrahedra per unit cell, and the ratio y/x usually has values ranging from 1 to ∞. The framework of the zeolite is built by TO_4 tetrahedra (T = Si, Al) with O atoms as bridges to connect the adjacent tetrahedra. Namely, each Si and Al shares one O atom in the framework. The arrangement of Si and Al in the zeolite framework is governed by Loewenstein's rule (Loewenstein, 1954) who proposed that the lowest ratio of Si/Al is equal to one. In other words, an Al–O–Al linkage is not allowed in the zeolite framework. For the pure silica units, the charge balance between Si^{4+} and two O^{2-} can be formed into neutral units. However, if tetravalent Si was substituted by trivalent Al, Al^{3+} and two O^{2-} will make the frameworks negatively charged. Therefore, it requires some extraframework cations such as alkalis and alkaline earth cations to balance the framework. The extraframework cations can be exchanged by other cations that make zeolites very important in industry.

For many decades, zeolites played an important role in various industries. Zeolites have applications in three main fields owing to their unique properties such as thermal stability, acidity, hydrophobicity/hydrophilicity of surfaces and ion-exchange capacity. As adsorbents, zeolites are very useful to remove the small polar or polarizable molecules and heavy metal ions such as Cu^{2+}, Pb^{2+}, Ba^{2+}, and Sr^{2+}. Zeolites can also be used as additive to detergents owing to their excellent ion-exchanged capacity. As catalysts, zeolites are widely used in petroleum industry in reactions such as cracking, alkylation, isomerization, shape-selective reforming, hydrogenation, and dehydrogenation. Fig. 1.2 provides the information about the main three applications of zeolites. Zeolites are majorly used in detergents. It seems that China consumes a large amount of natural zeolites (2.4 million tons per annum). In other area such as USA and Europe, only 8 wt% (0.15 million tons per annum) of natural zeolites were consumed.

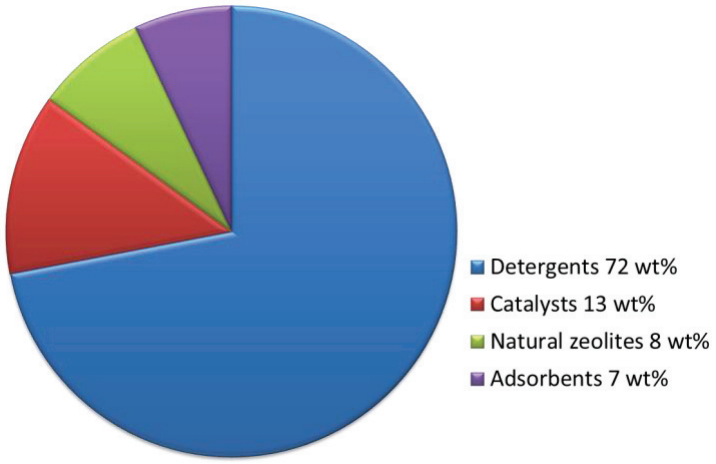

Fig. 1.2 Estimated annual zeolite consumption (wt% of total 1.8 million metric ton) by the major individual applications, excluding China's annual > 2.4 million metric ton of natural zeolite consumption (modified from Lauriente and Inoguchi.Y. (2005)).

Among all the synthetic zeolites, zeolite Na-A (LTA), with idealized composition (usually stated as $Na_{12}Al_{12}Si_{12}O_{48} \cdot 27H_2O$), is one of the most frequently studied zeolites. It is widely used as water softener because of its excellent properties instead of sodium tripolyphosphate (STPP) that leads to eutrophication and allows large growth of algae on the surface of water in lakes and rivers (Crutchfield, 1978; Gabrovšek, 1985). Zeolite Na-A is the first artificially synthesized zeolite that has the lowest Si/Al ratio (close to 1) in the zeolites family. About 350 crystal-structure refinements of aluminosilicate compounds with the LTA framework are listed in the Landolt-Börnstein series of microporous and other framework materials with zeolite-type structures (Fischer and Baur, 2006). More than 450 LTA type data sets are contained in the databank ZeoBase (Baur and Fischer, 2010). Zeolite A has an aluminosilicate framework formed by SiO_4 and AlO_4 tetrahedra.

In this thesis, a brief summary of the synthesis, structure, and applications of zeolite A are shortly introduced at the beginning. In the subsequent sections, the scope and objectives of this thesis are presented. The methods for the sample preparation and the instruments for the sample characterization are given in the third part. The main contribution of this thesis is included in results and discussion part. In the last section, conclusions, future perspectives, and the references of this thesis are presented. Manuscripts in preparation are listed in the final section.

1.1 Synthesis of zeolite A

The hydrothermal technique that is the pioneering method of synthesizing zeolite A has emerged as the basic and important method of producing zeolite A. Other new methods are also developed to obtain zeolite A.

(1) Hydrothermal method

Hydrothermal synthesis is widely used in the preparation of zeolites because of the high reactivity of reactants and easily controllable solution. This method is based on mixing an aluminate and silica solution in the presence of the organic and/or inorganic substance. The aqueous mixture is heated at around 100°C in a sealed autoclave or a polypropylene bottle. The aging time depends on different kinds of zeolites. Among the factors that influence the formation of zeolite A, many of them include the organic or inorganic additives. Sun and Shen (2012) reported that different organic additives have different influence on the crystallization process. For instance, sodium dodecyl sulphonate (SDS), Tween-80 (TWEEN), and poly (ethylene glycol) (PEG) can decrease the induction period, whereas sodium carboxymethyl cellulose (SCMC) works in the opposite way. Cetyltrimethylammonium bromide (CTAB) could destroy the crystal structure whereas poly (acrylamide) (PAM) could improve the stability of zeolite A. During the hydrothermal process, water is used as a common solvent particularly in the presence of an organic template to accelerate the chemical reactions. The hydrothermal techniques usually take place at low temperatures in an aqueous solution in a closed system. Therefore, fine polycrystalline powder samples are usually obtained. However, the synthesis of a large single crystal of zeolite A with a size larger than 50 μm is highly desirable for the analysis of the structure and growth mechanism, and has applications in zeolite functional materials (Ozin *et al.*, 1989).

The first time to obtain the large single crystal of zeolite A was used triethanolamine (TEA) as the complexing agent (Charnell, 1971). The solution of sodium metasilicate and aluminate was first mixed with TEA separately, then these two solutions were mixed together and kept for two or three weeks at 75–85°C for obtaining zeolite A or zeolite X. This method could produce approximately 60 μm on the edge of single crystal. Scott *et al.* (1990) studied the role of TEA in zeolite crystallization. It was found that the existence of

TEA can chelate aluminum through its hydroxyl groups, leading the release of aluminium nutrients deduce and then suppression of the nucleation rate of the zeolite crystal. However, an excess of TEA leads to the formation of zeolite X. Yang *et al.* (2006) proposed that TEA increases the viscosity of the system and reduces the reactivity of aluminum species in the precursors.

(2) Microwave-assisted hydrothermal synthetic route

The microwave-assisted synthesis has more advantages as compared with traditional hydrothermal synthesis. It is generally much faster and more efficient because the microwave energy significantly increases the heating rate of the synthesis mixture. Microwave irradiation can also result in a more uniform reaction. However, a sharp temperature increasing might also lead to some undesired phases. A special care on the preparation of the synthesis mixture for microwave heating was also required (Slangen *et al.*, 1997). Sathupunya *et al.* (2003) used alumatrane and silatrane as precursors to produce Na-A zeolite with crystal size of 1 μm by the sol–gel process combined with the microwave heating method. Bonaccorsi and Proverbio (2008) produced zeolite A by using the microwave process that was a real breakthrough for an industrial level.

(3) Microemulsion method

The microemulsion method is considered to be a useful approach to synthesize zeolites. Generally, this method involves a surfactant, co-surfactant, oil phase, and water phase. In the early 1990s, Dutta and Robins (1991) first investigated zeolite growth in microemulsion (Dutta *et al.*, 1995). Chen *et al.* (2005) reported the synthesis of template-free zeolite A by the means of a microemulsion technique assisted by microwave heating. In their study, the microemulsion included cetyl trimethyl ammonium bromide (CTAB), n-butanol, and cyclohexane that were used as the surfactant, co-surfactant, and oil phase, respectively. Eventually, the nanocrystals (40–80 nm) of zeolite A were also obtained. Esmaeili *et al.* (2011b) also reported the synthesis zeolite A with a microemulsion method but uses heptane as an oil phase. They pointed out that microemulsion is a reliable approach to prepare high–purity nanocrystallites of template-free zeolite materials.

1.2 Crystal structure of zeolite A

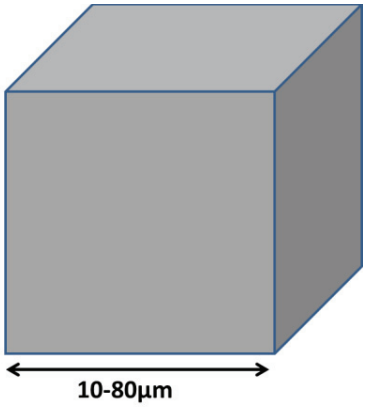

a

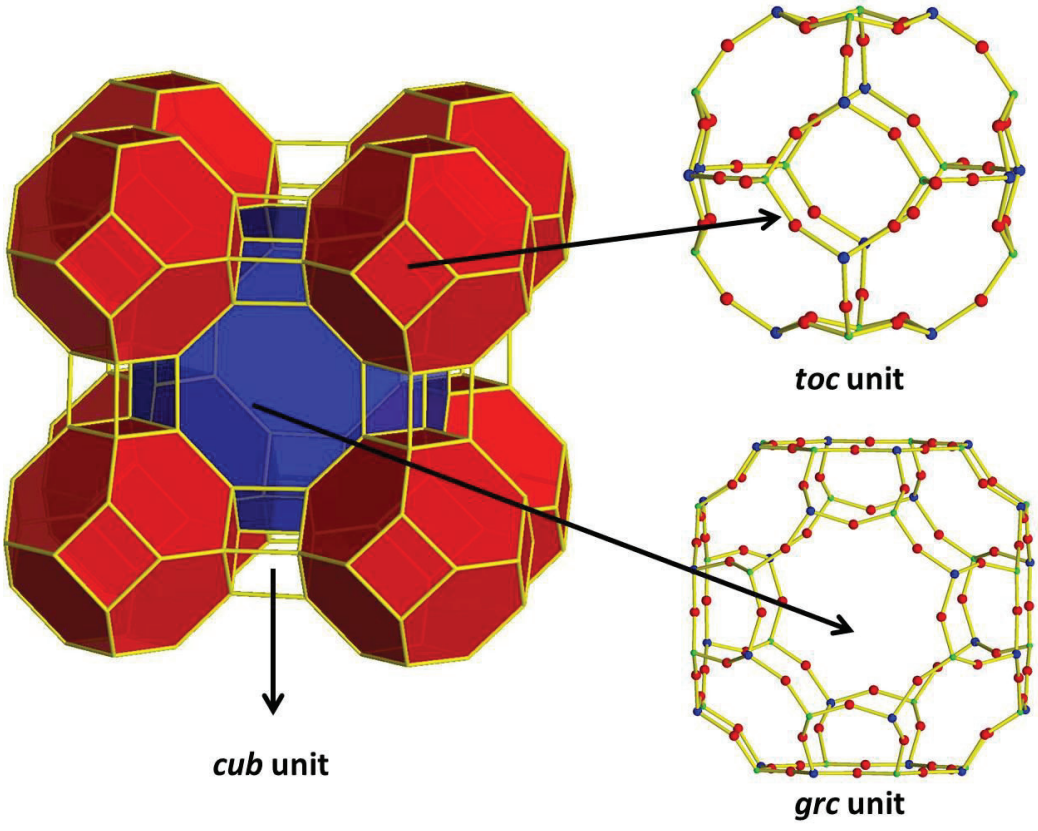

b

Fig. 1.3 Crystal structure of LTA. (a), cubic morphology; (b), crystal structure of zeolite A: the *toc* units [$4^6 6^8$] and *grc* units [$4^{12} 6^8 8^6$] blue=Al green=Si red=O.

The crystal structure of zeolite A is schematically shown in Fig. 1.3. Zeolite A possesses a three-dimensional structure of a cubic system. The lattice parameters of hydrated and dehydrated template-free zeolite A were estimated to be a = 24.6077(8) Å and a = 24.5693(3) Å, respectively, based on X-ray powder diffraction data (Ikeda *et al.*, 1998). For the hydrated zeolite A, which was synthesized by using triethanolamine, the lattice parameter was estimated to be a = 24.5498(28) Å based on a single-crystal synchrotron X-ray diffraction data (Fischer *et al.*, 2012). According to Loeweinstein's rule (Loewenstein, 1954), the framework of zeolite A has Si/Al = 1, which allows the Si atom and the Al atom to be arranged alternately in the framework. In Fig. 1.3, the oxygen atoms between Si and Al atoms are omitted. The unit cell of zeolite A consists of 12 AlO_4 and 12 SiO_4 tetrahedra. Zeolite A was constituted by three types of units: *grc* unit ($[4^{12}6^8 8^6]$, also called α cage) with an inside diameter of 11 Å, *toc* unit ($[4^6 6^8]$, also called β cage or sodalite cage) with a diameter of 6.6 Å and *cub* unit ($[4^6]$) (for designations see Smith (2000)). The *grc* units (Blackwell *et al.*, 1985; Hanson *et al.*, 1987) opened each other through eight-membered rings (8R) that are approximately 4 Å across. The opening size can be changed depending on the charge-balancing cations. Each *toc* unit was linked by double 4-ring (D4R). The six-membered rings (6R) are on the boundary between the *toc* units and *grc* units. In the framework, three crystallographical distinct oxygen sites exist: O1 forms the 6-ring and 4-ring part, O2 forms the 8-ring and 6-ring part, O3 forms the 8-ring and 4-ring part. The crystallographic ratios are 2:1:1 for O(1), O(2), and O(3) sites, respectively.

Zeolite A structure contains 96 Na^+ ions, which balance the surplus negative charge of AlO_4 tetrahedra. Na^+ could easily be changed by other cations such as alkali or alkaline earth metals. Water molecules are inside the pores of zeolite A, which could be released by the heating process. Generally, there are three sites for Na^+ in dehydrated zeolite Na-A (Ohgushi, 2007). S1: approximately 64 Na^+ are located in the 6-rings where they coordinate to the three framework oxygen atoms; S2: 24 Na^+ sit in/out 8-rings where they coordinate to the two framework oxygen atoms; S3: the remaining 8 Na^+ are usually located in the front of 4-rings where they coordinated to the two framework atoms. This 4R sites are not fully occupied. The water molecules distributed in both α cages and β cages.

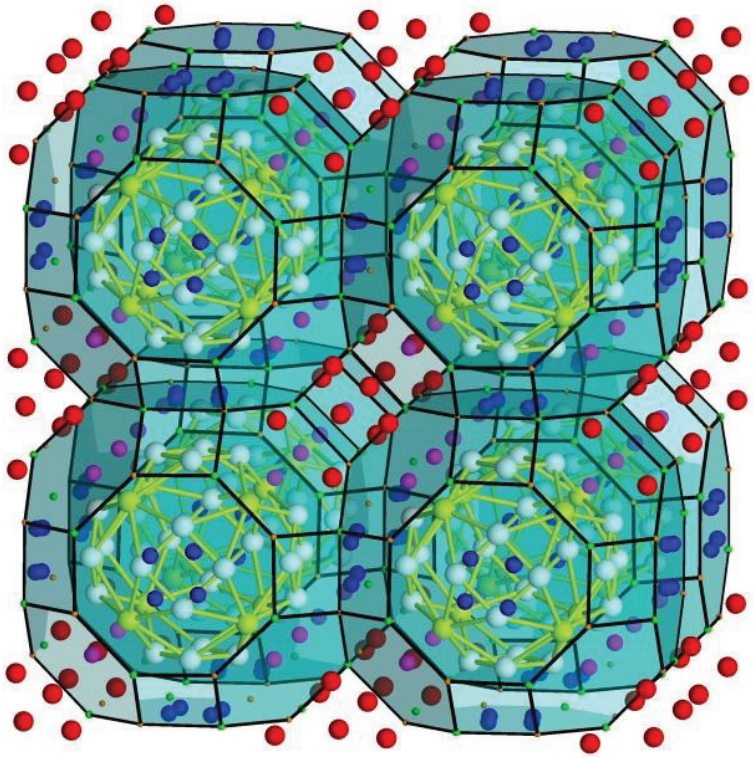

Fig. 1.4 Crystal structure of fully hydrated zeolite NaA (Fischer *et al.*, 2012) Na1=pink; Na2=blue; OW1=red; OW2=yellow; OW3=white.

Since the distance between water and framework oxygen is similar to the distance of Na^+ to framework oxygen atoms, it is hard to distinguish water molecules and Na^+ in hydrated Na-A. An authoritative refinement of the crystal structure of hydrated Na-A was reported by Gramlich and Meier (1971). In their work, five sites were observed for water molecules. Site 1 was occupied by four water molecules inside the small β cages. Site 2 and 3 were occupied by 20 water molecules inside the α cages. Site 4 probably included both sodium and water molecules. Site 5 was possibly occupied by one water molecules and one Na ion at the center of the dodecahedral cluster. Recently, our group reported the crystal structure of fully hydrated zeolite Na-A by single-crystal synchrotron methods in the space group $Fm\bar{3}c$ (Fischer *et al.*, 2012). In this work, two sites for Na^+ (Fig. 1.4) are shown. 64 Na^+ are located in large cages. 24 Na^+ are lying on the surface of 8-ring. There are three positions that are suitable for water molecules. Two of them are in the *grc* units (forming sodalite-cage-shaped clusters) and one was in the *toc* units (arranged octahedrally).

1.2.1 Space group assignment

The first report that describes the structure of zeolite Na-A was based on powder diffraction data provided by Reed and Breck (1956). They refined the structure in space group $Pm\bar{3}m$ with lattice parameter a = 12.3 Å. In space group $Pm\bar{3}m$, the Si and Al atoms are not discriminated. Later on Barrer and Meier (1958) observed two superstructure lines that indicate a doubled unit cell constant in the powder pattern Na-A. Smith and Dowell (1968) reported the structure of dehydrated Na-A in space group $Pm\bar{3}m$ using very small single crystal (an edge length of 23 μm). In 1971, the relatively large single crystals of zeolite Na-A were synthesized by Charnell (1971) with TEA as an additive. Gramlich and Meier (1971) described the structure of hydrated zeolite A in space group $Fm\bar{3}c$ with lattice parameter a = 24.6 Å. They refined the crystal structure in the subgroup but constrained the nonframework atoms to the symmetry of supergroup. In the double unit cell constant, they showed that the Si and Al atoms of the framework are ordered in this way.

So far, approximately 90% of the publications described the structure of zeolite A or different cation-exchanged zeolite A in space group $Pm\bar{3}m$. Only 10% of the publications are reported in subgroup $Fm\bar{3}c$. In this work, the main parts are concentrated on describing the structure of different cation exchanged zeolite A in space group $Fm\bar{3}c$.

1.2.2 Si/Al ratio

The detailed description of Si/Al ratio in zeolite A is presented in Chapter LTA.6.4 by Fischer and Baur (2006). A brief summary is presented in the following paragraph.

Table 1.2 The evolution of Si/Al ratio.

Year	Authors	method	Si/Al
1979	Pluth and Smith	Electron microprobe	1.03
1983	Bennett	Wet chemical analysis	0.94
1984	Seff and Mellum	^{29}Si NMR	1
1985	Blackwell	^{29}Si NMR	1.03±0.01
1987	Hanson	Proton inelastic scattering	1.04

The determination of the exact chemical composition of zeolite A is a controversial issue for many years. At the beginning, the Si/Al ratio in zeolite A synthesized by Charnell's method was assumed to be 1. Pluth and Smith (1979) used electron microprobe analysis on different cation-exchanged single crystal zeolite A and reported that the Si/Al was at least 1.03 corresponding to 97.4 Si and 94.6 Al in the F-centered unit cell. However, Seff and Mellum (1984) disputed that the Si/Al ratio is exactly one for strict alternation of Si and Al over tetrahedral nodes in the framework. They argued that the results that show the Si/Al ratio of more than one is due to the experimental error. Later Blackwell *et al.* (1985) reported that the Si/Al ratio is 1.03(1) by nuclear magnetic resonance spectrum. This is supported by Hanson *et al.* (1987) who determined the Si/Al = 1.04(1) by proton inelastic scattering. This issue is also discussed in this work.

1.3 Properties and applications of zeolite A

1.3.1 Thermal stability

In general, zeolites are widely used in extreme temperature conditions in industry. For instance, zeolites can be used as sorbents at high temperatures. Therefore, the thermal stability of zeolites is a very important feature. The thermal treatment introduces a framework of zeolites that collapses into intermediate amorphous phases. Subsequently, another crystalline phase is formed through a recrystallization process.

The sodium form of zeolite A transforms into a mixture of carnegeite and nepheline at 900°C and completely transforms into nepheline above 1000°C (MIMURA and KANNO, 1980). Ohgushi *et al.* (2001) investigated the thermal disintegration process of zeolite A by a microwave heating technique. They pointed out that zeolite A transformed into high-carnegieite 1 at 920°C. The transformation proceeded with increasing temperatures. Nepheline was formed at 990°C and high-carnegieite 2 at 1254°C. Further heating led to melting at 1526°C.

Generally, the thermal stability of the framework of zeolite varies depending on the nonframework cations. If sodium is replaced by potassium, the transformation at high temperature is different. The investigation from Kosanovic *et al.* (1997) showed that potassium-exchanged zeolite A (K-A) transformed into an amorphous aluminosilicate at 960°C. If the heating time was prolonged at the same temperature, it transferred into a

mixture of kalsilite and kaliophilite. Ferone *et al.* (2005) investigated the sequence of thermal transformation for Ba-exchanged zeolite A (Ba-A). The zeolite Ba-A became an amorphous phase at around 200°C by a partial disruption of the D4R units. The crystallization of small crystallites of monoclinic celsian started at 500°C and the crystallization of hexacelsian occurred above 800°C. With temperature up to 1400°C, the hexacelsian converted into monoclinic celsian. Radosavljevic-Mihajlovic *et al.* (2015) reported the transformation process for Pb-exchanged zeolite A (Pb-A). The framework of Pb-A was collapsed into amorphous intermediate products between 600°C and 650°C and yielded disordered Pb-feldspar$_{LTA}$ and Pb-feldspar$_{FAU}$ phases over 1100°C. Liguori *et al.* (2008) reported that the Sr-exchanged zeolite A (Sr-A) transformed into amorphous at approximately 900°C and followed by the formation of Sr-feldspar at 950°C and completely converted at 1150°C.

1.3.2 Ion exchange

The research on ion-exchange properties of zeolites has been a hot topic for many years. The ion-exchange applications of zeolites depend on many factors such as the framework of aluminum content, the structure of zeolite, and the positions of the charge-balancing cations within the structure.

Zeolite A has a high ion-exchanged capacity because it belongs to aluminum-rich zeolite. The excellent ion-exchange properties of zeolite A confer it to have applications as a "builder" in laundry detergents. Traditionally, phosphates are very popular for their use as detergent builders. However, in the early 1980s, high concentrations of phosphate compounds were found in the lakes and rivers, which led to eutrophication. Therefore, due to the environmental pressures, a new detergent was urgently needed to substitute the phosphate.

Zeolites are the excellent substitute for phosphatic builder materials in the formulation of detergents. Especially, zeolite A with high aluminum content is used to extract Ca^{2+} and Mg^{2+} by replacing soft ions such as Na^{+} and K^{+}. Several studies were reported on understanding the relevant cation-exchange processes (Barri and Rees, 1980; Franklin and Townsend, 1985a; Franklin and Townsend, 1985b). Coker and Rees (2005) investigated the kinetics of binary ion exchange of Ca^{2+} and Mg^{2+} in quasicrystalline and

crystalline zeolite A and found that the diffusion rates of calcium and magnesium ions in the crystalline zeolite A were relatively faster than that in the quasicrystallines precursors. Another important area where high ion-exchange properties of zeolites are exploited is the trapping and removal of heavy cations such as Pb^{2+}, Sr^{2+}, Ba^{2+}, Cs^{2+}, Cr^{3+}, and other cations from contaminated waste water. This application of zeolites to environmental pollution control has received very little attention, which might due to the necessary requirement for a low pH solution. Hui *et al.* (2005) found that the selectivity sequence of zeolite A depends on the initial concentration of the metal ions and the initial pH of the solution. They reported the sequence as $Cu^{2+} > Cr^{3+} > Zn^{2+} > Co^{2+} > Ni^{2+}$ at the tested concentration of 300 mg/L. El-Rahman *et al.* (2006) reported that the selectivity sequence from aqueous solution by synthetic zeolite A is $Sr^{2+} > Ca^{2+} > Mg^{2+} > Cs^{+} > Na^{+}$. Hashemian *et al.* (2013) also investigated the adsorption behavior of Fe^{3+} by synthesized zeolite A and found that a contact time of 60 min and a pH of 6 would be the best condition for removing iron.

Among the different cation exchanged zeolites, the NH_4^+ exchanged zeolites play important roles as catalysts in chemical and material industries due to their unique proprieties such as strong Brønsted acidity, high surface area, and shape selectivity.

Generally, the catalytically active sites, namely, Brønsted acidity, can be formed by a hydroxyl group that bridges framework Al and Si atoms (Si-OH-Al). Considerable attention has been paid to obtain the Brønsted acid sites by heating ammonium-exchanged zeolites. However, the heating of ammonium-exchanged zeolites could also lead to the breakdown of the framework due to removal of aluminum from the framework (dealumination). For Si-rich (Si/Al > 2.0) zeolites, the deammoniation process (removal of NH_3) and the dehydroxylation process (removal of framework OH groups) are well separated. Generally, the deammoniation occurs between 250 and 450°C whereas dehydroxylation occurs between 500 and 700°C (Beyer *et al.*, 1977; Weeks *et al.*, 1975). For instance, ammonium-exchanged zeolite Y (Kerr, 1969) could obtain the hydrogen forms of zeolite or even can attain an ultrastable status during the calcination process. For Al-rich zeolites (Si/Al < 2.0), it has been shown in experiment and quantum-chemical calculations that the protonated framework is unstable (Barthomeuf, 1987; Pelmenschikov *et al.*, 1992). Chu and Dwyer (1980) reported that NH_4X samples lost an

appreciable amount of crystallinity below 200°C. Kühl and Schweizer (1975) investigated that the partially NH_4^+exchanged zeolite X showed that zeolite X remains thermally stable if Na/Al atomic ratio is at least approximately 0.6.

In this study, the crystal structure and thermal stability of K^+, NH_4^+ and partially NH_4^+ exchanged zeolite A were investigated.

1.3.3 Adsorbents

According to the molecular sieving properties, zeolites are used as adsorbents because of their uniform micropores that allow small molecules to enter while blocking larger molecules. Zeolites act as selective regenerable adsorbants, and play an important role in the separation and purification of industrial pollutants.

The adsorption behavior of zeolites can be influenced by the following factors. The first factor is the size of the pores. For zeolite A, it has a pore diameter of 4 Å, which is just between the molecular size of O_2 and N_2 (O_2: 3.8 Å × 2.8 Å; N_2: 4.2 Å × 3.2 Å). Therefore, zeolite 4A membranes have a good application for air separation (Wang *et al.*, 2002). Alkane/alkene separation by using zeolite A was also studied by Granato *et al.* (2007). Owing to the high extraframework atoms, Na could be exchanged by calcium and potassium. When 75% of Na^+ is substituted by K^+, the effective diameter of pore is approximately 3 Å and it is denoted by zeolite 3A. Alternatively, if the Na^+ is substituted by Ca^{2+}, it produces zeolite 5A. Zeolite K-A is widely used in ethanol drying processes because the micropores are so small that the alcohol cannot penetrate (Carmo and Gubulin, 2002). Zeolite 5A has been used to separate CO_2 from several gas mixtures (Harlick and Tezel, 2004; Yin *et al.*, 2005). Yang *et al.* (1997) found that the zeolite 5A molecule sieve can produce highly pure H_2 by the adsorption of CH_4 and CO impurities.

The second factor is the interactions of the guest molecules with the framework atoms. In aluminum-rich zeolites (such as zeolite A), the abundance of negative framework charges is balanced by cations that make electrostatic interactions predominant. In contrast, in silicon-rich zeolites, the high amount of silicon increases the hydrophobic characters, therefore high van der Waals interactions was the master for the adsorption behavior. In addition, the pore topology is also considered to be an important factor to influence the adsorbent behaviors (Krishna and van Baten, 2013).

Chapter 2 Objectives and thesis outline

2.1 Objectives

Zeolite A was widely used in industry as water softeners in detergents (removing calcium and magnesium) and catalysts due to its excellent ion exchange capacity and adsorption behavior. The Si/Al ratio of LTA framework is close to 1. The high amount of Al in framework give rise to the negative charges that require more extraframework cations to neutralize. These extraframework cations that lived in the channel of zeolite A can be easily substituted by different valent cations. The chemical properties such as thermal stability are also influenced after different cations exchange. Especially the NH_4^+ exchanged zeolites draw more and more attention due to the introduce of catalytically active sites after the removal of NH_3. Most work was devoted to study the stability of NH_4^+ exchanged Si-rich zeolites (such as zeolite Y). Hence, it is significant to investigate the NH_4^+ exchanged Al-rich zeolite A and the thermal stability.

In addition to the cations, water molecules are also present in zeolite channels. The effect of water molecules can be divided in two aspects. One effect is to complete the coordination of the cations. Another is to decrease the electrostatic repulsion between framework oxygens (Higgins *et al.*, 2002). Generally, water molecules are coordinated to adjacent water and zeolitic framework atom and extraframework cations by hydrogen bonds and ion-dipole interactions (Crupi *et al.*, 2006). The existence of water molecules in zeolite has an important influence on the position of exchangeable cations and yields different properties of zeolite. Therefore, a detailed knowledge of water and cation position can be useful and is necessary to complete the description of crystal structure of cation exchanged zeolite A.

One important part of this thesis is to determine the crystal structure of different cation exchanged hydrated zeolite A including the description of the position of cations and water molecules. Another part is to study the thermal stability of zeolite A after different cation exchange (such as K^+ and NH_4^+ exchange). Meanwhile, an further study is continued to the previous work (Fischer *et al.*, 2012), which pointed out that the lattice patter *a* of synthetic zeolite A decreased, whereas the crystal size increased upon

increasing the TEA concentration during synthesis process. Some heavy atoms (Ba^{2+} and Sr^{2+}) exchanged zeolite A were prepared to interpret the lower X-ray diffraction intensity after heavy atoms exchange was due to the high absorption coefficient for X-rays.

Objective 1: Investigate the thermal stability and crystal structure of hydrated K^+ exchanged zeolite A

Prepare the pure powder and single crystal of K^+ exchanged zeolite A. Refine the crystal structure of hydrated K-A in space group $Fm\bar{3}c$ by single-crystal X-ray diffraction data. Investigate the thermal behavior at different temperature in air and under vacuum conditions by powder samples.

Objective 2: Investigate the thermal stability of partially NH_4^+ exchanged zeolite A and crystal structure of hydrated NH_4^+ exchanged zeolite A

Prepare different amount of K/NH_4 exchanged zeolite A and investigate the thermal stability under different atmosphere (air and vacuum). Describe the water and NH_4^+ positions in NH_4^+ exchanged zeolite A in space group $Fm\bar{3}c$ by single-crystal X-ray diffraction data.

Objective 3: Investigate the influence of TEA on synthesized zeolite A and crystal structure of heavy atom exchanged zeolite A.

The different zeolite A samples were synthesized based on different amount of TEA. It was found in the previous work (Fischer *et al.*, 2012) that lattice parameter *a* decreased with increasing the concentration of TEA. Different spectroscopy methods were employed to investigate these zeolite samples to find out the TEA effect. In addition, the effect of heavy atoms on the X-ray diffraction intensity of zeolite A was also studied.

2.2 Thesis outline

In this work, investigation of different cation exchanged zeolite A were the main task. For these results, the writing part were done by Li Wang based on the discussions from coauthors. The detail contributions were explained separately in the following.

(1) Powder and single-crystal K^+ exchanged zeolite A

All the sample preparation and sample measured by X-ray diffraction were done by Li Wang. The X-ray fluorescence analyses (XRF) were performed by Bernhard Schnetger (University of Oldenburg). The microprobe analyses for the single crystal were performed by Lennart A. Fischer, Karsten Goemann, Sandrin T. Feig (University of Tasmania, Hobart, Australia) and Dr. Andreas Klügel (University of Bremen). The thermal analyses (TG-DSC) measurements were done by Johannes Neumann (IFAM in Oldenburg). The crystal structure refinements for both single crystals and powder data were done by Li Wang with support from Prof. Reinhard X. Fischer and Dr. Johannes Birkenstock. All the data evaluation from XRF, EMPA and TG-DSC results was done by Li Wang with support from Dr. Iris Spieß, and Prof. Reinhard X. Fischer.

All the results in this section are based on the manuscript "*The thermal stability and crystal structure of zeolite K-A*", which is in preparation for publication.

(2) Powder and single-crystal NH_4^+ exchanged zeolite A

All the sample preparations and sample measurements by X-ray diffraction were done by Li Wang. The characterization of TG-FTIR was performed by Johannes Neumann (IFAM in Oldenburg). The X-ray fluorescence analysis were performed by Bernhard Schnetger (University of Oldenburg). The single-crystal structure refinement was done by Li Wang with support from Prof. Reinhard X. Fischer and Dr. Johannes Birkenstock. The data evaluation for TG-FTIR and XRF were done by Li Wang with support from Dr. Iris Spieß and Prof. Reinhard X. Fischer.

All the results in this section are based on the manuscript "*The thermal stability and crystal structure of zeolite NH_4-A*", which is in preparation for publication.

(3) The TEA effect and heavy atoms exchanged zeolite A

The sample syntheses were done by Li Wang and Malik Šehović. The XRF were performed by Bernhard Schnetger (University of Oldenburg). All the other analyses including powder X-ray diffraction (University of Bremen), Infrared spectroscopy (University of Bremen) and UV/vis spectroscopy (University of Bremen) were discussed

with Prof. Reinhard X. Fischer and Dr. Iris Spieß. The writing part was done by Li Wang based on the discussions.

All the results in this section are based on two manuscripts, which are in preparation for publications.

Chapter 3 Material and methods

3.1 Synthesis

In this study, most of the lab works are focused on the synthesis of different cation exchanged zeolite A. For all the powder samples and the single-crystal samples, the preparations were done using static methods. Powder samples of zeolite A (idealized composition $Na_{12}Al_{12}Si_{12}O_{48}\cdot 27H_2O$) were used as starting material. For the K^+ and NH_4^+ exchanged zeolite A, the parent Na-A was supplied from Degussa. For heavy atoms exchanged zeolite A, the original zeolite was synthesized in the laboratory using Charnell's methods (Charnell, 1971). The single crystals zeolite Na-A (size up to 80 μm) are kindly supplied from Karl Seff. The raw materials that used during the sample preparation are listed in Table 3.1.

Table 3.1 The raw materials used during the sample preparation

Materials	purity	Company	CAS number
$Na_2SiO_3\cdot 9H_2O$	≥98%	Sigma-Aldrich	13517-24-3
$NaAlO_2$	≥99.95%	Sigma-Aldrich	11138-49-1
Triethanolamine	≥99%	Sigma-Aldrich	102-71-6
NH_4NO_3	≥95%	Merck Millipore	6484-52-2
KCl_2	≥99%	Sigma-Aldrich	7447-40-7
$BaCl_2$	≥99%	Sigma-Aldrich	10326-27-9
$Ba(NO_3)_2$	≥99%	Sigma-Aldrich	10022-31-8
$SrCl_2$	≥99%	Sigma-Aldrich	10025-70-4

3.1.1 K^+ and NH_4^+ exchanged single crystal Na-A

The single crystals were synthetized by Charnell's method (Charnell, 1971) and provided for these studies. For K^+ exchanged zeolite A, single crystals of Na-A (cube shaped with an edge length of 0.08 mm) were placed into the 1M KCl solution for 5 days at 80°C. The resulting colorless crystals were mounted on the tip of a glass fiber for further characterization. For NH_4^+ exchanged zeolite A, single crystals of Na-A were contract with 1M NH_4^+ solution for two days at ambient temperature. The NH_4^+ exchange solution

was prepared by solving NH_4NO_3 into ammoniacal solution to avoid the H_3O^+ generation during exchange process. Then the crystals were mounted on tip of glass fiber. The data collection for X-ray diffraction start immediately after fixing the crystal and the result was abbreviated as NH_4-A_0d. The crystal was stored at room temperature for 16 days and the data was collected again. The obtained data was accordingly labeled as NH_4-A_16d.

3.1.2 K^+ and NH_4^+ exchanged powder Na-A

The preparation method for K-exchanged samples was described by Lührs *et al.* (2012). Exchange was performed in a KCl solution for a total of six times. The obtained white solid product was filtered and washed carefully by doubly distilled water and dried at 50°C yielding the final product of zeolite K-A.

Powder samples of dehydrated K-A were obtained at 500°C for 12 h under vacuum conditions. The sample stored in air for 2 days at ambient temperature yielded rehydrated K-A.

The completely NH_4-exchanged samples (denoted as NH_4-A) were prepared by static methods. Powder zeolite A was put into NH_4NO_3 solution and maintained for 12 h. The solid was separated by filtration and again contacted with the fresh NH_4NO_3 solution for a total of eight times. The final samples were dried at 40°C to avoid NH_3 dissociation from ammonium cations.

The intermediate compositions between completely K-exchanged and NH_4-exchanged zeolite A are also obtained by static methods. Powder samples of K-A (produced from Na-A) were contacted with different concentrations of NH_4NO_3 solution for 12 h at 60°C. The separated solid was dried at 40°C in case of NH_3 evaporation. The chemical compositions of intermediate samples were determined by X-ray fluorescence. They are denoted as $K_{9.6}$-A and $K_{7.8}$-A, respectively.

3.1.3 Zeolite Na-A with different amount of TEA

Powder samples of zeolite Na-A were synthesized using a modified procedure after Charnell (Charnell, 1971) with various concentrations of TEA. The precursors were

consisted of aluminate and silicate solution mixed with different amount of TEA, respectively. The details for the preparation were described in the previous work (Fischer *et al.*, 2012). The synthesized zeolite A was denoted according to the concentration of TEA. For example, NaA_0.25 means the sample was synthesized with 0.25 mol/L TEA. Another experiment about zeolite A synthesized with 0.25 mol/L TEA was repeated. The only difference is the mixing precursors were transformed into autoclave instead of polypropylene bottles. This sample was denoted as NaA_0.25_a.

3.1.4 Ba^{2+} and Sr^{2+} exchanged Na-A

The synthesis method of zeolite Na-A was similar as the previous report (Fischer *et al.*, 2012). The only difference is that the sealed autoclave instead of polypropylene bottle was used as container for the mixture of sodium metasilicate and aluminate solution. To obtain completely Ba^{2+} exchanged zeolite A, powder zeolite A was contacted with $Ba(NO_3)_2$ and $BaCl_2$ solution at 65°C for a total of eight times. This sample was noted as Ba-A. Sr^{2+} exchanged zeolite A was prepared through placing parent zeolite Na-A into fresh $SrCl_2$ solution for a total of six times. After exchange, the solid was separated from the liquid by filtration and washed with doubly distilled water. Finally, the products were dried at 60°C for overnight. The details for the Ba^{2+} and Sr^{2+} exchanged conditions are presented in Table 3.2.

Table 3.2. The exchange process of Ba^{2+}, Pb^{2+} and Sr^{2+} exchanged zeolite A

Samples	Sequence of refresh times	Salt solution	concentration of solution	Solid/liquid ratio	Temperature	interval time
Ba-A	1st-4th	$Ba(NO_3)_2$	0.1M	1/25	338K	12h
	5th	$BaCl_2$	0.1M	1/50	338K	12h
	6th	$BaCl_2$	0.002M	1/20	338K	12h
	7th	$BaCl_2$	0.04M	1/30	338K	12h
	8th	$BaCl_2$	0.04M	1/40	338K	12h
Sr-A	6	$SrCl_2$	0.1M	1/50	298K	24h

3.2 Analytical methods

The analytical methods including diffraction and spectroscopic techniques are employed for this study. Among the different analytical methods, the powder and single-crystal X-ray diffraction experiments and thermal analysis under synthetic air were performed in the group of Crystallography, FB05 Geosciences, University of Bremen. Other instruments are introduced in the sections below.

3.2.1 Single-crystal X-ray diffraction

A Bruker AXS D8 VENTURE diffractometer equipped with a KAPPA four-circle goniometer with a curved graphite crystal TRIUMPH as monochromator and a PHOTON 100 detector based on CMOS (Complementary Metal Oxide Semiconductor) technology with an active area of 100 cm^2 ($K\alpha_1$, λ = 0.7093 Å; $K\alpha_2$, λ = 0.7136 Å) was used for data collection at ambient temperature. For data collection of single crystal zeolite K-A and zeolite NH_4-A, each reflection was scanned with a speed of 0.5°/f and 80 s/f. The data was collected in a full sphere at the beginning and integrated all the reflections using large unit cell. Multiscan absorption correction was applied on the data.

3.2.2 Powder X-ray diffraction

X'pert:

The temperature-dependent X-ray diffraction measurements were performed on a Bragg-Brentano PANalytical X'Pert MPDPRO diffraction system, equipped with a high-temperature chamber HTK 1200N (Anton Paar Co.), Cu-Kα radiation (λ = 1.5418Å), ¼ fixed divergence, primary and secondary Soller slits with 0.04 rad aperture, secondary Ni-filter and X'Celerator detector system (127 channels, channel width 0.01671 $^o2\theta$).

Measurements for sample K-A and intermediate samples were performed from 30°C to 1000°C during heating with a rate of 20°C/min in air and under vacuum conditions, respectively. Only NH_4-A were performed in steps of 10°C from 30°C to 220°C. Under vacuum conditions, the sample was put into the chamber and then the pump started immediately. After one hour, the pressure in the chamber achieved 10^{-4} mbar, the data collection was started. Before the isothermal data collection at each temperature, the

sample was equilibrated for 5 min. Scanning was performed in the range from 3–120 °2θ, with a step width of 0.01672 °2θ.

PW1800:

For heavy atoms exchanged zeolite A, the data was collected on the Philips PW1800 diffractometer with Bragg-Brentano geometry, equipped with a PW1711 proportional detector, a graphite monochromator and Cu-Kα radiation.

3.2.3 X-ray fluorescence (XRF)

The chemical composition of the powder sample of zeolite K-A was analyzed by X-ray fluorescence spectroscopy (Panalytical Axios Max), equipped with a Rh (4kW maximal power) X-ray tube. This experiments were carried out in University of Oldenburg. 400 mg of powder samples were mixed with 4.5 g lithium tetraborate before measurements. For zeolite K-A, the analyzed elements were Na, K, Si and Al. The result indicated that the all Na^+ was completely exchanged by K^+ since no Na^+ was detected. The chemical composition was $K_{88.2}Al_{94}Si_{98}O_{384}$ without considering water content. For zeolite NH_4-A and intermediate samples, since XRF cannot quantify light element such as nitrogen and oxygen, the elements analyzed were Na, K, Si and Al in the powder samples. The results are shown in the results and discussion section (Chapter 4).

3.2.4 Thermal analyses (TG)

Thermogravimetric analyses were performed on a Netzsch 449 F3 Jupiter (Netzsch) STA apparatus. Under synthetic air (80% N_2, 20% O_2), samples (20 mg) zeolite K-A were heated from ambient temperature to 800°C with heating and cooling rate of 10 K/min and a controlled gas flowed with a rate of 20 ml/min. An empty corundum crucible was used as a reference.

3.2.5 In situ thermogravimetric analyses coupled with Fourier transform infrared spectroscopy (TG-FTIR)

The TG–FTIR analyses were performed using simultaneous thermogravimetry (Netzsch STA 449 F3 upiter) coupled with FTIR spectrometer (Bruker Tensor 27). The samples

were first maintained at 35°C for 2 h under Ar gas with a flow rate of 20 ml/min. Later the samples were measured at a heating rate of 5 K/min under vacuum in the temperature range of 35–800°C. Although some different ionic species were produced during heating process, in this work, only water and ammonia were specially studied. The qualitative determination of NH_3 and H_2O removed from the NH_4^+ exchanged zeolite A during their thermal decomposition was carried out by gas IR spectroscopy. All the experiments were done in the Department of Elec. Energy Storage, Fraunhofer Institute for Manufacturing Technology and Advanced Materials IFAM, Oldenburg.

3.2.6 Electron microprobe analyzer (EMPA)

Electron microprobe analyses were performed to do the elemental analysis for single crystal K^+ exchanged zeolite A. The crystal was mounted in epoxy and polished to expose their cross-section and coated with a thin carbon film to avoid charge accumulation. The same single crystal was measured with two different instruments to check the accuracy of the chemical composition. Analyses at the University of Tasmania, Hobart, Australia were performed with a CAMECA SX-100, which equipped with 5 tunable wavelength dispersive spectrometers, an acceleration voltage of 15 kV, a beam current of 10 nA and a beam diameter of 10 μm. Raw data were corrected with the software "Probe for EPMA", "ZAF" matrix (Armstrong, 1988) and the intensity data was corrected for time dependent intensity (TDI) loss. The counting time was 6s for Si and Al, 10s for Na and K, and 20s for Ca, respectively. The standards were clinopyroxene for Si and Ca, plagioclase for Al, anorthoclase for Na, and microcline for K, respectively. The general chemical formula was obtained by averaging 10 points analyses. Insignificant amounts of Ca, which are possibly from the exchange KCl solution, were also detected by electron microprobe analysis without showing in the chemical formula.

Another measurement was performed in CAMECA SX-100 electron microprobe at the group of Petrophysics Geochemistry, FB05 Geoscience, University of Bremen. This measurement was performed at operating voltage of 15 kV, a beam current of 4 nA, and a beam diameter of 5 μm. The detailed discussion for these results are discussed in section 4.1.1.

3.2.7 Scanning electron microscopy and energy dispersive X-ray spectroscopy (SEM/EDX)

The scanning electron microscopy (SEM) micrographs and the energy dispersive X-ray spectroscopy (EDX) data were performed on JMS-6510 instrument equipped with X-Flash detector 410-M operated at an accelerating voltage of 20 kV. This experiment was performed in group Chemical Crystallography of Solids, FB02 Biology/Chemistry, University of Bremen.

3.2.8 Fourier Transform Infrared Spectroscopy (FTIR)

FTIR measurements were performed on Nicolet Nexux 8700 FTIR spectrometer (Thermo Electron corporation, Madison, WI), which equipped with the Smart iTR^{TM} (ATR) sampling accessory. The powder samples were mixed with KBr (in a mass ratio of 1:250) and pressed into tablets for FTIR measurements. The samples were measured under air conditions at room temperature with the wave number range of 4000–400 cm^{-1} at 4 cm^{-1} resolution. All the experiments are used the instrument in University of Jacobs.

3.2.9 Ultraviolet-visible Spectroscopy (UV/vis)

UV/vis spectra of various samples were obtained on a Shimadzu UV/vis spectrophotometer UV-2600， which equipped with ISR-2600 plus two-detector integrating sphere. The reference is $BaSO_4$. The wavelength was ranging from 185 nm to 1400 nm. The spectra of different samples were taken at ambient conditions without any special precautions. This experiment was performed in the Department of Production Engineering, FB04 IWT, University of Bremen.

3.2.10 Raman Spectroscopy

One single crystal of zeolite K-A was measured by Raman Spectroscopy. The spectra were performed on a Horiba LabRam Aramis spectrometer. Data collection was started from 100cm^{-1} to 4000 cm^{-1} Raman shift at room temperature. This experiment was performed in group Chemical Crystallography of Solids, FB02 Biology/Chemistry,

University of Bremen. The figure of the Raman spectroscopy was not shown in this thesis but discussed in Chapter 4.

3.2.11 Computer programs used

The Rietveld refinements for powder samples were performed with the programs BRASS (Birkenstock *et al.*, 2012) and Topas (Bruker, 2009). The structure refinements of single crystals were performed with the SHELXL-97 program (Sheldrick, 2008). The visualization of the crystal structure were performed in program VESTA (Momma and Izumi, 2011) and STRUPLO (Fischer and Messner, 2010). For the evaluation of the thermal analyses the Netzsch software was used (NETZSCH, 2010).

Chapter 4 Results and discussion

4.1 K^+ exchanged zeolite A (K-A)

In this section, the crystal structure and thermal stability of zeolite K-A were investigated based on single-crystal and powder data. About 90% of the crystal structures of zeolite A are described in space group $Pm\bar{3}m$ which was first reported by Reed and Breck (1956). However, the true space group is assumed to be $Fm\bar{3}c$ with an ordered distribution of Si and Al and a doubled lattice parameter *a* (Gramlich and Meier, 1971). In addition, space groups $R\bar{3}c$ (Bennett *et al.*, 1983) and $Fm\bar{3}m$ (Armstrong *et al.*, 1994) were assigned to LTA type compounds with partial ordering of Na and K, respectively.

In fully hydrated zeolite K-A, water molecules and K^+ have similar distances to framework oxygen atoms (about 3 Å), thus it is difficult to distinguish between K^+ and H_2O by crystal-chemical considerations. Therefore, most of the previous work was devoted to describing the structure of the dehydrated K^+ exchanged zeolite A. Pluth and Smith (1979) described the crystal structures of dehydrated zeolite K-A proving the absence of zero-coordinated potassium as reported before. Adams and Haselden (1983) studied the dehydrated partially K^+ exchanged zeolite A based on neutron powder diffraction in space group $Fm\bar{3}c$ with three K^+ and one Na^+ position. Sun and Seff (1993) investigated the location of cationic tetrahedral K_4 and/or trigonal K_3 clusters formed by over exchange under potassium metal vapor. To our knowledge, the first structure description of hydrated zeolite K-A was reported by Leung *et al.* (1975). They studied both the hydrated and dehydrated zeolite K-A based on single-crystal X-ray diffraction methods in space group $Pm\bar{3}m$. In the hydrated structure, K^+ is distributed inside the large cage, found near the center of the 8-ring and near the center of the unit cell. Water molecules were distributed in both the *toc* unit (for designations see Smith (2000); also named sodalite cage or β cage) and the large *grc* (α cage) cavity.

4.1.1 EMPA analysis

The EMPA analyses of K^+ exchanged zeolite A yielded a chemical composition of $Na_{9.3}K_{61.9}Al_{95.36}Si_{96.6}O_{384}$ which is not charge balanced. The water content was not determined. The results showed that approximately 25% positive charges are missing in zeolite K,Na-A. The microprobe analysis was repeated on a different instrument on the same single crystal to check the precision of the result. However, the second measurement still indicated that more than 25% positive charges are missing.

Based on the results, two assumptions for the missing positive charges were inferred in this work. One assumption is that positively-charged H_3O^+ that cannot be detected by EMPA was incorporated in the structure. To check whether H_3O^+ exists or not, Raman spectroscopy was used on measuring the single crystal K-A. Four different locations from the single crystal were selected for the data collection. Generally, frequencies around 1135 cm^{-1}, 1680 cm^{-1}, and 2800 cm^{-1} are assigned to H_3O^+ (Ronald W.T. Wilkins *et al.*, 1974). However, there are no typical stretching and bending bands for H_3O^+ in the zeolite K,Na-A.

Another hypothesis for the missing positive charges could be that alkali ions especially Na are lost under the intense electron beam. Pluth and Smith (1979) reported that the monovalent alkali ions are very mobile compared with multicharged ions, therefore, the microprobe analysis on the element sodium and potassium might be unreliable. In their work, they focused on the analysis of Si, Al, and Ca rather than of Na and K. Similarly, in this work, the mobility of Na and K under the electron beam could also lead to a partial loss. The loss of Na and K can be reduced to a minimum level through the analytical setting such as operating with low beam currents and large beam diameters or monitoring intensities over time in case of decreasing. In this case, the TDI correction provided by the "Probe for EPMA" software package was used. However, it seems that the monitored intensities did not show a decrease with time in this measurement. In other words, all the detected elements were collected. Therefore, it is also possible that the H_3O^+ (if exist) partially decreased due to the protonation effect during the measurements.

Up to now, it is still an open question which hypothesis is the proper interpretation for the missing positive charges. It still needs more work to be answered.

Although the contents of Na and K are unreliable, the analysis on the multicharged ions Si and Al was still helpful. For years, it is a controversial issue for determining the exact chemical composition of zeolite A (summarized in Chapter 1). Different methods such as electron microprobe analyses (Pluth and Smith, 1979), ^{29}Si NMR-spectroscopy (Blackwell *et al.*, 1985) and proton inelastic scattering (Hanson *et al.*, 1987) were employed to determine the Si/Al ratio. All these methods indicated that the Si/Al ratio in zeolite A prepared following Charnell's method (Charnell, 1971) is higher than one. In this work, the electron microprobe analysis shows that the Si/Al ratio is 1.01(3).

In conclusion, it is worth noting that in our present work the chemical composition of $Na_{33.46}K_{61.9}Al_{95.36}Si_{96.6}O_{384}$, that is to say the missing charge was due to the undetected Na^+, was preferred to compare with the following structure refinement.

4.1.2 Single-crystal structure refinement

The single-crystal structure was refined using the SHELXL-97 program (Sheldrick, 2007) in space group $Fm\bar{3}c$. Crystal structure projections were performed with the program STRUPLO (Fischer and Messner, 2010). All the details of the refinement are listed in Table 4.1.

The original single-crystal Na-A was provided by Karl Seff (Hawaii). Initial framework atomic parameters for the refinements were taken from the single-crystal studies of Gramlich and Meier (1971). Isotropic refinement of the framework atoms converged to the indices R_1 = 0.3590 for 643 F_o> 4 sig (F_o) and weighed R_2 = 0.7560. The initial difference Fourier maps revealed one large peak position at (0.131, 0.131, 0.131) with highest maximum at 19.06 e/Å^3. This position was defined as K1. Subsequent difference Fourier maps revealed two positions of (0.0496, 0.0496, 0.0496) and (0.1327, 0.1327, 0.25) for water molecules and one position (0.0324, 0.2289, 0.2212) for K2. Since Na^+ was not completely exchanged by K^+ in this single crystal sample, it is possible that K1 and K2 position are mixed occupancy. However, the refinement results showed that no occupancy for sodium if K2 position was considered to be a mixed position. In this refinement, the K1 position was considered to be occupied by Na^+ and K^+. After introducing the nonframework atoms, the isotropic refinement converged to the indices R_1 = 0.1576 for 643 F_o> 4 sig (F_o) and weighed R_2 = 0.5589. The refinement with

anisotropic thermal parameters for all atoms revealed that the water position at (0.13, 0.13, 0.25) should be split into two separate positions (OW2 and OW3).

Table 4.1 Data collection and refinement parameters for zeolite K,Na-A.

Crystal data	Zeolite K,Na-A
Crystal system	cubic
Lattice parameter *a* [Å]	24.5714(8)
Unit cell volume[Å^3]	14835.054
Space group	$Fm\bar{3}c$ (No. 226)
Z	1
Crystal dimensions [mm^3]	0.08×0.08×0.08
Maximum 2θ range [^{o}]	54.99
T for data collection [K]	293
Reflection range	-31≤ h ≤31
	-31≤ k ≤31
	-31≤ l ≤31
No. of measured reflections	174177
No. of unique reflcetions	777
No. of reflections [F_o>4σ(F_o)]	643
Inconsistent equivalents	0
R_{int}	0.0427
R1 [F_o>4σ(F_o)] [b]	0.1213
R1(all data) [b]	0.1269
wR2 (all data) [c]	0.4711
No. of least-squares parameters	62
Weighting parameter *a*[d]	0.2
Goodness of fit	2.304
Final $\Delta\varrho_{min}$[e$^-$/ Å^3]	-1.03(1.65 Å from O3)
Final $\Delta\varrho_{max}$[e$^-$/ Å^3]	2.75 (2.08 Å from OW1)

a: The number of water molecules were derived from thermal analysis of powder sample zeolite K-A.

b: $R_1 = \sum ||F_o| - |F_c|| / \sum |F_o|$

c: $wR_2 = (\sum (w(F_o^2 - F_c^2)^2) / \sum (w(F_o^2)^2))^{1/2}$

d: $w = 1/(\sigma^2(F_o^2)+(aP))$ $P = (2F_c^2+\max(F_o^2, 0))/3$

In the final refinement, simultaneous position, occupancy and anisotropic refinement of all but OW2 and OW3 which were refined isotropically, decreased the R_1 to 0.1213 and weighted R_2 to 0.4711. The highest peak in the Fourier maps was at (0, 0, 0). Refining this position yielded distance of 2.08 Å to OW1, which was too close to water molecules. The deepest peak in the final difference Fourier map appeared at (0.0000, 0.0447, 0.2502) (–1.03 e/Å^3) which was too close to framework O3 (1.65 Å). All shifts in the final cycles of refinement were less than 5% of their corresponding estimated standard deviations.

4.1.3 Single-crystal structure analysis

The refinement results and selected interatomic distances and angles are presented in Table 4.2 and Table 4.3. Distances and angles between atoms are calculated by program STRUPLO (Fischer and Messner, 2010).

The distances of Al-O and Si-O are similar to the corresponding distances in the hydrated zeolite Na-A (Fischer *et al.*, 2012). The mean distance of Si-O is 1.612 Å indicating full occupancy by Si. The mean distance of Al-O was calculated to be 1.713 Å which is slightly shorter than the expected value of 1.746 Å (Baur and Ohta, 1982). The shorter distance might indicated that Al1 position is partially occupied by Si, which conforms to the microprobe analysis yielding a Si/Al more than one.

Table 4.2 Atomic position, Wyckoff positions, site occupancies and anisotropic displacement parameters. OW denotes water molecules. Numbers in parentheses are the estimated standard deviation.

Atom	Wyckoff site	x	y	z	Occ.
Si1	96i	0	0.09246(8)	0.18503(8)	1
Al1	96i	0	0.18610(9)	0.09034(8)	1
O1	192j	0.0538(3)	0.0574(2)	0.1713(4)	1
O2	96i	0	0.1470(2)	0.1480(2)	1
O3	96i	0	0.1117(4)	0.2474(2)	1
K1	64g	0.1297(1)	0.1297(1)	0.1297(1)	0.45(6)
Na1	64g	0.1297(1)	0.1297(1)	0.1297(1)	0.55(6)
K2	192j	0.039(1)	0.2254(7)	0.2242(7)	0.125
OW1	64g	0.0488(4)	0.0488(4)	0.0488(4)	0.72(4)
OW2	192j	0.125(1)	0.141(1)	0.249(1)	0.26(3)
OW3	192j	0.167(3)	0.105(3)	0.250(2)	0.23(5)

Atom	U_{11}	U_{22}	U_{33}	U_{23}	U_{13}	U_{12}	Ueq[Å^2]
Si1	0.018(2)	0.016(2)	0.015(2)	0.0036(7)	0.0000	0.0000	0.016(1)
Al1	0.017(2)	0.015(2)	0.015(2)	0.0040(7)	0.0000	0.0000	0.015(1)
O1	0.034(3)	0.035(3)	0.083(5)	0.024(3)	0.023(3)	0.013(2)	0.051(2)
O2	0.047(3)	0.017(3)	0.016(3)	0.001(3)	0.0000	0.0000	0.027(2)
O3	0.12(1)	0.028(4)	0.023(4)	-0.002(2)	0.0000	0.0000	0.056(4)
K1	0.031(2)	0.031(2)	0.031(2)	0.006(1)	0.006(1)	0.006(1)	0.031(2)
Na1	0.031(2)	0.031(2)	0.031(2)	0.006(1)	0.006(1)	0.006(1)	0.031(2)
K2	0.07(1)	0.07(1)	0.07(1)	-0.03(1)	-0.028(8)	-0.033(9)	0.068(6)
OW1	0.032(5)	0.032(5)	0.032(5)	0.007(3)	0.007(3)	0.007(3)	0.032(5)
OW2							0.030(8)
OW3							0.05(1)

Table 4.3 Selected interatomic distances and angles.

	Distances [Å]		Angles [^{o}]		Distances [Å]
Si-O1 2×	1.612(6)	Si-O1-Al	145.7(5)	K1-O1 3×	2.771(7)
Si-O2	1.619(6)	Si-O2-Al	158.3(4)	K1-OW2 3×	2.97(1)
Si-O3	1.604(5)	Si-O3-Al	145.1(7)	K1-OW2 3×	2.98(1)
Mean	1.612	Mean	148.7	K2-O2	2.85(2)
Al-O1 2×	1.712(6)	O3-Si-O1	110.9(4)	K2-O3	3.00(2)
Al-O2	1.712(6)	O3-Si-O2	107.1(4)	K2-O3	3.01(2)
Al-O3	1.715(6)	O1-Si-O1	110.1(3)	K2-K2	2.59(3)
Mean	1.713	O1-Si-O2	108.9(3)	K2-K2 2×	1.24(3)
O1-O1(Si)	2.642(9)	Mean	109.5	K2-K2	1.75(3)
O1-O2 2×	2.629(8)	O3-Al-O1	111.2(3)	K2-K2	1.91(4)
O1-O3 2×	2.649(10)	O3-Al-O2	106.4(4)	K2-K2 2 ×	2.28(4)
O2-O3	2.592(8)	O1-Al-O1	111.0(3)	K2-OW2	2.99(3)
Mean	2.632	O1-Al-O2	108.4(3)	K2-OW2	3.02(3)
O1-O1(Al)	2.823(8)	Mean	109.43	K2-OW3	3.13 (4)
O1-O2 2×	2.777(8)			K2-OW3	3.15(4)
O1-O3 2×	2.829(10)			OW1-O1 3×	3.02(1)
O2-O3	2.744(7)			OW1-OW1 3×	2.40(1)
Mean	2.797			OW2-O3	3.20(2)
				OW2-O1	3.37(2)
				OW3-O3	2.94(4)

Numbers in parentheses are the estimated standard deviation.

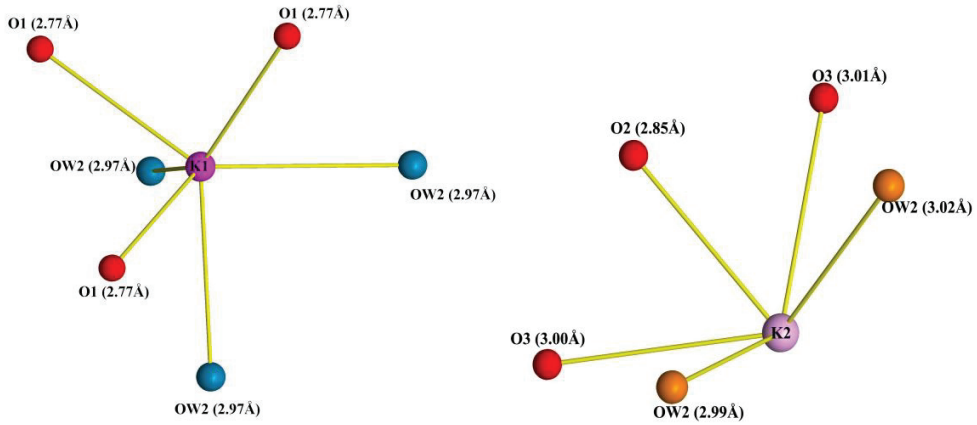

Fig. 4.1 Coordination environment of K1 and K2.

In fully hydrated zeolite K,Na-A, the K^+ ions occupy two different sites. The coordination environment for K^+ position was shown in Fig. 4.1. The K1 position is located inside the big *grc* unit along the 6-fold axes and projected into the center of the 6-ring. In zeolite A structure, small cations (such as Li^+ and Na^+) usually can be fit in the center or very close to the center of 6-ring on 6-fold axes. But with large ionic radius of K^+, positions on the 6-fold axes require off the 6-ring plane. From the normalized microprobe analysis result, Na^+ was not completely substituted by K^+. A trial that refine the Na^+ and K^+ in different positions independently near K1 location increased the index R1 to 0.17. In this situation, the K1 position was considered to be fully occupied by K^+ and Na^+. Other trials that K1 position was partially occupied by Na^+ and K^+ increased the index R1 as well. The framework oxygen atoms O1 from 6-ring are coordinated to the most populated K1 position with the distance of 2.77 Å. This distance is considered to be reasonable from the sums of their respective ionic radii (2.74 Å (Shannon, 1976)). Other water molecules OW2 are close to K1 position with the distance between 2.97 Å and 2.98 Å to complete the coordination of potassium. This position is considered to be stable due to the small anisotropic parameters.

The K2 position resides inside of the *grc* units. The same reason with K1 (larger ionic radius for K^+), K2 is located off the 8-ring window. If this position was located in the center of 8-ring, the distance between K^+ and framework oxygen atoms become 3.43 Å, which is significantly larger than 2.74 Å. Hence, the refined position for K2 in this work

seems reasonable. This position generates eight symmetry-equivalent positions and each four occupied one side of 8-ring. The eight symmetry equivalent positions in such a local arrangement are too close to each other, consequently, this limits the maximum occupancy in this position to 1/8. Refine the occupancy of this position freely yielded higher occupancy values. Therefore, the occupancy was constrained to 1/8 during the refinement. K^+ in this position is coordinated to three framework oxygen atoms with distances ranging from 2.85 Å to 3.00 Å and four water molecules with distances ranging from 2.90 Å to 3.17 Å (considering the distance up to 3.2 Å as coordination contracts) in OW2 and OW3 position. The long distance may be ascribed to the elongated thermal ellipsoid of K2.

The OW1 position is located in the *toc* unit on the 6-fold axis, the water molecules of which are connected with each other by hydrogen bonds with an interatomic distances of 2.40 Å (Fig. 4.2). The water molecules in the OW1 positions form a cube in the *toc* unit and approach to three framework oxygen atoms O1 with only weak bonds of 3.02 Å. It has been reported that this position was occupied by 8 water molecules per primitive unit cell in hydrated K-A (corresponding to 64 per F-centered cell with eight-fold volume) (Leung *et al.*, 1975). In Gramlich and Meier's work, 5.5 water molecules were found in the *toc* unit in Na-A (Gramlich and Meier, 1971). In hydrated Cd-A, 4 water molecules per primitive unit cell also resides in this position (McCusker and Seff, 1981b).

The OW2 and OW3 positions are placed in the *grc* unit near the 4-ring. Water molecules in these two positions approach framework oxygen at long distance. The position OW2 is surrounded by two framework oxygen atoms O3 and one O1 with the distance of 3.20 Å and 3.37 Å respectively. The position OW3 is neighbored by one framework oxygen atoms O3 with 2.94 Å. Water molecules in these two position form a sodalite-cage-shaped *toc* cage (Fig. 4.2). In the previous work, a similar position was reported for water molecules with full occupation in the *grc* unit (Leung *et al.*, 1975). But in the refinement of this work, this position is split into the OW2 and OW3 positions. The short distance between OW2 and OW3 indicate that it is impossible to place two water molecules simultaneously in these two positions. This is compatible with the low site occupancies of OW2 and OW3 of less than 0.5.

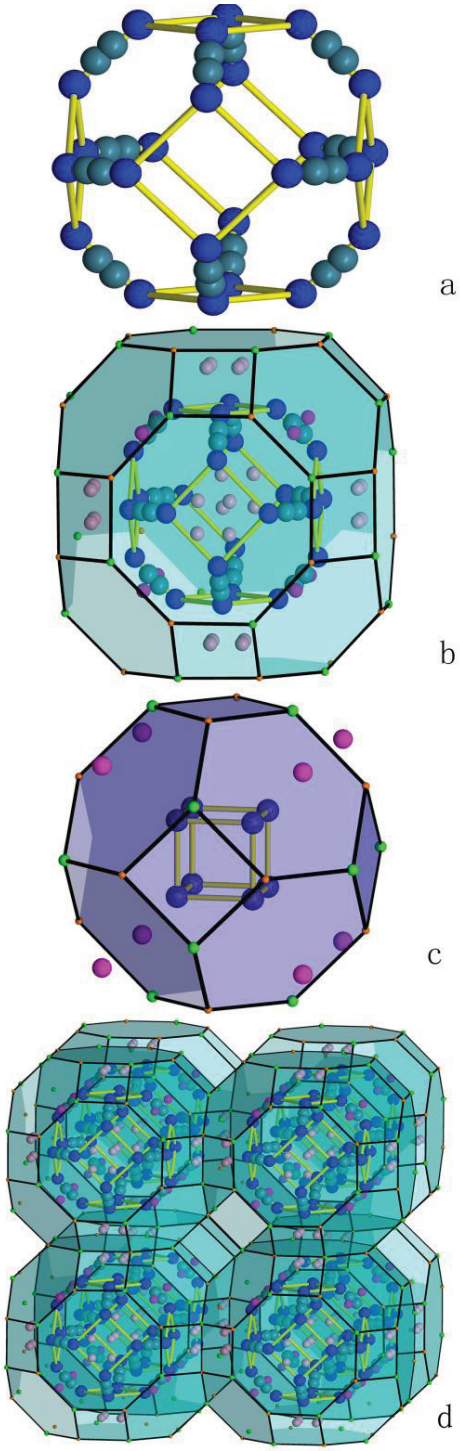

Fig. 4.2 Crystal structure projections of fully hydrated zeolite K,Na-A drawn with STRUPLO. (a) Sodalite-cage-shaped cluster of OW2 molecules (light blue) and OW3 molecules(blue); (b) *grc* unit with water cluster inside; (c) *toc* unit with a cubic arrangement of OW1 positions. K1 atoms are shown in red; (d) The *grc* units enclosing the *toc* units made up of OW2 and OW3 positions in the center.

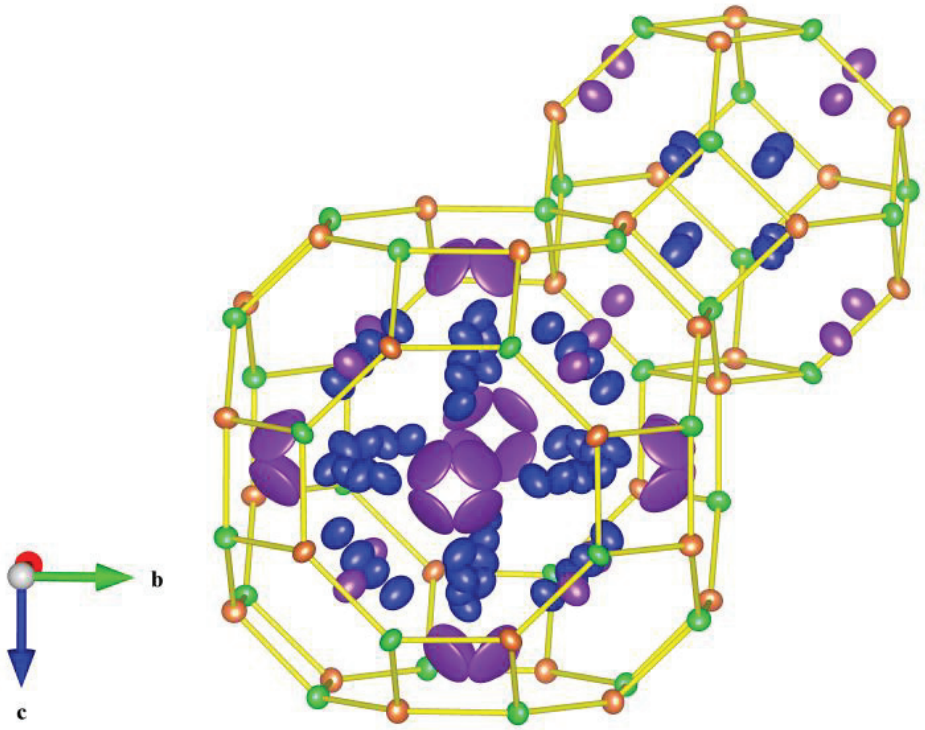

Fig. 4.3 Crystal structure projection of zeolite K,Na-A showing the anisotropic displacement ellipsoids (90% probability) except OW2 and OW3 drawn in VESTA (Momma and Izumi, 2011). Green=Al, orange=Si, purple=K, and blue=OW.

Fig. 4.3 shows the position of K^+ and water molecules in hydrated K,Na-A. The location of Na^+ in hydrated zeolite A (Fischer *et al.*, 2012) is similar to that of K^+ here. Both cations reside in the *grc* unit along the 6-fold axes near the 6-ring windows and in (Na^+) or off (K^+) the plane of 8-ring window, respectively. The Na^+ was calculated to be 35 while K^+ was 53 from the occupancy factor. About 9 K^+ was not found in the refinement. The possibility that K^+ distributed in water molecules position cannot excluded. The number of water molecules was ca.148 per unit cell which is slightly smaller than the number obtained by Leung *et al.* (1975) (160 OW/unit cell). Compared the water molecules obtained from TG analysis based on powder samples (192 OW/unit cell), 44 water was still missing. Inconsistencies that were reported for the numbers of water molecules between XRD and TG analysis were found to be due to the positional disorder and large atomic displacement parameters for H_2O, which increased the difficulty to locate water positions (Bish and Carey, 2000).

The crystal structure of hydrated zeolite K,Na-A was studied at ambient temperature. It is equally important to investigate the thermal behavior using X-ray powder diffraction. In the following, the lattice parameter a of zeolite K-A at different temperatures were obtained by the LeBail method (Le Bail, 2005) in space group $Fm\bar{3}c$. However, due to the fact that the X-ray diffraction data of powder sample exhibits a comparatively low resolution and that the strong pseudo symmetry in LTA can hardly be resolved in powder diffraction data, the Rietveld refinements of powder zeolite K-A were performed in space group $Pm\bar{3}m$ using the correspondingly eight-fold smaller unit cell which assumes disorder of silicon and aluminum.

The powder samples K-A were characterized by in situ powder X-ray diffraction, XRF and TG analysis.

4.1.4 In situ powder X-ray diffraction data analysis

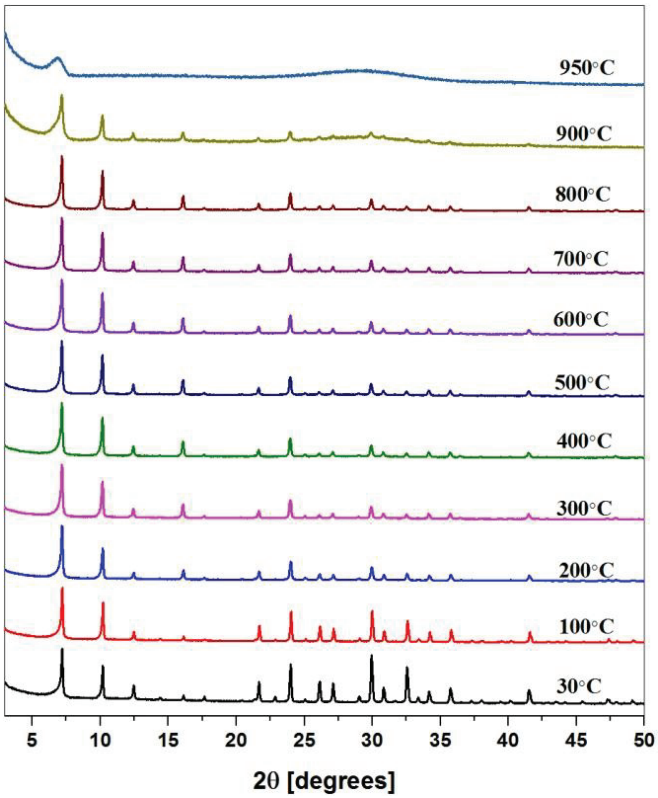

Fig. 4.4 In situ high temperature X-ray diffraction patterns of zeolite K-A collected between 30°C and 950°C in air.

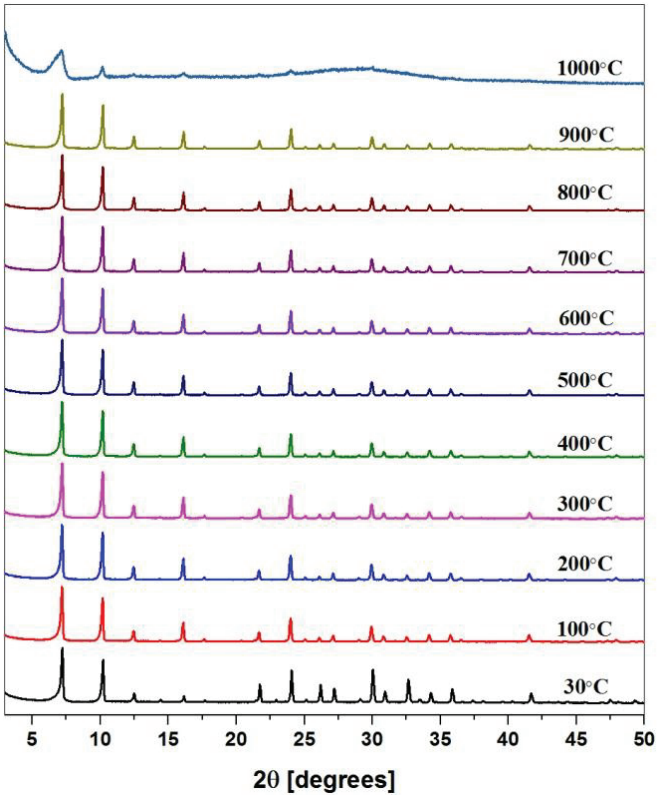

Fig. 4.5 In situ high temperature X-ray diffraction patterns of zeolite K-A collected between 30°C and 1000°C under vacuum conditions (10^{-4} mbar).

A very useful technique to study the thermal stability of zeolite is in situ X-ray diffraction. The XRD patterns of zeolite K-A heated in air and under vacuum are shown in Fig. 4.4 and Fig. 4.5, respectively. It can be seen that in both conditions, the intensity of the reflections at low 2θ angles increased until approximately 200°C. A possible interpretation is that the electron scatting density drop in the channels due to release of water (Agostini Giovanni *et al.*, 2009). Further increasing the temperature up to 800°C did not yield a significant intensity change. In other words, the framework of zeolite K-A remained stable up to temperatures of 800°C under both atmospheric and vacuum conditions. Zeolite K-A became completely amorphous at 950°C in air and 1000°C under vacuum conditions. It was reported that the potassium-exchanged zeolite A transforms into an amorphous phase when heated at 960°C for 30 min (Kosanovic *et al.*, 1997). The results in this work are in good agreement with these results.

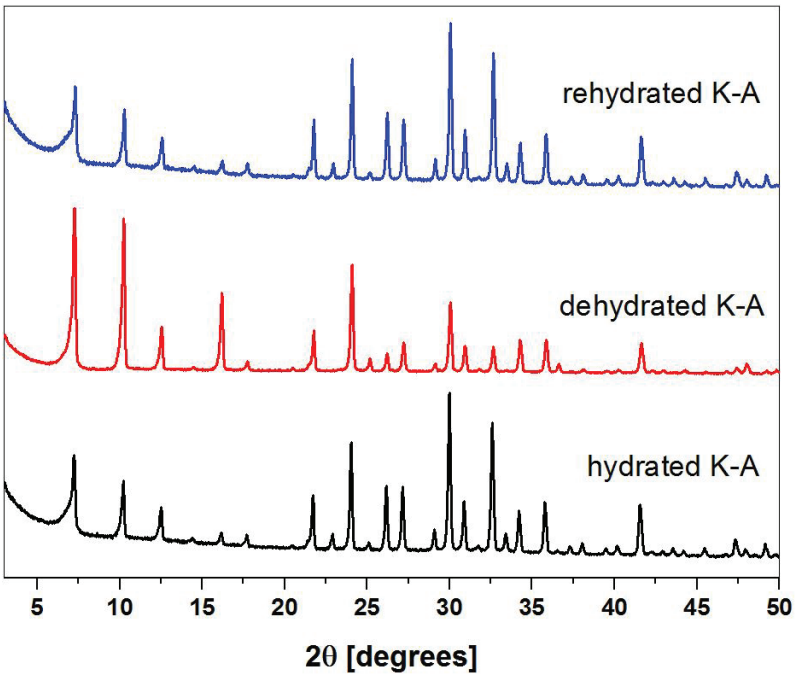

Fig. 4.6 X-ray diffraction patterns of hydrated K-A, dehydrated K-A, rehydrated K-A.

It is known that some dehydrated zeolites undergo irreversible structural changes and lead to total structural collapse. The XRD patterns of hydrated K-A, dehydrated K-A and rehydrated K-A are shown in Fig. 4.6. The similar diffraction patterns in these three samples indicate that water molecules can be removed and adsorbed back to the structure without leading to structural destruction. The dehydration and rehydration of K-A can be monitored by lattice parameter *a*. The lattice parameter of hydrated K-A measured at room temperature was calculated to be 24.6050(5) Å. After water release, the lattice parameter of dehydrated K-A decreased to 24.5586(7) Å. With exposure of the sample to air for 2 days, the lattice parameter a of rehydrated K-A was calculated to be 24.5937(6) Å, which was slightly smaller than the initial hydrated K-A.

To understand the process that takes place during heating, the analysis of lattice parameter *a* should be considered under both conditions. Structure-independent profile refinements using the LeBail (Le Bail, 2005) method describing peak intensities with a pseudo-Voigt peak shape function were performed to determine the lattice parameter *a* in space group $Fm\bar{3}c$ (F-cell, No.226) with the program BRASS (Birkenstock *et al.*, 2012). Instrumental profile parameters were specified by refinement of a LaB_6-standard.

The following parameters were refined: scale factor (s), zero point error (zero), background points were modeled by spline interpolation, Lorentzian and Gaussian peak width parameters (iPl, iPG, iSl, iSG) and lattice parameter *a*.

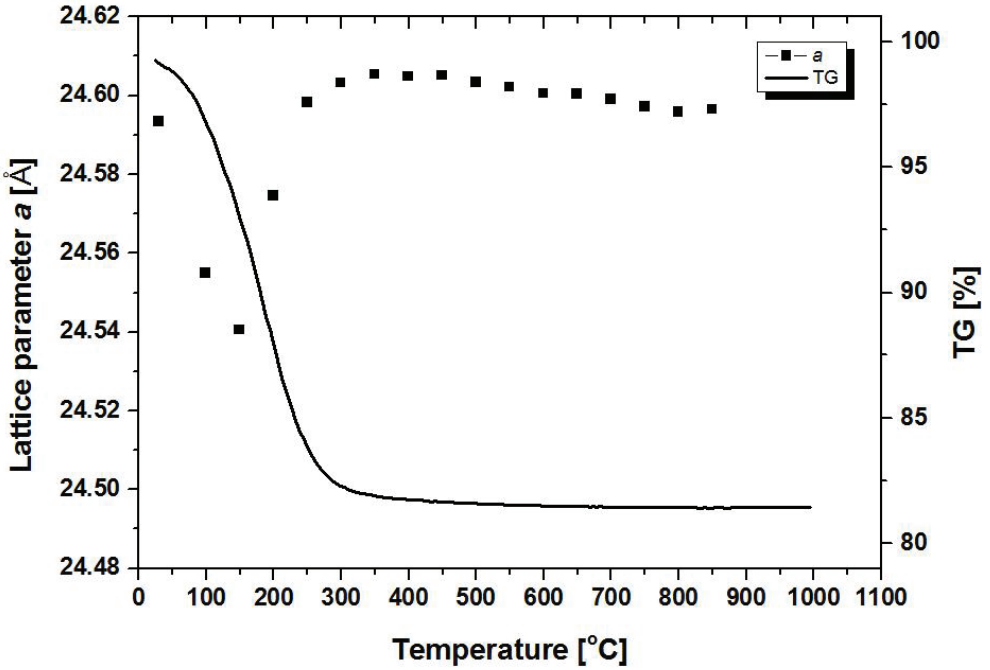

Fig. 4.7 Lattice parameter *a* and TG of zeolite K-A as a function of temperature in air.

The lattice parameter *a* and TG curve of zeolite K-A as a function of temperature in air are shown in Fig. 4.7. The water loss from K-A in air started around 50°C and continued up to approximately 400°C. The overall weight loss measured up to 800°C is 18.6%, which indicates that the number of water molecules in the zeolite K-A is 24.02, referring to the P-cell (192 referring to the F-cell). The calculated lattice parameters were plotted as a function of temperature in Fig. 4.7. There are some significant variations of lattice parameter of K-A heated in air. At 30°C the lattice parameter *a* of K-A was calculated to be 24.5934(4) Å, which was in a good agreement with previously reported calculation of hydrated K-A in space group $Pm\bar{3}m$ (a = 12.301 Å) (Leung *et al.*, 1975). The lattice parameter *a* shows a strong decrease from 30°C to 150°C due to the water release. From 150°C to 350°C, the lattice parameter increases which is attributed to the normal thermal expansion(caused by the repulsive forces of the K^+ ions after the loss of coordinated water) (Habersberger, 1987). The lattice parameter remained more or less constant from

400°C to 850°C in the range of 24.5959(8) Å to 24.6049(8) Å. At 900°C, the lattice parameter decreased dramatically indicating the thermal decomposition of zeolite framework.

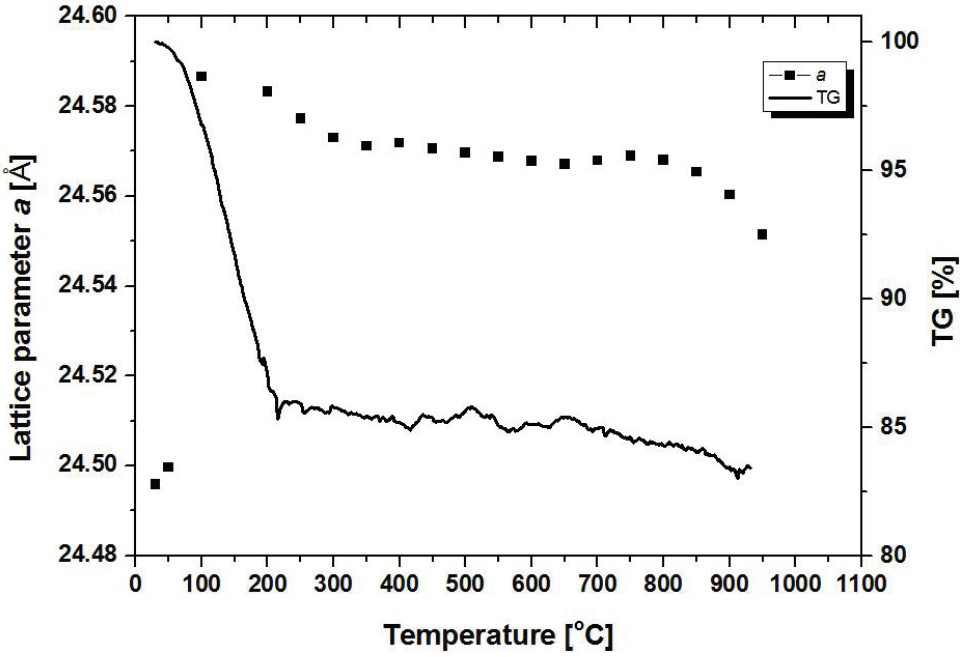

Fig. 4.8 Lattice parameter *a* and TG of zeolite K-A as a function of temperature under vacuum conditions.

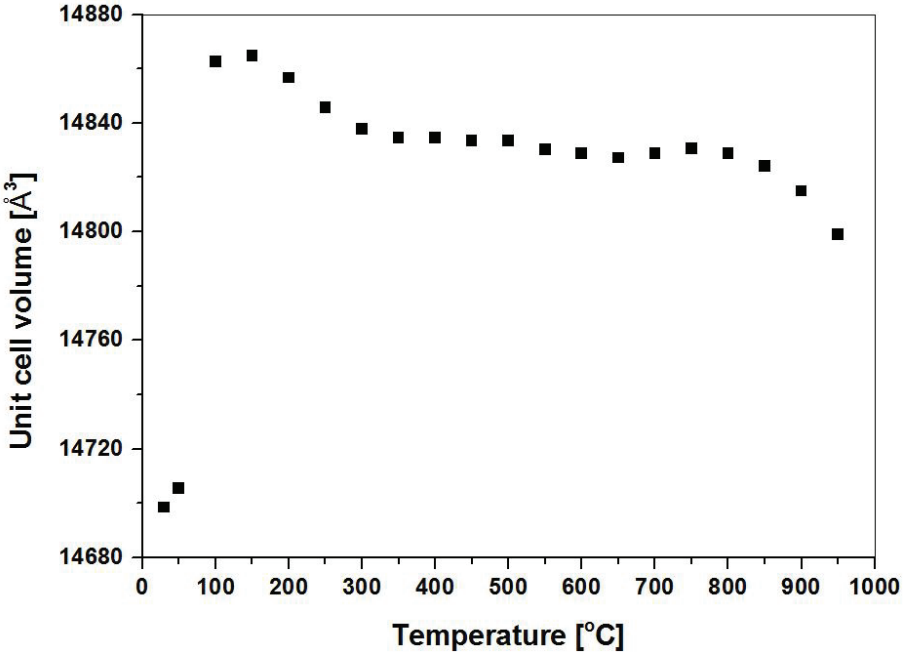

Fig. 4.9 Unit-cell volume of zeolite K-A as a function of temperature under vacuum conditions.

The lattice parameter *a,* the thermogravimetric curve, and the unit-cell volume as a function of temperature under vacuum conditions are presented in Fig. 4.8 and Fig. 4.9, respectively. The fluctuations in the range of 200–900°C may be related to the instrument noise. From TG analyses, the number of water molecules in K-A was calculated to be 20, which is slightly less than the number calculated from TG curve in air. The discrepancy may be ascribed to that partially physically absorbed water was involved under atmospheric condition while they are extracted under vacuum condition before the data collection started. Under vacuum condition, the variation of lattice parameter *a* is different from K-A under atmospheric condition. At 30°C, the lattice parameter is calculated to be 24.4958(5) Å, which is significantly lower than that of K-A at 30°C under atmospheric condition. This is probably due to that the water molecules were extracted out when the pump started to work in order to obtain vacuum, therefore the lattice parameter decreased remarkably. In the temperature range of 30°C–150°C, the lattice parameter increases with a consequently positive volume expansion from 14698.5(5) to 14864.8(7) $Å^3$. From 150°C to 300°C, the lattice parameters showed a drastic decrease which resulted in a negative volume expansion with a rate $\Delta V/\Delta T$ of -0.179. In the same temperature range, the rate of weight loss is -0.039 (Δweight/ΔT). Compared with the two different rates, it can be assume that the effect of water molecules on the thermal behavior in the temperature range could be negligible. A small decrease was observed up to approximately 800°C. After 800°C, the lattice parameter shows a stronger decrease. These results confirmed a weak negative thermal expansion effect on K-A with a unit cell volume contraction of 0.2% upon elevated temperature. After 800°C, the lattice parameter decreases due to the partial collapse of structure.

4.1.5 Powder structure refinement

To investigate the negative thermal expansion, Rietveld structure refinement was carried out by analyzing the powder XRD data of zeolite K-A at different temperatures. The crystal-structure refinement of K-A was performed in supergroup $Pm\bar{3}m$ to understand the variation over the full temperature range.

Rietveld structure refinement of zeolite K-A was performed in space group $Pm\bar{3}m$ (P-cell) which assumes disorder of silicon and aluminum using the software TOPAS

(A.Bruker, 2009). The occupancies of framework Si, Al, O were fixed while the atom positions and isotropic displacement parameters B varied during the refinement. For the extraframework atoms, the B_{iso} values were fixed at B(K) = 1 $Å^2$ and B(water) = 2 $Å^2$. The structure refinement results are shown in Fig. 4.10 and Fig. 4.11, respectively.

Generally, there are four principal mechanisms to interpret the negative thermal expansion as summarized by Sleight (1998). 1) the average metal-oxygen (M-O) distance decreased; 2) the anisotropic thermal behavior (expand in one or two directions while contract in others) of different bonds; 3) extrinsic effect (interstitial cations change positions upon heating); 4) the transverse thermal vibrations of oxygen atoms in M-O-M linkages. In the opposite, the longitudinal thermal vibrations lead to the expansion of lattice. Due to the strong metal-oxygen bonds, the expansion of the MOx polyhedra is negligible and the polyhedra are rotated freely as rigid units. This mechanism is so-called rigid unit mode (RUM), which was developed by Bieniok and Hammonds (1998).

4.1.6 Powder structure analysis

The mean T-O distance and O-T-O angles of K-A as a function of temperature are shown in Fig. 4.10 (T = Si, Al). The T-O distance at 30°C is slightly higher than other distances at high temperatures. The bias may be resulted from the process of the refinement. Becasue a R_{bragg} value high up to 9.472% was obtained at 30°C, comparatively less than 5% at high temperatures. Too much water molecules at 30°C may partially explain the poorer refinement. There are no significant changes in the T-O bond distances and O-T-O bond angles considering the estimated standard deviations found in the Rietveld refinements from 100°C to 800°C. Hence, changes in the TO_4 tetrahedra do not seem to be responsible for the contraction of the framework. In other words, the TO_4 tetrahedra can be treated as rigid bodies. Therefore, the negative thermal expansion was correlated to the transverse vibrations of the two-coordinate bridging oxygen atoms.

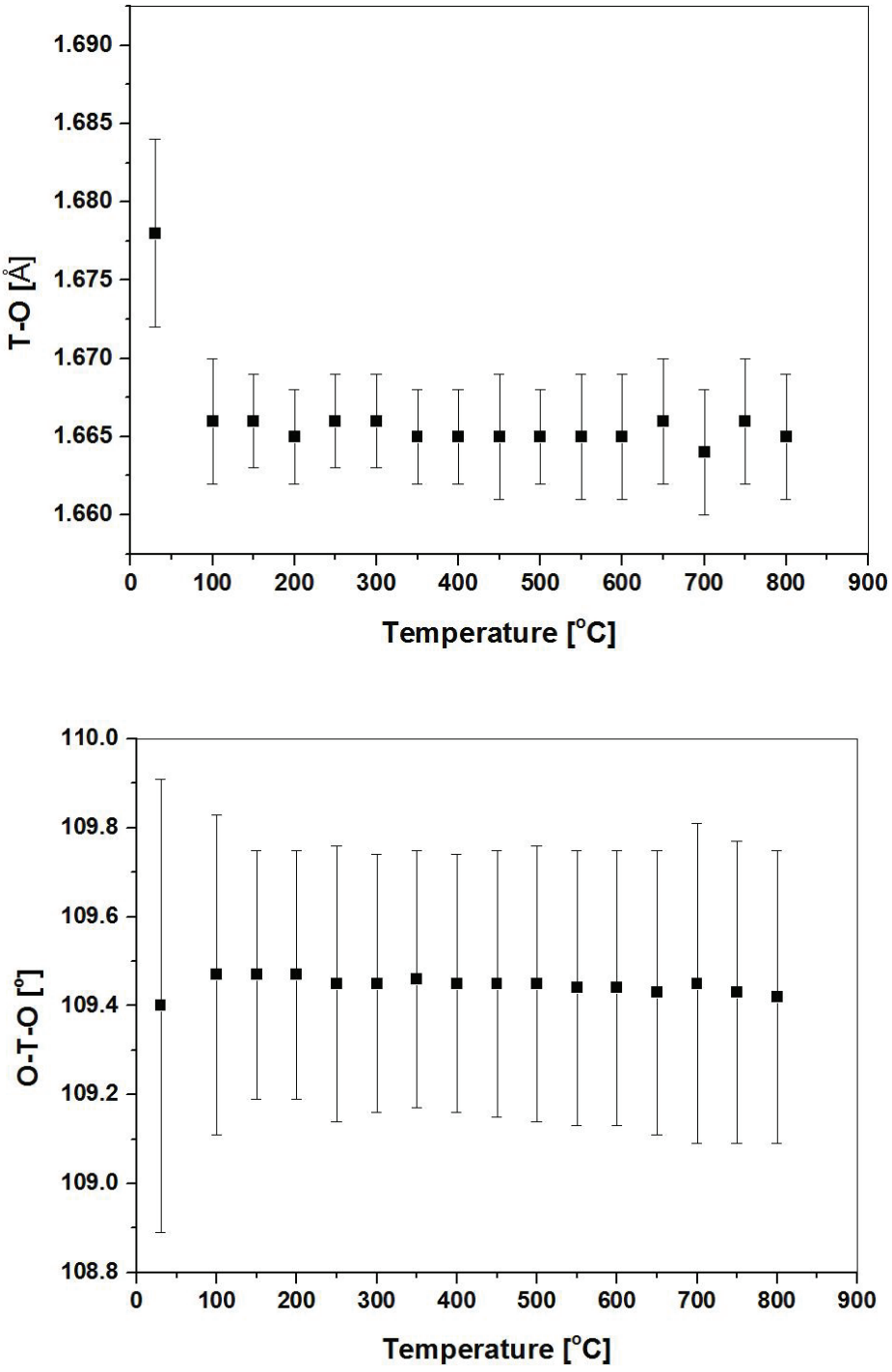

Fig. 4.10 Mean T-O distance and O-T-O angles of K-A as a function of temperature.

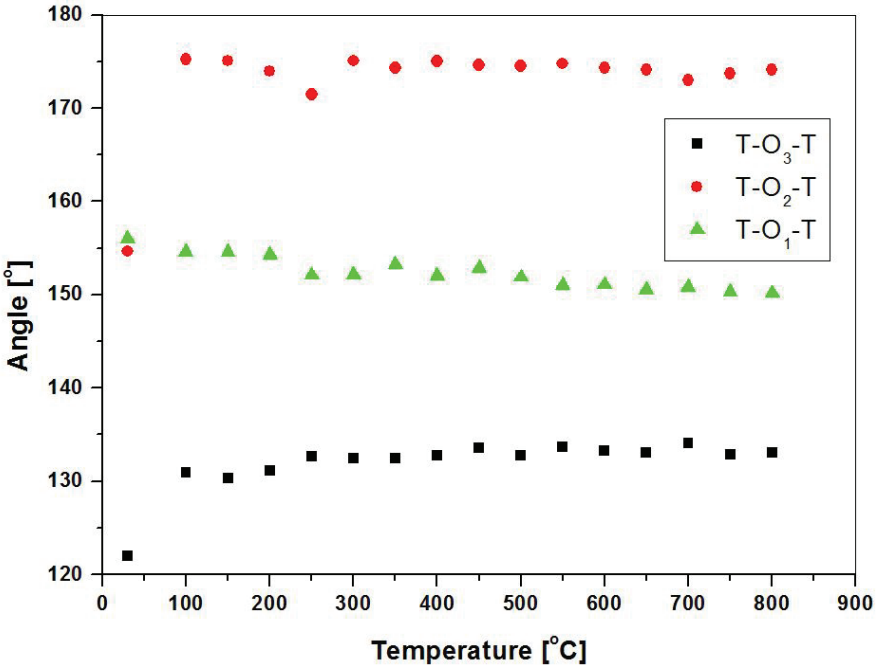

Fig. 4.11 T-O-T bond angles of zeolite K-A as a function of temperature.

Fig. 4.11 illustrates the specific T-O-T bond angles as a function of temperature for K-A. From room temperature to 100°C, significant increases in the angles T-O2-T and T-O3-T were observed. These changes indicate that the channels of eight-ring become broader. From 150°C to 250°C. The angle T-O1-T and T-O2-T decreased upon heating. The T-O1-T angles decreased by 2.48°, leading to a shift of O1 from the center of D4R. The T-O2-T decreased by 3.6°, consequently, O2 shifted from the plane of S6R upon heating. On the contrary, the T-O3-T angle increased by 2.3° (moving O3 shift from the center of the S8R). After 300°C, all the T-O-T angles remained roughly constant until 700 °C. The changes of these transverse vibration of T-O-T angles indicated a weak rotation of the tetrahedra with heating, which led to the volume contraction. The directions of tetrahedra rotation are shown in Fig. 4.12.

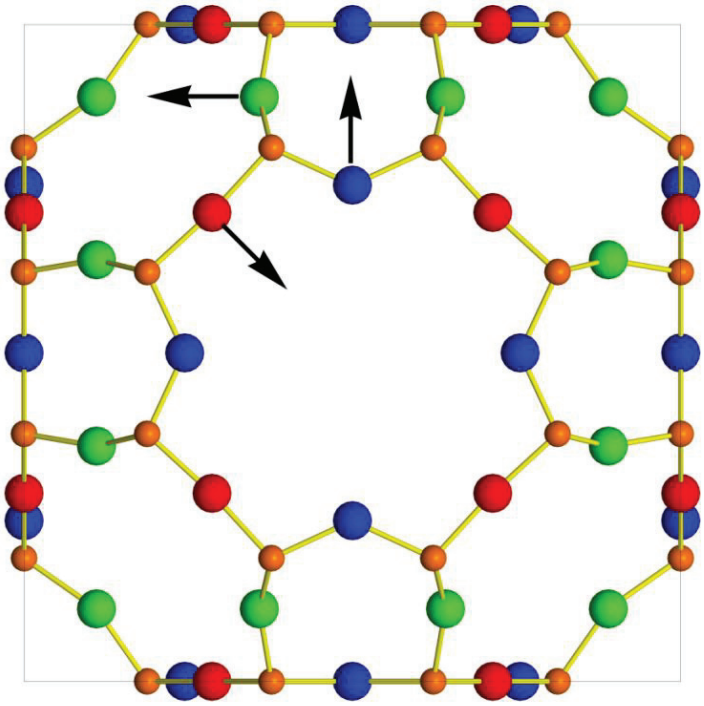

Fig. 4.12 Diagram of the LTA α-cage illustrating the changes in T–O–T bond angles upon heating (orange=T, green=O1, red=O2, blue=O3). The arrows indicate the directions of movement of atoms from 150°C to high temperature.

Generally, the negative thermal expansion would be stronger when there were no extra-framwork cations in the pores. Carey *et al.* (2014) reported that the purely siliceous ITQ-29 has the strongest negative thermal expansion resulting from the rotation of rigid TO_4 tetrahedra upon heating. It was reported that the dehydrated zeolite Na-X showed negative thermal expansion behavior below 227°C (Couves *et al.*, 1993). Changing the pore contents made the rotation restricted. Hence, in this work, with Na^+ exchanged by K^+ in zeolite A, it seems reasonable that only weak negative thermal expansion was found upon heating.

4.2 NH_4^+ exchanged zeolite A (NH_4-A)

The single crystal structure of zeolite NH_4-A was refined in space group $Fm\bar{3}c$ based on single-crystal X-ray diffraction data. EDX analysis was used to check whether the Na^+

was completely exchanged or not. The powder samples of NH_4-A were characterized by in situ X-ray powder diffraction and thermal analysis.

In fully hydrated NH_4-exchanged zeolite A, NH_4^+ and water molecules show almost identical scatter amplitude in X-ray diffraction, thus it is difficult to distinguish their positions. Patalinghug and Seff (1990) and Lee *et al.* (1982) investigated the structure of cation (Ni^{2+}, Cu^{2+}) and NH_4-exchanged zeolite A by single-crystal X-ray diffraction technique in the cubic space group $Pm\bar{3}m$. McCusker and Seff (1981a) prepared the NH_4-exchanged zeolite A by flow methods and determined the crystal structure in space group $Fm\bar{3}c$ (a = 24.568 Å) in dehydrated state. Hence, it is interesting to determine the crystal structure of hydrated NH_4-A.

4.2.1 EDX analysis

In order to check whether Na^+ was exchanged completely or not, one single crystal from the same batch was selected for the EDX analysis. Since EDX analysis has low accuracy for light elements and the Si/Al ratio of is determined by EPMA analysis in zeolite K-A, the main focus was the determination of the sodium content to estimate roughly whether Na^+ still exist or not. The EDX results are shown in Fig. 4.13.

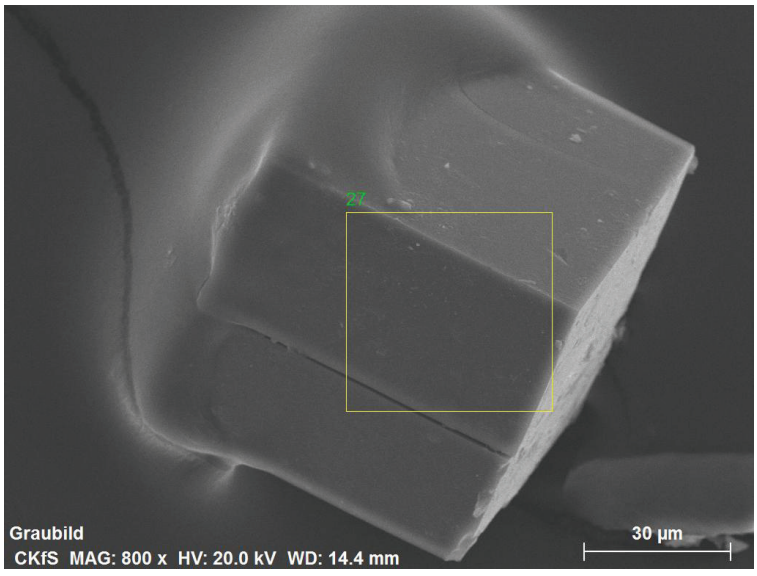

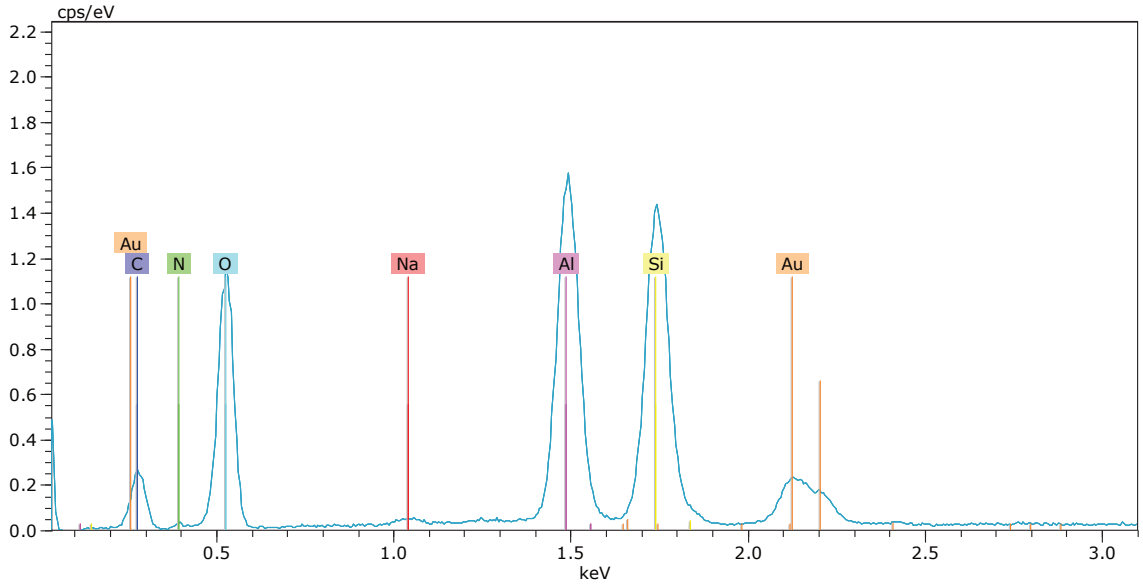

Fig. 4.13 The EDX elemental mapping and spectrum.

As shown in Fig. 4.13, the elements Au and C were from the sample preparation. The other elements Al, Si, O, N, and Na were detected. The selected elemental mapping demonstrated that there was almost no Na^+ in the crystal (very weak peak intensity). Therefore, in the following section, the single crystal of zeolite NH_4-A was considered to be exchanged completely. However, due to the inaccuracy of EDX analysis, some fraction of Na^+ might still be there in the structure.

4.2.2 Single-crystal structure refinement

The single crystal structure was refined using the SHELXL-97 program in space group $Fm\bar{3}c$ (Sheldrick, 2007). The visualization of the crystal structure were performed in program VESTA (Momma and Izumi, 2011). The original single crystal Na-A was provided by Karl Seff (Hawaii). Details of data collection and crystal data are listed in Table 4.4. The refinement results and selected interatomic distances and angles for each datasets are presented in Table 4.5 and Table 4.6, respectively. Distances and angles between atoms are calculated by program STRUPLO (Fischer and Messner, 2010).

Table 4.4 Data collection and refinement parameters for zeolite NH_4-A.

Crystal data	NH_4-A_0d	NH_4-A_16d
Crystal system	cubic	cubic
Lattice parameter *a* [Å]	24.5996(3)	24.3378(3)
Unit cell volume[$Å^3$]	14886.27	14415.97
Space group	$Fm\bar{3}c$ (No. 226)	$Fm\bar{3}c$ (No. 226)
Z	1	1
Crystal dimensions [mm^3]	0.08×0.08×0.08	0.08×0.08×0.08
Maximum 2θ range [^{o}]	54.92	55
T for data collection [K]	293	293
Reflection range	-31≤ h ≤31	-31≤ h ≤31
	-31≤ k ≤31	-31≤ k ≤31
	-31≤ l ≤31	-31≤ l ≤31
No. of measured reflections	433832	98604
No. of unique reflcetions	777	730
No. of reflections [$F_o>4\sigma(F_o)$]	671	570
No. of systematic absence violations	82	16
Inconsistent equivalents	0	0
R_{int}	0.0626	0.0706
R1 [$F_o>4\sigma(F_o)$][b]	0.0636	0.1074
R1(all data)[b]	0.0690	0.1184
wR2 (all data)[c]	0.2065	0.3643
No. of least-squares parameters	57	59
Weighting parameter [d]	0.137/89.499	0.2
Goodness of fit	1.112	1.629
Final $\Delta\varrho_{min}$[$e^-/Å^3$]	-0.35 (0.65 Å from Si)	-0.72 (1.24 Å from O3)
Final $\Delta\varrho_{max}$[$e^-/Å^3$]	1.94 (2.05 Å from OW1)	1.76 (0.47 Å from OW1)

a: the chemical position was obtained from EDX analysis; the number of water molecules was calculated from the thermal analysis based on powder data NH_4-A.

b: $R_1 = \sum ||F_o| - |F_c|| / \sum |F_o|$

c: $wR_2 = (\sum (w(F_o^2 - F_c^2)^2) / \sum (w(F_o^2)^2))^{1/2}$

d: $w = 1/(\sigma^2(F_o^2)+(aP))$ $P = (2F_c^2+\max(F_o^2, 0))/3$

Full-matrix least-squares refinement was done on F_o^2 using all data. Initial framework atomic parameters for the refinements were taken from the work of single-crystal studies (Gramlich and Meier, 1971). The initial refinement used isotropic thermal parameters and

converged the indices R1= 0.1843 and R1= 0.2543 for the two datasets, respectively. Subsequent difference Fourier maps immediately yielded two independent positions for NH_4^+ and three positions for water molecules. For data NH_4-A_0d, the final cycles of the refinement were done with anisotropic for all positions except OW2 and OW3. For data NH_4-A_16d, all the water molecules were refined isotropically in the final cycles of the refinement. The final refined weighting-scheme parameters and the final error index R1 for each dataset are given in Table 4.4. The highest peak and deepest hole in the final difference Fourier maps were not assigned in the refinement due to these positions are too close to either framework atoms or water molecules.

In single crystal NH_4-A_16d, another aluminum position was assigned on (0, 0, 0) position. The difference Fourier maps revealed high electron density (approximately 20 e/Å^3) at this position that located in the center of the sodalite unit during the entire refinement process. As water molecules or NH_4^+, this peak was too close to OW1. At this point, it was inferred that the original site was occupied by cationic Al^{3+}. This is also consistent with the results obtained by Pluth and Smith (1982) who reported that aluminum-oxygen complex located at the original sites in dehydrated Sr^{2+} exchanged zeolite A. Bae *et al.* (1999) also reported that the Al position derived from dealumination process was also in sodalite cage in dehydrated Zn-exchanged zeolite X. Seo *et al.* (2014) found the Al^{3+} ion at the center of the sodalite cages in Mn^{2+} exchanged zeolite Y. In this work, isotropic refinement for this (0, 0, 0) position as Al^{3+} yielded the index R1 significantly decreased. The result showed that it approach to water molecules OW1 with a distance of 1.92 Å. In other words, dealumination could proceed for the single crystal NH_4-A_0d even at room temperature.

4.2.3 Single-crystal structure analysis

The previous work showed that the lattice parameter *a* of zeolite Na-A is 24.5498(28) Å based on single-crystal synchrotron experiments (Fischer *et al.*, 2012). In this work, after NH_4^+ exchange, the lattice parameter *a* was calculated to be 24.5996(3) Å by means of single-crystal X-ray diffraction methods. The increased lattice parameter is reasonable as cation NH_4^+ need more space than Na^+ in the cages. However, the lattice parameter *a* of zeolite NH_4-A decreased significantly to 24.3378(3) Å as well as unit cell

volume after exposure in the air at room temperature for 16 days (Table 4.4). The data implied that the unit cell underwent a contraction process at room temperature. Since there was no heating and cation exchanges on the mounted single crystal, the only reason for this change could be ascribed to the removal of framework Al. It was reported that dealumination of zeolite 4A at room temperature could be done with thionyl chloride (Shu *et al.*, 2007). However, in this work, for single crystal zeolite NH_4-A, it seems that dealumination process occurred at room temperature even without any special treatment. The contractible lattice parameter and the high electron density at position (0, 0, 0) might give the indication for the presence of Al^{3+}.

Table 4.5 Atomic coordinates, displacement factors, site symmetries, Wyckoff positions, site occupancies (occ), and anisotropic displacement parameters. OW denotes water molecules.

Atom	Wyckoff site	x	y	z	Occ
NH_4-A_0d					
Si1	96i	0	0.09307(3)	0.18545(3)	1
Al1	96i	0	0.18673(4)	0.09069(4)	1
O1	192j	0.0535(1)	0.0578(1)	0.1727(1)	1
O2	96i	0	0.1460(1)	0.1474(1)	1
O3	96i	0	0.1134(2)	0.2473(1)	1
N1	64g	0.1338(2)	0.1338(2)	0.1338(2)	0.834(6)
N2	96i	0.228(2)	0.0000	0.232(3)	0.25
OW1	64g	0.0482(7)	0.0482(7)	0.0482(7)	0.25
OW2	192j	0.124(1)	0.150(1)	0.2493(9)	0.14(1)
OW3	192j	0.184(1)	0.096(1)	0.2510(7)	0.22(2)
NH_4-A_16d					
Si1	96i	0	0.09235(6)	0.18455(6)	1
Al1	96i	0	0.18567(6)	0.09013(6)	1
O1	192j	0.0535(3)	0.0574(3)	0.1685(4)	1
O2	96i	0	0.1495(2)	0.1506(2)	1
O3	96i	0	0.1069(3)	0.2474(1)	1
N1	64g	0.1385(5)	0.1385(5)	0.1385(5)	0.77(2)
N2	96i	0.00000	0.221(3)	0.252(2)	0.25
OW1	64g	0.0452(9)	0.0452(9)	0.0452(9)	0.25
OW2	192j	0.123(2)	0.153(2)	0.2492(7)	0.18(4)
OW3	192j	0.095(2)	0.186(2)	0.2496(5)	0.34(5)
Al2	8b	0	0	0	0.026(2)

Atom	U11	U22	U33	U23	U13	U12	Ueq[Å^2]
NH4-A_0d							
Si1	0.0145(6)	0.0121(6)	0.0112(6)	0.0022(3)	0.000	0.00	0.0126(5)
Al1	0.0135(6)	0.0112(6)	0.0130(6)	0.0024(3)	0.000	0.00	0.0125(5)
O1	0.035(1)	0.034(1)	0.064(2)	0.024(1)	0.023(1)	0.022(1)	0.0443(9)
O2	0.026(1)	0.020(1)	0.021(1)	0.010(1)	0.00	0.000	0.0221(7)
O3	0.104(4)	0.029(2)	0.008(1)	-0.0002(10)	0.0000	0.000	0.047(1)
N1	0.050(3)	0.050(3)	0.050(3)	0.013(2)	0.013(2)	0.013(2)	0.050(3)
N2	0.06(4)	0.33(7)	0.06(3)	0.000	-0.02(2)	0.000	0.15(2)
OW1	0.066(7)	0.066(7)	0.066(7)	0.006(8)	0.006(8)	0.006(8)	0.066(7)
OW2							0.06(1)
OW3							0.10(1)
NH4-A_16d							
Si1	0.021(1)	0.020(1)	0.016(1)	0.0021(5)	0.000	0.00	0.019(1)
Al1	0.020(1)	0.016(1)	0.019(1)	0.0027(5)	0.000	0.00	0.018(1)
O1	0.063(3)	0.063(3)	0.107(6)	0.056(3)	0.055(4)	0.045(3)	0.078(3)
O2	0.040(3)	0.026(2)	0.027(2)	0.009(2)	0.00	0.000	0.031(1)
O3	0.21(1)	0.028(4)	0.024(3)	-0.001(1)	0.0000	0.000	0.086(4)
N1	0.058(6)	0.058(6)	0.058(6)	0.016(5)	0.016(5)	0.016(5)	0.058(6)
N2	0.3(2)	0.10(5)	0.05(3)	-0.01(3)	0.000	0.000	0.16(5)
OW1							0.05(1)
OW2							0.07(2)
OW3							0.12(2)
Al2							0.008(4)

Table 4.6 Selected interatomic distances and angles.

NH_4-A_0d					
	Dist. [Å]		Angles [°]		Dist. [Å]
Si-O1 2×	1.607(3)	Si-O1-Al	147.1(2)	N1-O1 3×	2.883(6)
Si-O2	1.603(3)	Si-O2-Al	161.4(2)	N1-OW2 3×	2.88(2)
Si-O3	1.600(2)	Si-O3-Al	142.9(3)	N1-OW2 3×	2.91(2)
Mean	1.604	Mean	149.6	N2-N2 2×	0.97(9)
Al-O1 2×	1.726(3)	O3-Si-O1	110.8(2)	N2-N2	1.37(9)
Al-O2	1.718(3)	O3-Si-O2	107.5(2)	N2-OW3 2×	2.65(4)
Al-O3	1.717(3)	O1-Si-O1	109.8(1)	N2-OW3 2×	2.70(4)
Mean	1.722	O1-Si-O2	108.9(1)	N2-O3	2.87(6)

NH_4-A_0d					
	Dist. [Å]		Angles [°]		Dist. [Å]
O1-O1(Si)	2.630(4)	Mean	109.5	N2-O2	2.91(7)
O1-O2 2×	2.612(3)	O3-Al-O1	111.2(1)	N2-O3	2.97(7)
O1-O3 2×	2.640(4)	O3-Al-O2	106.7(2)	N2-OW3 2×	3.18(6)
O2-O3	2.583(4)	O1-Al-O1	110.9(1)	OW1-OW1 3×	2.37(3)
Mean	2.620	O1-Al-O2	108.3(1)	OW1-O1 3×	3.07(2)
O1-O1(Al)	2.842(3)	Mean	109.4	OW2-OW2	0.88(4)
O1-O2 2×	2.791(4)			OW2-OW3	1.10(4)
O1-O3 2×	2.841(4)			OW2-OW3	1.98(4)
O2-O3	2.757(4)			OW2-O3	3.18(3)
Mean	2.811			OW3-OW3 3×	2.28(4)
				OW3-O3	2.95(3)
NH_4-A_16d					
	Dist. [Å]		Angles [°]		Dist. [Å]
Si-O1 2×	1.604(7)	Si-O1-Al	143.0(6)	N1-O1 3×	2.95(1)
Si-O2	1.617(5)	Si-O2-Al	151.6(3)	N1-OW2 3×	2.74(2)
Si-O3	1.569(4)	Si-O3-Al	152.8(5)	N1-OW2 3×	2.78(2)
Mean	1.599	Mean	147.6	N2-O2	2.96(7)
Al-O1 2×	1.708(7)	O3-Si-O1	110.9(4)	N2-O3	2.79(8)
Al-O2	1.716(5)	O3-Si-O2	107.6(3)	N2-O2	3.01(7)
Al-O3	1.681(4)	O1-Si-O1	108.6(3)	N2-N2	0.99(9)
Mean	1.703	O1-Si-O2	109.4(3)	N2-N2	1.4(1)
O1-O1(Si)	2.602(9)	Mean	109.5	N2-OW3 2×	2.46(6)
O1-O2 2×	2.631(8)	O3-Al-O1	111.3(3)	N2-OW3 2×	2.84(6)
O1-O3 2×	2.610(9)	O3-Al-O2	106.8(3)	N2-OW3 2×	2.90(6)
O2-O3	2.574(6)	O1-Al-O1	109.7(3)	N2-O2	2.96(7)
Mean	2.610	O1-Al-O2	108.8(3)	N2-O2	3.01(7)
O1-O1(Al)	2.787(9)	Mean	109.5	OW1-OW1 3×	2.20(3)
O1-O2 2×	2.785(8)			OW1-O1 3×	3.02(2)
O1-O3 2×	2.793(9)			OW1-OW1 3×	3.11 (5)
O2-O3	2.728(6)			OW2-OW2	1.04(2)
Mean	2.779			OW2-OW3	1.05(7)
				OW2-OW3	2.09(7)
				OW3-OW3 2×	2.21(5)
				Al2-OW1 8×	1.90(2)

Numbers in parentheses are the estimated standard deviations for the corresponding parameter.

Although Na^+ ions were considered completely exchanged by NH_4^+ ions during the refinement, a partial occupancy of Na^+ at N position cannot be ruled out completely. The Si-O distance in NH_4-A_0d is 1.604 Å, which is reasonable for the full occupancy of Si in this position. However, the Al-O distance (1.722 Å) was shorter than the expected value of 1.746 Å (Baur and Ohta, 1982). This observation concords with zeolite K-A (discussed in section 4.1) and Na-A (Fischer *et al.*, 2012), which indicates that the Al position was partially occupied by Si. After storing the crystal in air, the mean Si-O and Al-O distances reduced to 1.599 Å and 1.703 Å, respectively, which resulted in the lattice parameter as well as unit cell volume decreasing.

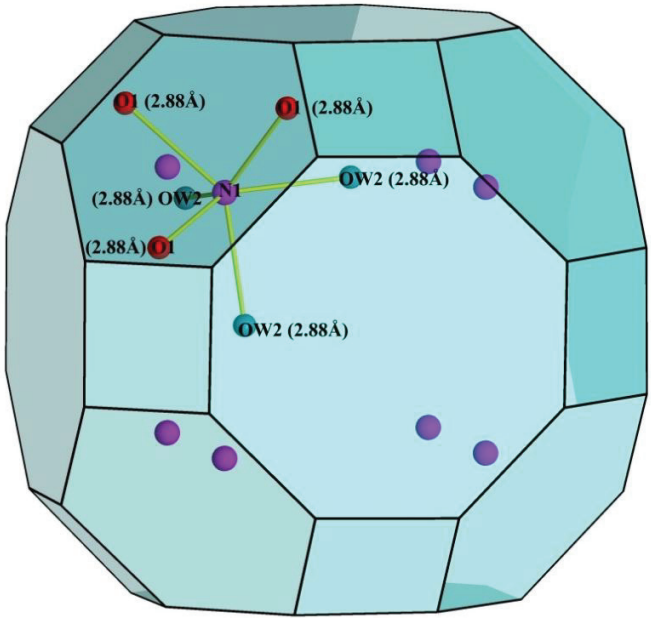

Fig. 4.14 The distribution and coordination environment of NH_4^+ in N1 position in datasets NH_4A_0d.

In fully hydrated zeolite NH_4-A for both the datasets, the cations NH_4^+ occupy two independent crystallographic positions: N1 and N2. The N1 position resides inside the big *grc* unit along 6-fold axes and projects into the center of the 6-ring (Fig. 4.14). This position is not fully occupied in both the datasets. NH_4^+ in N1 position is coordinated to three framework oxygen atoms O1 at 2.88 Å. This distance has a good agreement with the sum of the ionic radii (1.49+1.36 = 2.85 Å) (Khan and Baur, 1972). In addition, some water molecules surround the N1 position. There are six water molecules in OW2 position close to N1 position with the distances of 2.88 Å and 2.91 Å, respectively.

However, the short distance between OW2−OW2 (0.88 Å) prevents the simultaneous occupation of all the six sites. Therefore, the water molecules are distributed over three out of the six sites to coordinate to N1 position. The N1 position has similar coordination numbers in NH_4-A_16d datasets. Only the distance to framework oxygen is longer (2.95 Å) whereas to water molecules is shorter (2.74 Å and 2.78 Å).

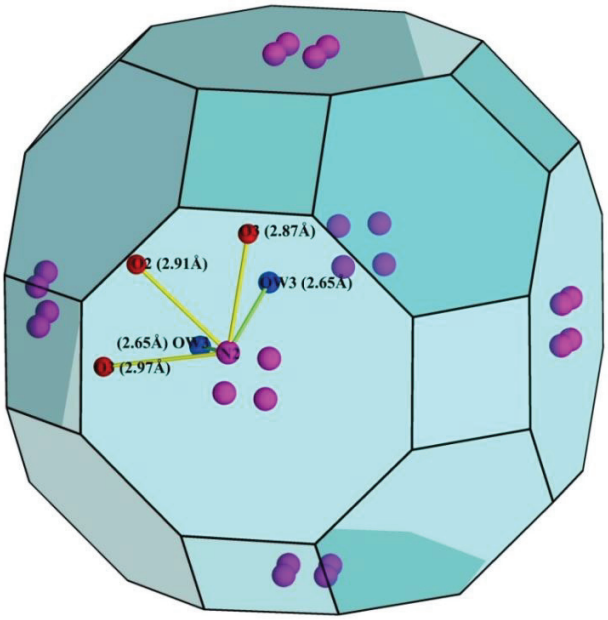

Fig. 4.15 The distribution and coordination environment of NH_4^+ in N2 position in datasets NH_4A_0d.

The N2 position is located in the plane of the 8-ring in the *grc* units (Fig. 4.15). The same situation was reported earlier in hydrated Na-A for Na^+ position (Fischer *et al.*, 2012). In McCusker's work, this position in dehydrated NH_4A shifted from the surface of the 8-ring into the *grc* units (McCusker and Seff, 1981a). The N2 position is not completely occupied because its symmetrical-equivalent positions are too close (less than 1.5 Å). During the refinement, the occupancy of this position was constrained to the maximum level because the independent refinement leads to a higher value than the maximum possible one. In NH_4-A_0d, there are three framework oxygen atoms coordinated to NH_4^+ in this position with a distance of 2.87 Å, 2.91 Å and 2.97 Å, respectively. Other four water molecules in OW3 position are close to N2 position with a distance of 2.65 Å and 2.70 Å, respectively. The short distance between position OW3 and OW3 (2.28 Å) prevents simultaneous occupation of all sites. Therefore, the coordination environment of

NH_4^+ in N2 position includes three framework oxygen atoms and two water molecules in OW3 position.

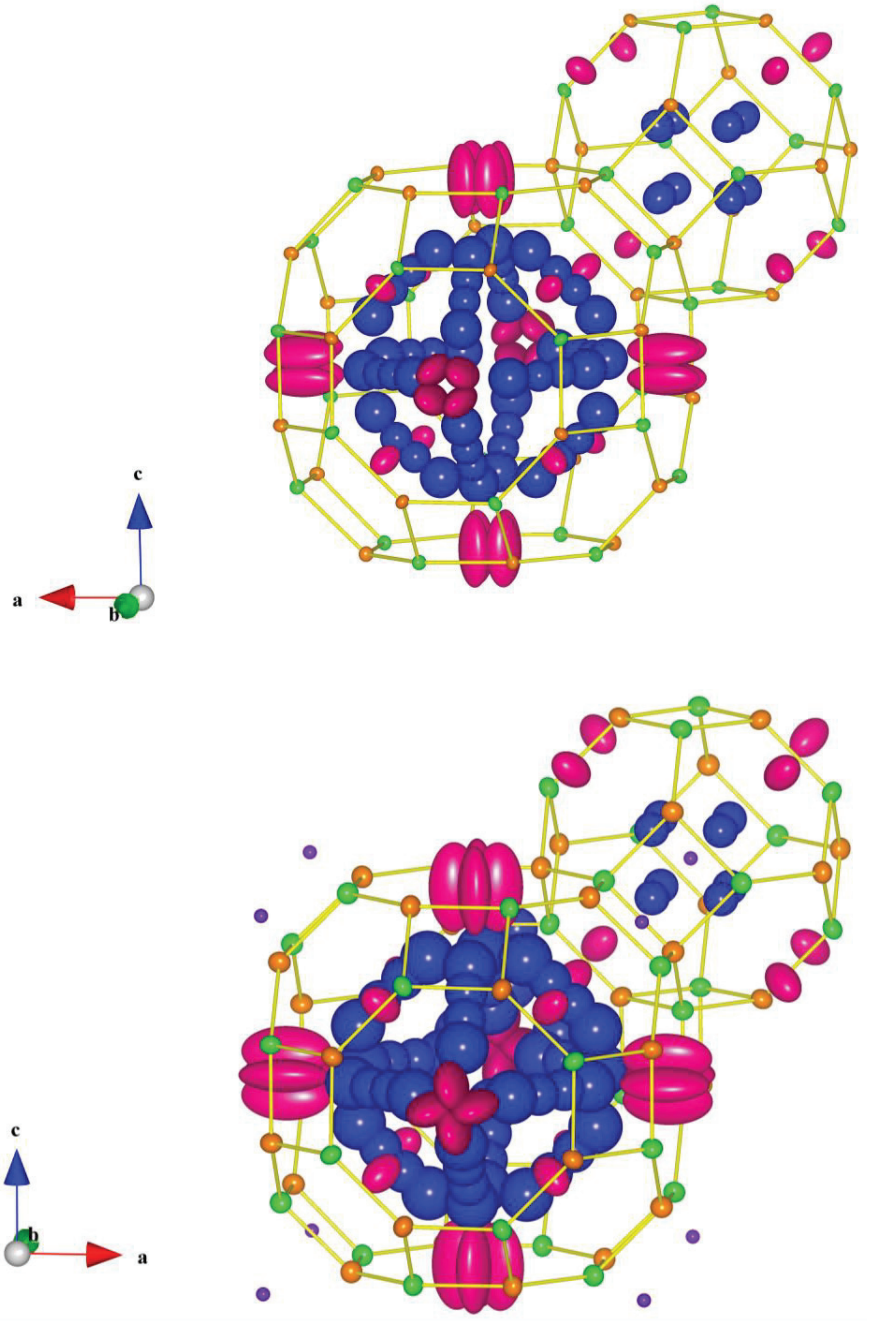

Fig. 4.16 Crystal structure projection showing the anisotropic displacement ellipsoids (90% probability) except OW2 and OW3 drawn in VESTA. Green = Al, orange = Si, pink = NH_4^+, blue = OW. (a) NH_4-A_0d; (b) NH_4-A_16d, purple = Al^{3+}.

Compared with these two datasets, the number of NH_4^+ was calculated to be less in the dataset NH_4-A_16d from the occupancy factor in the refinement results. The lower number of NH_4^+ was probably due to the dissociation of NH_3 from crystal. Namely, a partial deammoniation process occurs during storage of the single crystal at room temperature, which is consequently, accompanied by a dealumination process.

The OW1 position is located on the 6-fold axes in the *toc* unit in both datasets (Fig. 4.16). This position generates other three neighbors that are very close to each other. Therefore, the occupancy of OW1 position was fixed to 0.25 during the refinement.

The OW2 and OW3 positions are placed in the *grc* unit. Water molecules in these two positions have a long distance from framework oxygen atoms, therefore, they can make only weak bonds with these framework oxygen atoms. In Leung's work with hydrated KA, a similar position (0.2683, 0.2683, 0.5) in space group $Pm\bar{3}m$ for water molecules was observed to be fully occupied (Leung *et al.*, 1975). However, in this refinement, the position was split into OW2 and OW3 positions. The distribution of water position in both datasets are similar with zeolite K,Na-A.

It is known that density refined in high symmetry such as origin in our work could be an artifact in the refinement. However, in NH_4-A_16d, the (0, 0, 0) position was inferred to be occupied by six Al^{3+} ions per unit cell as discussed above. The numbers of NH_4^+ in both the datasets are calculated to be 77 and 73 per unit cell from the occupancy factors, respectively (Table 4.5). While an analogous calculation for water molecules results in the numbrs to be 85 and 115 per unit cell. It is possible that some water molecules are randomly located in the pores with low occupancy; and consequently, the difference Fourier maps cannot show them.

The high framework aluminum content yields more negative framework charges and requires more cations to be neutralized. Therefore, zeolite A has a high ion-exchange capacity. For NH_4-exchanged zeolite A, it is difficult to obtain completely stable hydrogen zeolite A because too many framework aluminum ions are converted into hydroxy-aluminum, which leads to the tetrahedra collapse during the deammoniation and dehydroxylation processes.

4.2.4 In situ powder X-ray diffraction data analysis

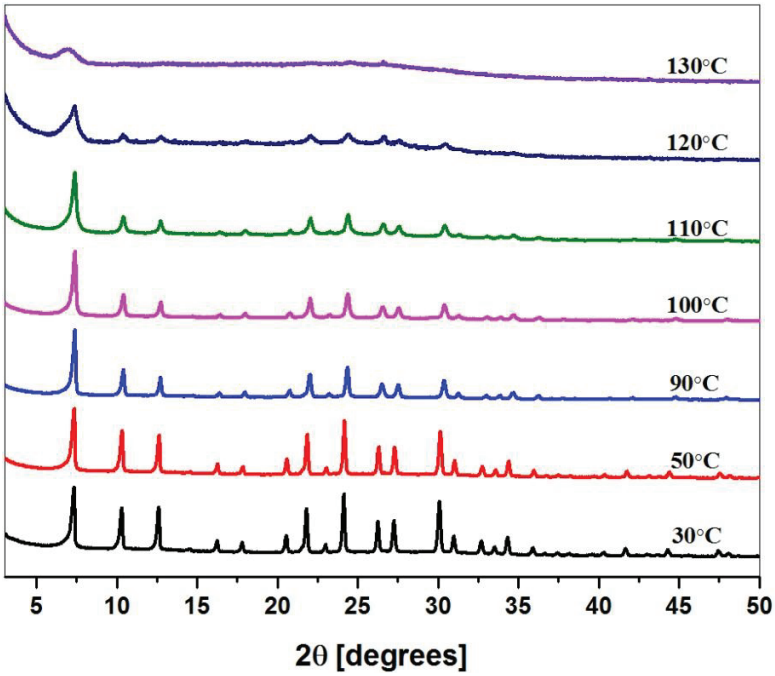

Fig. 4.17 In situ high temperature X-ray diffraction patterns of NH_4A collected between 30°C and 130°C in air.

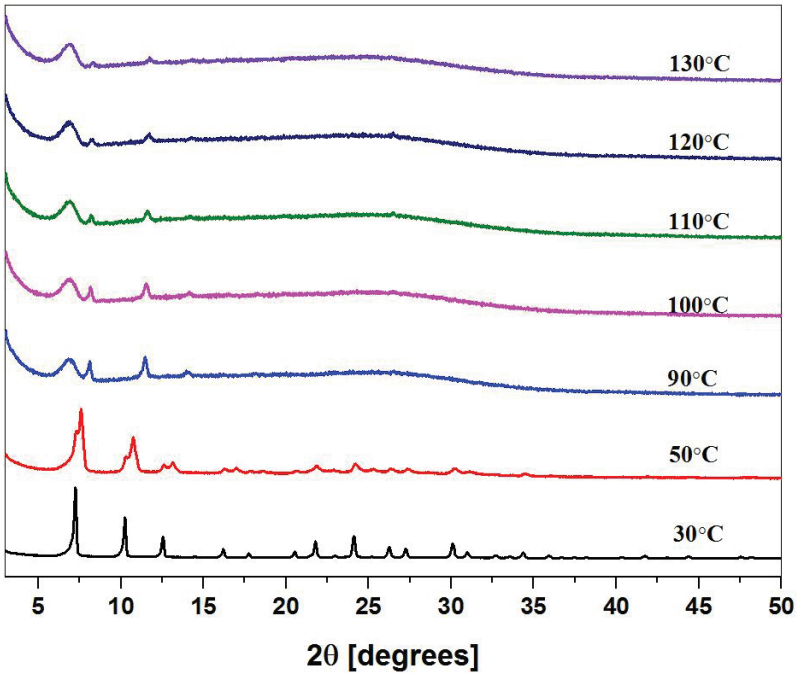

Fig. 4.18 In situ high temperature X-ray diffraction patterns of NH_4A collected between 30°C and 130°C under vacuum conditions.

X-ray diffraction data of sample NH_4A in air and vacuum condition are shown in Fig. 4.17 and Fig. 4.18, respectively. In air, the NH_4-A sample retained its characteristic diffraction peaks until 100°C but peak width broadening occurred. As temperature increases, the intensity of diffraction peaks decreases significantly, which indicates that the sample starts losing crystallinity until it becomes completely amorphous at 130°C. It can be seen in Fig. 4.18 that NH_4-A loses a great amount of crystallinity and splits into two diffraction peaks at low angles from 50°C. At high angles, only few single weak peaks exist. The intensity of split diffraction peaks that shift to the right direction becomes weak with the increasing temperature. This indicates that the newly formed phase is not stable at high temperatures.

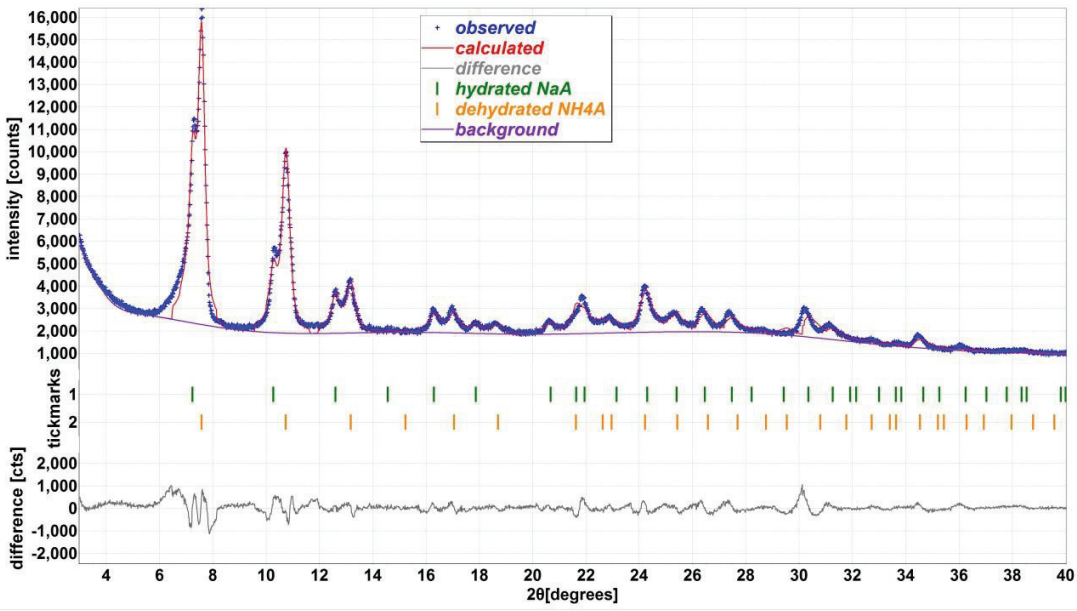

Fig. 4.19 Two phases refinement of NH_4A at 50°C using LeBail method. The two row of tick marks correspond to the reflection positions of hydrate NaA (green) and dehydrated NH_4A (orange).

Dong *et al.* (2013) reported the XRD pattern of HA while heating NH_4A. In that case, zeolite HA showed strong intensity of diffraction peaks at low angels. Compared with the XRD patterns of NH_4-A, the diffraction peaks of HA were also shifted to the right direction. Therefore, we can infer that the framework of zeolite A is partially formed into zeolite HA, which collapses with increasing temperature. Since no crystallographic data are available for zeolite HA due to the difficulty in preparation, it is hard to give a direct

proof to confirm the inference. However, it is possible to prove that the newly formed phase belongs to zeolite A. The matching refinement of the two phase profile using LeBail method (Le Bail, 2005) was performed by software BRASS (Birkenstock *et al.*, 2012). The pseudo-Vogit function was used as peak profiles function. Two structural models of hydrated zeolite NaA (Gramlich and Meier, 1971) and dehydrated zeolite NH_4A (McCusker and Seff, 1981a) were chosen for the refinement. Both of the structural were performed in space group $Fm\bar{3}c$. Fig. 4.19 shows the obtained refinement for NH_4A at 50°C under vacuum conditions. The split peaks showed a good fit with dehydrated NH_4A phase. In other words, as the temperature increased, the newly formed phase is the zeolite A phase. The two phases refinement might give the indirect evidence for the presence of zeolite HA when NH_4A was heated under vacuum conditions.

4.2.5 Thermal analysis

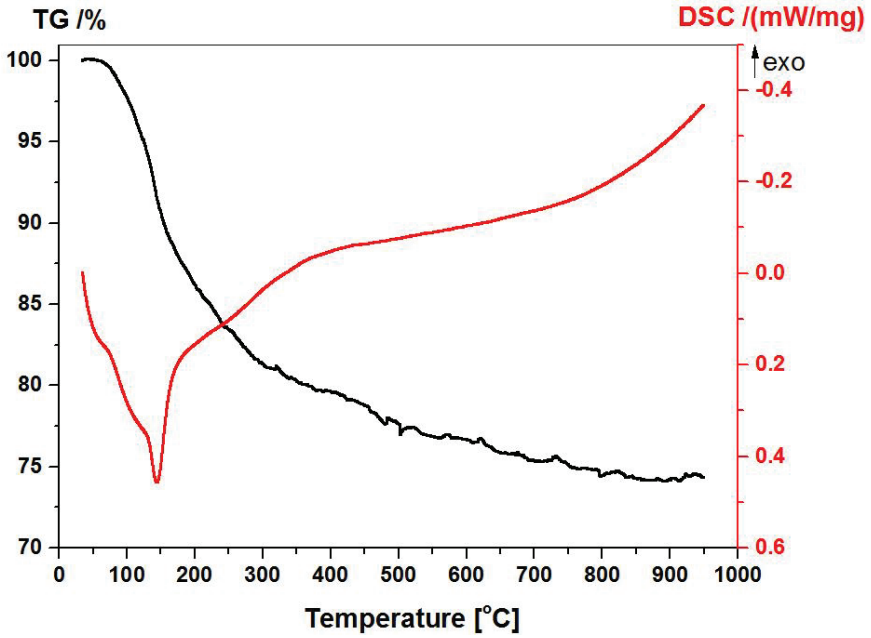

Fig. 4.20 Thermal analysis diagrams of NH_4-A under vacuum conditions.

Fig. 4.20 presents the TG and DSC curves for NH_4-A under vacuum conditions. The TG curve shows that most of the mass loss (20%) occurs in the range from room temperature up to 300°C, while the remaining weight loss about 5% occurs slowly up to 900°C. The

DSC diagram of NH_4-A exhibits two endothermic peaks at 55°C and 145°C, a shoulder peak range from 83°C to 120°C, and another wide shoulder between 220°C and 320°C. The small peak at 55°C may be related to the low level water and ammonia desorption, which can be inferred from the changes in the XRD patterns. As shown by X-ray diffraction, the zeolite HA phase appears around 50°C. Therefore, it is possible that the dehydration and deammoniation both occur simultaneously at this temperature. The shoulder between 83°C and 120°C and the large endothermic peak around 145°C may be related to the desorption of water and ammonia from different positions and achieved the maximum rate at 145°C. The shoulder peak between 220°C and 320°C could probably be associated with the zeolite structure changes. In NH_4^+ exchanged zeolite X (Si/Al=1.25), two endothermic peaks at 100°C, 175°C and a shoulder between 180°C and 350°C are assigned to water desorption, NH_3 dissociation from small pores and large pores, respectively. The dehydroxylation and deammoniation process occurs simultaneously in NH_4X (Chu and Dwyer, 1980). Similar observation has been made in NH_4^+ exchanged zeolite Y (Si/Al=2.5) but at high temperature for deammoniation and a separate dehydroxylation around 650°C (Chu, 1976). Combined with these results, it can be concluded that the temperature of deammoniation and dehydroxylation processes decreases with decreasing the Si/Al ratio in zeolites.

4.3. Partially NH_4^+ exchanged zeolite A

It is difficult to obtain 100% pure hydrogen zeolite A, but partially NH_4-exchanged zeolite A (the Na/Al ratio surpasses 0.5) can remain crystalline even after calcination at high temperatures (Dondur *et al.*, 1985; Kühl, 1973). Recently, it has been reported that the thermal deammoniation of partially ammonium-exchanged zeolite A is accompanied by a weak dealumination in the framework (Dyballa *et al.*, 2015). Thermal stability of zeolite K-A was improved compared with zeolite Na-A as discussed above. However, the zeolite NH_4-A is unstable even at lower temperatures. Therefore, it is interesting to study the thermal stability range of partially NH_4^+ exchanged zeolite K-A.

4.3.1 XRF analysis

The chemical compositions, the number of water molecules, and lattice parameter *a* for different samples are listed in Table 4.7.

Table 4.7. The chemical composition, thermal gravimetric analysis, and lattice parameter *a* for different samples.

sample	Chemical composition *	H_2O [mole in P-cell]	Lattice parameter *a* [Å]
NH_4A	$(NH_4)_{11.7}Al_{11.7}Si_{12.3}O_{48}$	22.03	24.6417(4)
$K_{9.6}A$	$K_{9.6}(NH_4)_{2.1}Al_{11.7}Si_{12.3}O_{48}$	22.09	24.5981(3)
$K_{7.8}A$	$K_{7.8}(NH_4)_{3.9}Al_{11.7}Si_{12.3}O_{48}$	22.82	24.6325(3)

* The chemical composition were given in primitive unit cell.

The XRF results revealed that the different levels of K/NH_4^+ ratio were obtained successfully as expected. In sample NH_4-A, almost no Na^+ ions were detected by XRF. Consequently, in order to balance the charge from the framework, the number of NH_4^+ could be inferred as 11.7 in the primitive unit cell.

It is worth noticing that the Si/Al ratio in $K_{9.6}$-A and $K_{7.8}$-A is more than unity, which has been controversial over many years. The previous works have analyzed a series of Na-A, Ca-A, and Na, K-A samples, which were prepared by Charnell's method (Lührs *et al*., 2012). An average value for Si/Al ratio of 1.07 was determined. The water content was calculated by deducting the ammonia from total weight loss. The lattice parameter *a* for these three samples followed a fixed trend, i.e., it increased along with the decreasing of K/NH_4^+ ratio. After NH_4^+ exchange, the NH_4^+ group forms hydrogen bonds with the framework oxygen, therefore NH_4^+ group needs more space compared to the alkaline and alkaline earth cations. This results in the increasing lattice parameter as well as unit cell volume.

4.3.2 In situ powder X-ray diffraction data analysis

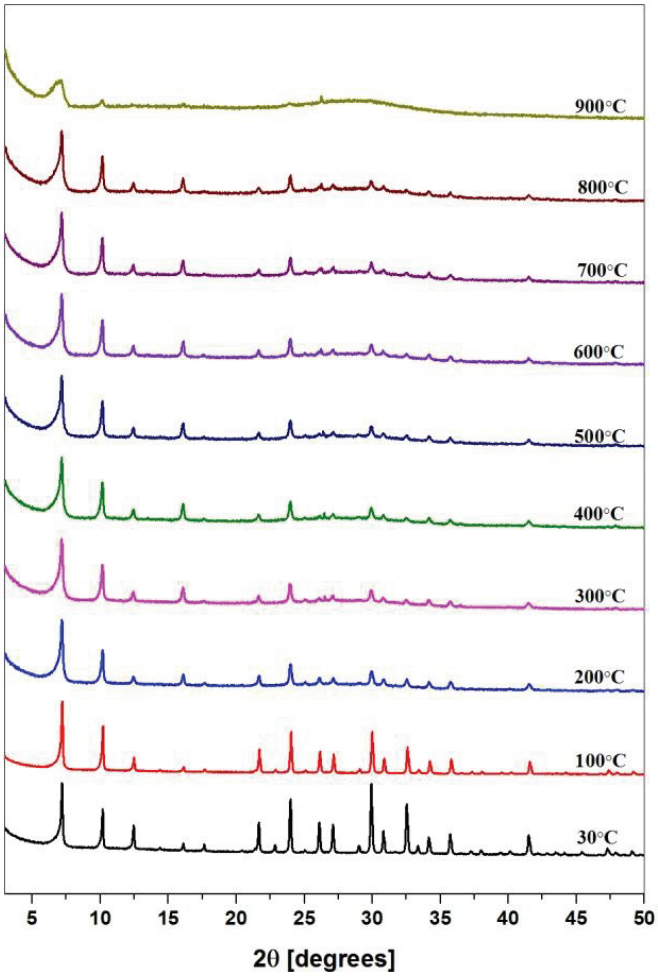

Fig. 4.21 In situ high temperature X-ray diffraction patterns of $K_{9.6}$-A collected between 30°C and 900°C in air.

The X-ray diffraction patterns of $K_{9.6}$-A at different temperatures in air are shown in Fig. 4.21. The relative intensities of the peaks changed along with the elevated temperatures. From 30°C to 100°C, water and/or NH_3 evaporation yielded a peak position shift to right direction, indicating the shrink of the unit cell in the crystalline framework. This result was consistent with LeBail fits, confirming a decrease in the lattice parameter *a* and the cell volume. The overall intensity showed a dramatic reduction especially after 200°C. Interestingly, a hump was observed between 25–35° 2θ, indicating the presence of amorphous aluminosilicate in the diffraction pattern at 200°C. Complete structure of sample $K_{9.6}$-A collapsed at a temperature of 900°C in air.

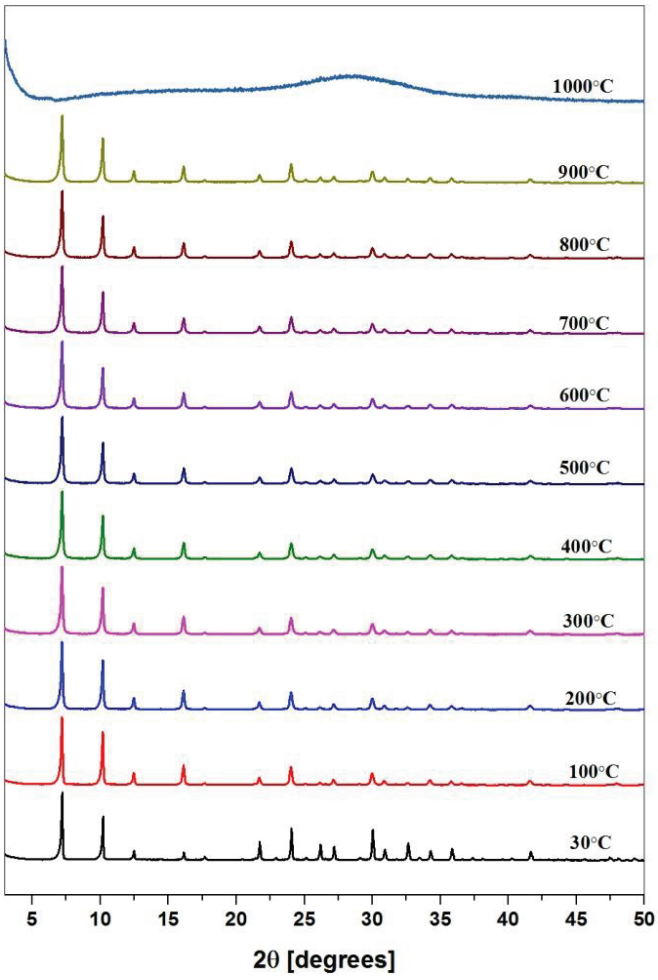

Fig. 4.22 In situ high temperature X-ray diffraction patterns of $K_{9.6}$-A collected between 30°C and 1000°C under vacuum conditions.

The X-ray diffraction patterns of $K_{9.6}$-A taken under vacuum conditions are shown in Fig. 4.22. In this case, no appreciable change occurred in the diffraction patterns up to 900°C, which indicates the structure of sample $K_{9.6}$-A remains intact at 900°C. The intensity loss started at approximately after 900°C and the sample became completely amorphous at 1000°C under vacuum conditions. In other words, the thermal stability of $K_{9.6}$-A under vacuum conditions is slightly higher than in air.

The heating results of sample $K_{9.6}$-A in air and under vacuum conditions assert that if the absorbed water in ammonium zeolite is not removed, the water vapors would attack the proton site which was formed after NH_3 evaporation (Kühl and Schweizer, 1975). Hence, aluminum was removed from the framework and resulted in the structure collapse. When

the NH_3 was pumped out under vacuum conditions, the structure became stable. However, this theory does not hold true for the samples that have lower K/NH_4 ratio.

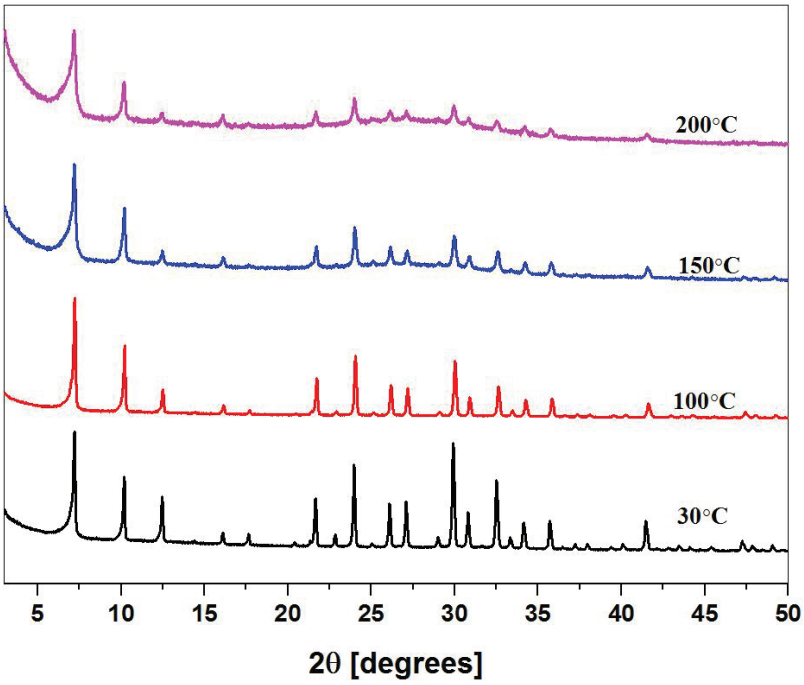

Fig. 4.23 In situ high temperature X-ray diffraction patterns of $K_{7.8}$-A collected in air.

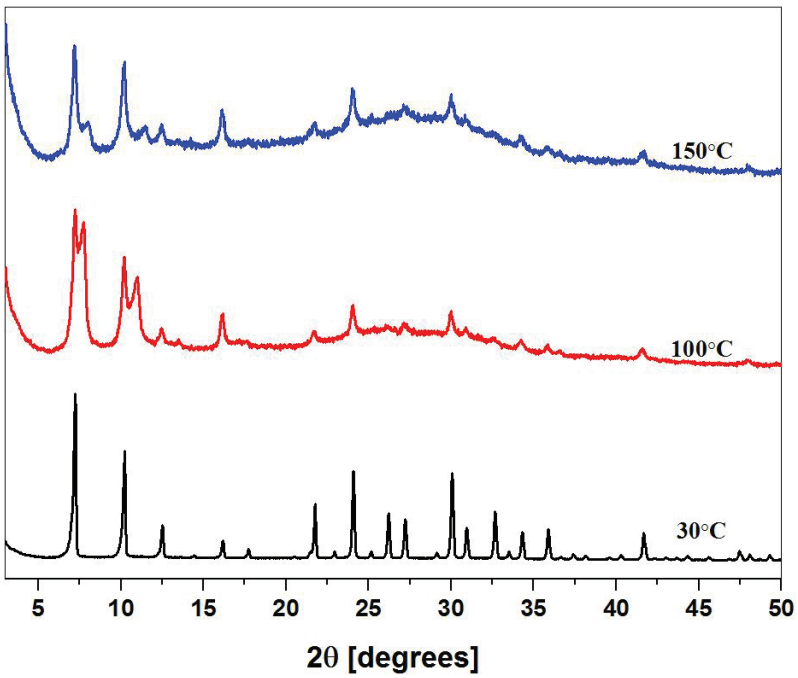

Fig. 4.24 In situ high temperature X-ray diffraction patterns of $K_{7.8}$-A collected under vacuum conditions.

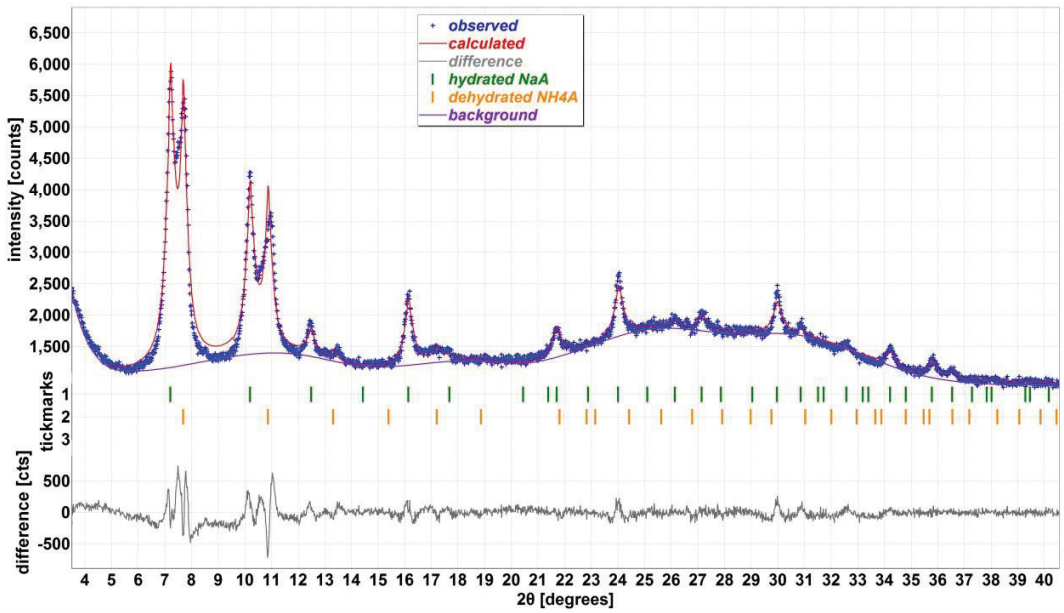

Fig. 4.25 Two phases refinement of $K_{7.8}$-A at 100°C using LeBail method. The two row of tick marks correspond to the reflection positions of hydrate NaA (green) and dehydrated NH_4A (orange).

Diffraction patterns of sample $K_{7.8}$-A at representative temperatures in air are shown in Fig. 4.23. As the temperature increased, the intensity became markedly weaker, indicating a decrease in the crystallinity. Apparently the hump between 20−35° 2θ emerged at 150°C, similar to the observation made for $K_{9.6}A$. This indicates the formation of amorphous phase. Under vacuum conditions (Fig. 4.24), at room temperature, it seems that one single zeolite phase is formed after K^+ and NH_4^+ exchange. When the temperature increased to 100°C, the diffraction peak of sample $K_{7.8}$-A at low angles splits into two small peaks. This splitting peaks is similar to that of NH_4A heating under vacuum conditions. Therefore, it could be assumed that partially zeolite HA was formed but it became unstable with increasing temperature. Two phases refinement was performed by LeBail method and is shown in Fig.4.25. It seems that split reflections belong to zeolite A phase.

4.3.3 TG-FTIR analysis

For the K^+ and NH_4^+ exchanged zeolite A, it is known that both water and ammonia evaporate at high temperatures. However, the common TG-DSC analysis can only give the corresponding desorption behavior for water and ammonia together. In other words, it

is difficult to know the dehydration and deammoniation temperature separately. Therefore, in this work, a convenient method, in situ TG-DSC analysis coupled with FTIR spectroscopy was used to monitor the behavior of water and ammonia during the heating process.

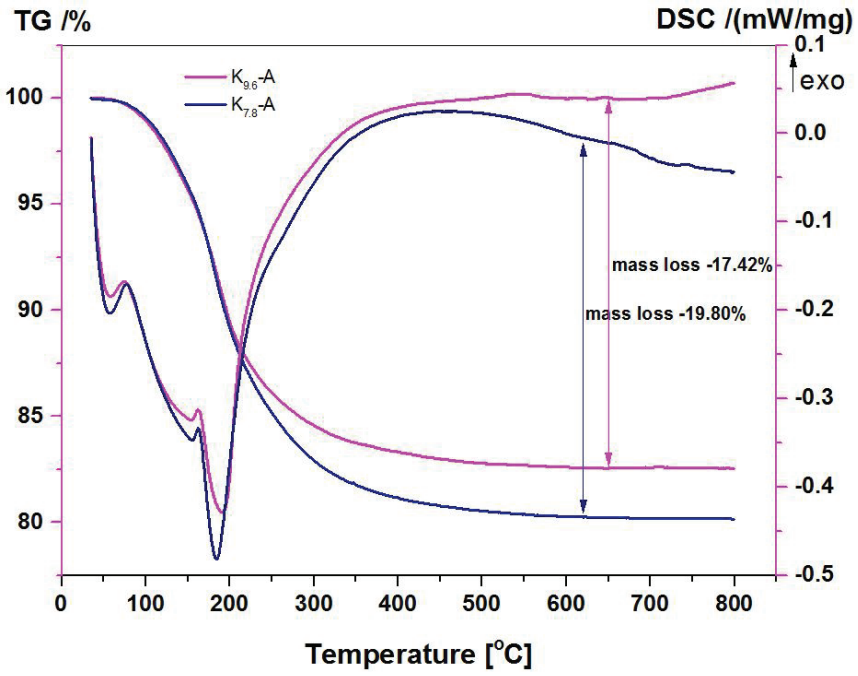

Fig. 4.26 Thermal analysis diagrams of $K_{9.6}$-A and $K_{7.8}$-A.

Fig. 4.26 illustrates the thermogravimetric and differential scanning calorimetric (TG-DSC) curves for both samples $K_{9.6}$-A and $K_{7.8}$-A. Mass loss of about 17.42% and 19.8% was observed for sample $K_{9.6}$-A and $K_{7.8}$-A, which seems to be reasonable because of the different amount of NH_4^+ exchange. The large weight loss is mainly due to the desorption of ammonia and water molecules during the heating process. Three endothermic peaks were found in the DSC curves. The first weak endothermic peak appears at 60°C corresponding to the desorption of loosely held moisture from the zeolite (Park *et al.*, 1994). The second appears at 150°C and the third endotherm peak at 180°C could be attributed to the simultaneously occurring water and ammonia desorption. Since water and NH_3 are distributed at several different positions, an escaping of them from zeolite will need different amounts of energy. This could be further confirmed by the gas IR spectroscopy.

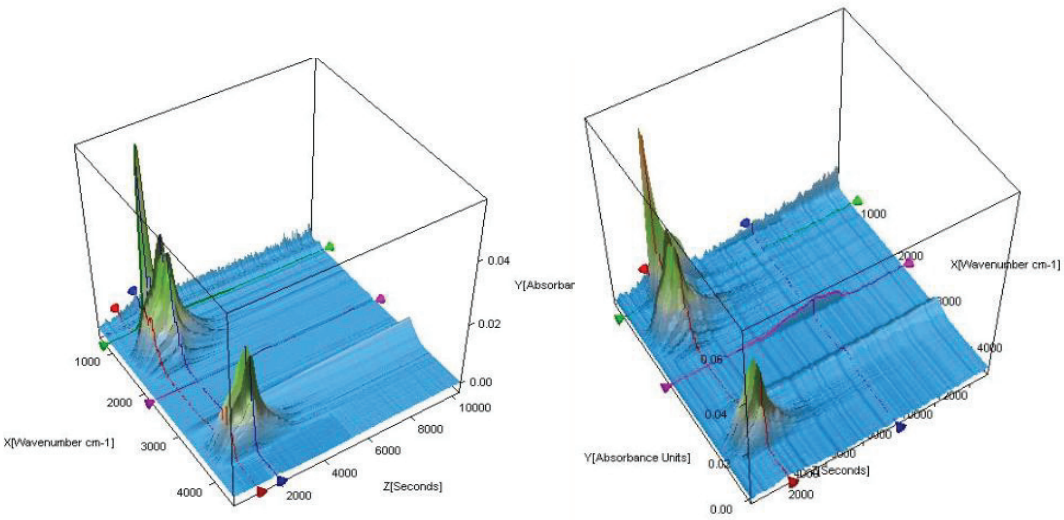

Fig. 4.27 3D FTIR spectra of the evolved gases for $K_{9.6}$-A (left) and $K_{7.8}$A (right).

In order to monitor the gas evolution at the corresponding temperature, three-dimensional diagrams (3D diagrams) of the FTIR spectra of sample $K_{9.6}$-A and $K_{7.8}$-A were constructed (Fig. 4.27). The FTIR spectra correctly identified the released gas species. The gas evolution lasted approximately 4000s (corresponding to 370°C), this concords with the results of thermal analysis. Three absorbance bands corresponding to water and ammonia are shown in Fig. 4.27. From the 3D FTIR spectra, the relative intensity of different gases was also obtained.

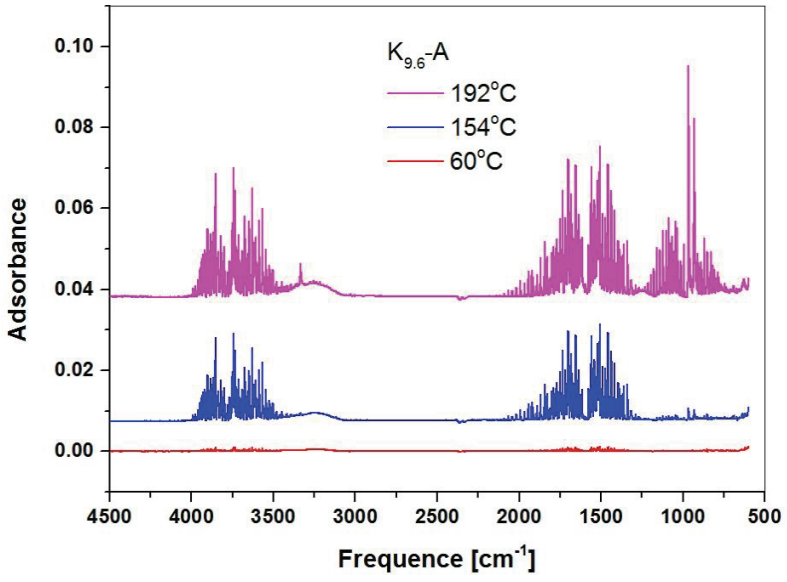

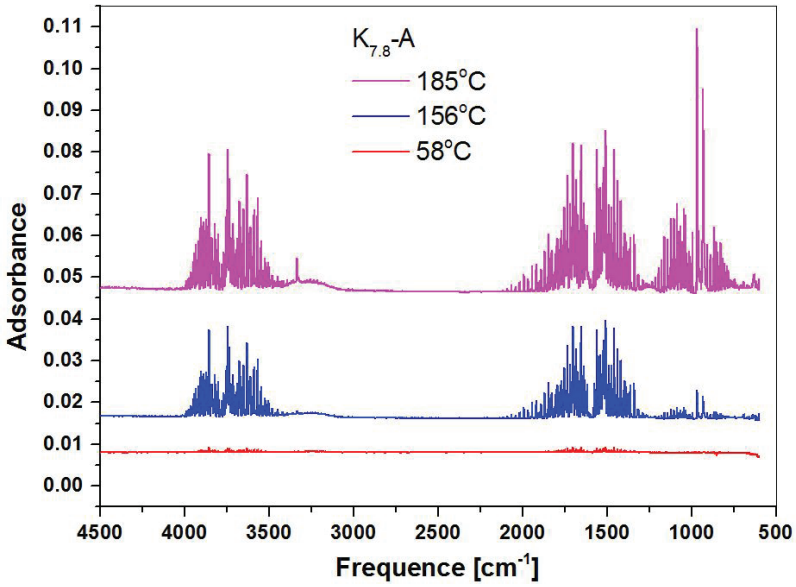

Fig. 4.28 Infrared spectroscopy analysis of evolved gases for sample $K_{9.6}$-A and $K_{7.8}$-A .

In order to obtain the detail information of the gas evolution, three spectra at different temperatures corresponding to three endothermic peaks were selected for further analysis. Fig. 4.28 shows the IR spectrum of the evolved gases at different temperatures. The characteristic water bands in the infrared spectroscopy lie in the broad ranges of 3900–3500 cm^{-1} and 1900–1300 cm^{-1}, while the bands for ammonia lie in 3335 cm^{-1} and 1180–680 cm^{-1} (Madarász *et al.*, 2004). For $K_{9.6}$-A, at 60°C, very weak bands for water molecules were observed in the spectra. As temperature increased, at 154°C, the bands for water molecules became stronger while only weak NH_3 signals were detected from IR spectroscopy. A154°C, roughly 6% decomposition of NH_3 occurred as gleaned from the intensity of NH_3 IR signals. At 192°C, the emission of both water and ammonia attained its maximum rate. For $K_{7.8}$-A, the detected dissociation of NH_3 from the samples started at 156°C accompanied with large amount of water release. Apparently, the intensity of NH_3 in $K_{7.8}$-A at 156°C was higher than in $K_{9.6}$-A at same temperature. This is in accordance with the endotherm peak that appeared stronger than $K_{9.6}$-A. Similar with $K_{9.6}$-A, the dehydration and deammoniation processes achieved maximum at 185°C.

4.4. Ba^{2+} and Sr^{2+} exchanged zeolite A

In this section, powder X-ray diffraction, thermal analysis, and XRF analysis were employed for the characterization.

Since zeolite A has high ion-exchange ability, it is very useful to remove undesirable heavy metals from waste water. However, after heavy atoms exchange, the properties of zeolite A was changed. Sherry (1966) observed that the X-ray diffraction intensity of zeolite A decreased after Ba^{2+} exchange and proposed that the low intensity of Ba-A was due to the high absorption coefficient of barium for X-rays. The similar phenomenon was observed by other reports. Dell'Agli *et al.* (2000) inferred the reason for the depression is that the crystallinity of the zeolitic structures was lost after barium exchange.

4.4.1 Powder X-ray diffraction data analysis

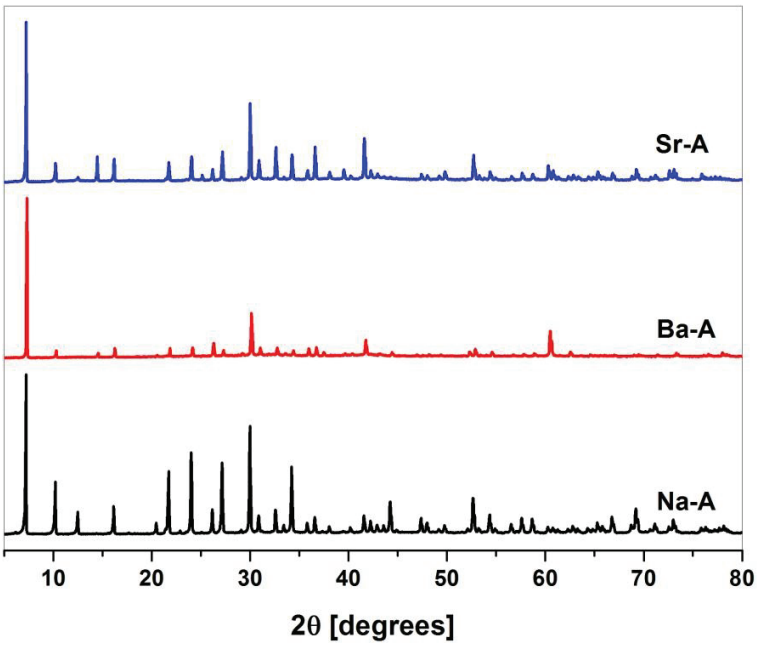

Fig. 4.29 X-ray powder diffraction patterns of synthesized zeolite Na-A, Ba-A, and Sr-A

X-ray powder diffraction patterns of the Na-A and cation exchanged zeolite A are shown in Fig. 4.29. For Na-A, it is clear that all the diffraction peaks are reasonable, which ascertain the successful synthesis of zeolite Na-A. After Ba^{2+} or Sr^{2+} exchange, the samples still retain the characteristic peaks of zeolite A. This indicates that even after six

or eight times of repetitive ion exchanges, no extraneous phases are present. The lattice parameter of Na-A, Ba-A, and Sr-A, calculated by the LeBail method (Le Bail, 2005), are shown in Table.4.8. The lattice parameter of zeolite Na-A was calculated to be a = 24.5680(3) Å. After heavy atoms exchange, both lattice parameter of zeolite Ba-A and Sr-A decreased as shown in Table 4.8.

After heavy atoms exchange, not only the lattice parameters changed but also the peak intensity decreased. Especially for sample Ba-A, it results in a dramatic reduction of peak intensity in zeolite A pattern. This result is in good agreement with the report by Ferone *et al.* (2010). They found a progressive reduction of peak intensity with increasing the Ba/Sr ratio in (Ba, Sr)-exchanged zeolite A. The linear absorption coefficient after different cation exchange could be obtained through the equations 1 and 2.

$$\rho = \frac{M_{X-A} \cdot Z}{N_A \cdot V} \quad , \qquad (1)$$

$$\mu = \rho \sum \frac{P_n}{100} \cdot \left(\frac{\mu_m}{\rho} \right)_n \quad , \qquad (2)$$

where ρ is the density of the material in units of g/cm^3, n is the number of the different elements, M is the molar mass, X means the Na^+, Ba^{2+}, or Sr^{2+}, N_A is Avogadro's number, $P_n/100$ is the mass fraction of each elements in the materials, μ_m/ρ is mass attenuation coefficients of each elements that could obtained from international tables in the units of cm^2/g (Arndt, 2006).

The calculated absorption coefficients of different samples are listed in Table 4.8. For the synthesized zeolite Na-A, the absorption coefficients is calculated to be 42.67 cm^{-1}. After Ba^{2+} or Sr^{2+} exchanged, this value increased especially for Ba-A. The X-ray diffraction intensity of one single phase can be given as

$$I_{(hkl)\alpha} = \frac{I_0 \lambda^3}{64\pi r} \left(\frac{e^2}{m_e c^2} \right)^2 \frac{M_{(hkl)}}{V_\alpha^2} \left| F_{(hkl)\alpha} \right|^2 \left(\frac{1 + \cos^2(2\theta)\cos^2(2\theta_m)}{\sin^2\theta \cos\theta} \right)_{hkl} \frac{v_\alpha}{\mu_s} \quad ,$$

where $I_{(hkl)\alpha}$ is the intensity of reflection of *hkl* in phase α, I_0 is the intensity of incident beam, λ is the wavelength of X-ray, r is the distance from specimen to detector, e is the charge on an electron, m is the mass of electron, c is the rate of light, $M_{(hkl)}$ is the multiplicity of the reflection *hkl* of phase α, $V\alpha$ is the volume of the unit cell of phase α,

$F_{(hkl)\alpha}$ is the structure factor, $2\theta_m$ is the diffraction angle of the monochromator, ν_α is the volume fraction of phase α, and μ_s is the linear absorption coefficient of the specimen (Connolly, 2012). For the same experimental system, the X-ray diffraction intensity is inversely proportional to absorption coefficient from the equation. Therefore, when the Na^+ was exchanged by Ba^{2+} and Sr^{2+}, the increased linear absorption coefficients resulted in the decreased peak intensity.

Table 4.8 lattice parameter, Number of water molecules, and absorption coefficients of different samples.

sample	Lattice parameter *a* (Å)	No. of water molecules *	Linear absorption coefficients (cm^{-1})
Na-A	24.5680(3)	184	42.67
Ba-A	24.5031(3)	209.4	278.33
Sr-A	24.5588(3)	234.6	97.81

* The number of water molecules was determined from thermal analysis.

4.4.2 XRF analysis

The chemical compositions of three samples were reports in Table 4.9 from XRF analysis. It seems that almost all Na^+ was exchanged by Ba^{2+} and Sr^{2+} by using the static methods. The Si/Al ratio is more than one. These results are in good agreement with the previous work (Lührs *et al.*, 2012). In that work, a series of K^+ and Ca^{2+} exchanged zeolite A was prepared. The EDX results show that the Si/Al ratio is more than one (i.e., 1.06).

Table 4.9 The chemical composition of different samples.

composition	Na-A	Ba-A	Sr-A
Al_2O_3	27.6	22.1	23.8
SiO_2	33.6	26.6	29.0
Na_2O	16.8	0.251	0.22
BaO	<0.011	32.2	<0.011
PbO	<0.002	<0.002	0.011
SrO	<0.03	<0.03	23.8
LOI	22.01	18.9	16.2
Sum	99.9	100.1	99.9
Chemical formula	$Na_{94.08}Al_{94.4}Si_{97.6}O_{384}$	$Ba_{46.08}Na_{1.77}Al_{94.88}Si_{97.12}O_{384}$	$Sr_{46.25}Na_{1.43}Al_{94.32}Si_{97.68}O_{384}$
Si/Al	1.03	1.02	1.04

4.5 TEA effect on zeolite A

The previous work reported that the lattice parameter *a* of synthesized zeolite A decreased whereas the crystal size increased with increasing the concentration of TEA (Fischer *et al.*, 2012). In this work, different spectroscopic methods were employed to study the influence of TEA on the crystal structure of zeolite A.

The typical synthesis method for zeolite A (channel dimensions ranging from 0.2 to 2.0 nm (Moloy *et al.*, 2002)) is the traditional hydrothermal method, which contains the silicate and aluminate solutions in the precursor. It has been reported that several factors such as silica and alumina sources, structure-directing agents, alkalinities, SiO_2/Al_2O_3, aging time, and temperature play important roles during the synthesis process (Zhou *et al.*, 2012). Because of the crucial application for small-sized zeolites as films in membrane or as seeds for zeolite powders, several studies focused on producing nanocrystals. Alfaro *et al.* (2007) studied the effect of the aging time on the influence of synthesis small crystals of zeolite Na-A. The result showed that when the aging time was 144 h, the crystal size ranged from 200 to 500 nm. Bayati *et al.* (2008) investigated the factors including the initial reaction composition, reaction time and temperature that affect the synthesis of nanostructure Na-A. It was reported that the optimum condition for synthesized Na-A is the use of the molar ratio $10NaO:Al_2O_3:50SiO_2:1000H_2O$ at 60–90°C with a maximum time of 24 h.

Large zeolite crystals are important in single-crystal determination. The best conditions for growing large size crystals depend on the following three aspects (Schmitz *et al.*, 1987): (1) slowing down the reaction rate, (2) increased solubility of the zeolites, and (3) the region of concentration yielding maximum crystal size. One effective way to obtain the large single crystal for zeolite A is the uses of organic additives. Among all the organic additives, 2,2',2"-nitrilotriethanol (triethanolamine, TEA, $N(C_2H_4OH)_3$, scheme1) is the most commonly used for preparing the large-sized zeolite A crystals. The first time to add TEA to the reaction mixture for synthesis zeolite A and X was reported by Charnell (1971). In his procedure, the size of zeolite A could be up to 60 μm whereas the size of zeolite X is over 100 μm. They proposed that the large-sized zeolite A was produced due to the "stabilizing and buffering" effect of TEA. In other words, TEA could chelate with Al^{3+} by its hydroxyl groups in the initial gel. Therefore, the distribution of

aluminum in the initial gel would be decreased with high amount of TEA. As a consequence, the rate of the nucleation process is reduced. Subsequent research confirmed this assumption (Basaldella and Tara, 1998; Scott *et al.*, 1990). A recent study concerning the preparation of large zeolite A was reported by Yang *et al.* (2006). Zeolite A with crystal size up to 35–40 μm was obtained by the addition of TEA. They pointed out that the TEA, as an organic additive, not only increases the viscosity of the system but also forms chelated complex with aluminum species, which reduces the nucleation and crystal growth processes. In addition, Tetra Methyl Ammonium (TMA, scheme 4.1) was also in the synthesis zeolite A as organic additives. It was reported that the Si/Al ratio of synthetic zeolite A varied from 1 to high ratios (up to 1.7), if TMA was used during the synthesis procedure (Esmaeili *et al.*, 2011a). In contrast, the template-free synthesis led to Si/Al = 1.

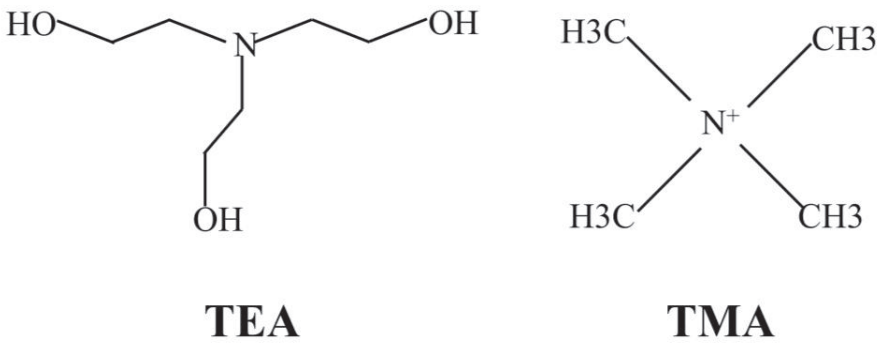

Scheme 4.1. Scheme for TEA and TMA.

It is worth mentioning that this effect of chelation of aluminum causes an increase in the Si/Al ratio in the precursor suspensions. Therefore, the production of zeolite LTA and FAU with a high Si/Al ratio would be obtained. Although the addition of TEA could yielded large-sized zeolites, the reaction requires more time to achieve complete crystallinity than the solution without TEA (Coker *et al.*, 1993).

4.5.1 XRF analysis

The chemical composition of selected samples, determined by XRF as percentage of oxides, is shown in Table 4.10.

Table 4.10 Chemical composition of selected zeolite A with different amount of TEA from XRF analysis (weight percent less than 0.1% are not listed in the table)

composition	Sample				
	NaA_0.25	NaA_0.25_a	NaA_1.0	NaA_1.75	NaA_2.5
SiO_2	33.3	32.9	33.5	33.7	37.1
Al_2O_3	29.1	28.4	28.0	27.4	26.9
Na_2O	17.1	16.5	17.0	16.9	16.5
Si/Al	0.972	0.982	1.017	1.043	1.169

As shown in Table 4.10, zeolite A is primarily composed of Al_2O_3, SiO_2, and Na_2O. It is worth noticing that the Si/Al ratio increases with the increase in the amount of TEA during the synthesis process. In the sample with lowest TEA concentration, the Si/Al ratio is less than one (0.972 as shown in the table 4.10). It seems that the result violated the Loewenstein's rule, which requires that the minimum Si/Al ratio should be 1 for aluminum in four-fold coordination (Loewenstein, 1954). In order to check this low Si/Al ratio is not derived from the experimental mistake, a repeat synthesis experiment (sample NaA_0.25_a) was carried out. The result indicated that the Si/Al ratio is still less than 1 (0.982 as shown in the table 4.10). However, this "violation" was discovered many years ago. Barrer and Meier (1958) analyzed the composition of zeolite A and found that the molar ratio SiO_2/Al_2O_3 is 1.87. They assumed that the excess Al was occluded in the β-cages as sodium aluminate molecules. However, at that time, there was no direct crystallographic evidence to support it. In the following years, some authors reported this assumption with the incomplete cation-exchange phenomenon. A. Marocco *et al.* (2011) reported that a small part of Na^+ in zeolite A cannot be further exchanged, which involves the possible presence of $NaAlO_2$ in the zeolite framework. Feoktistova and Ryzhikov (2004) reported two indirect evidence for the above assumption. First, they synthesized zeolite NaS (recrystallized from zeolite A) because its framework only consists of cuboctahedron (also called sodalite cage). The chemical composition showed that the SiO_2/Al_2O_3 ratio is 2.0, which means that the $NaAlO_2$ was absent. Therefore, they inferred that the steric hindrance caused by higher electron density prevented the occlusion of large $NaAlO_2$ in zeolite NaS. Second, the adsorption ability of zeolite A was decreased, which was attributed to the excess $NaAlO_2$.

4.5.2 FTIR spectra analysis

The previous work showed that the lattice parameter *a* decreased with increasing the concentration of TEA during the synthesis process. Therefore, it is important to check whether the TEA was completely washed out or not. FTIR spectroscopy was used for further evaluation. The FTIR spectrum of the selected samples in the range 4000–400 cm^{-1} is illustrated in Fig. 4.30.

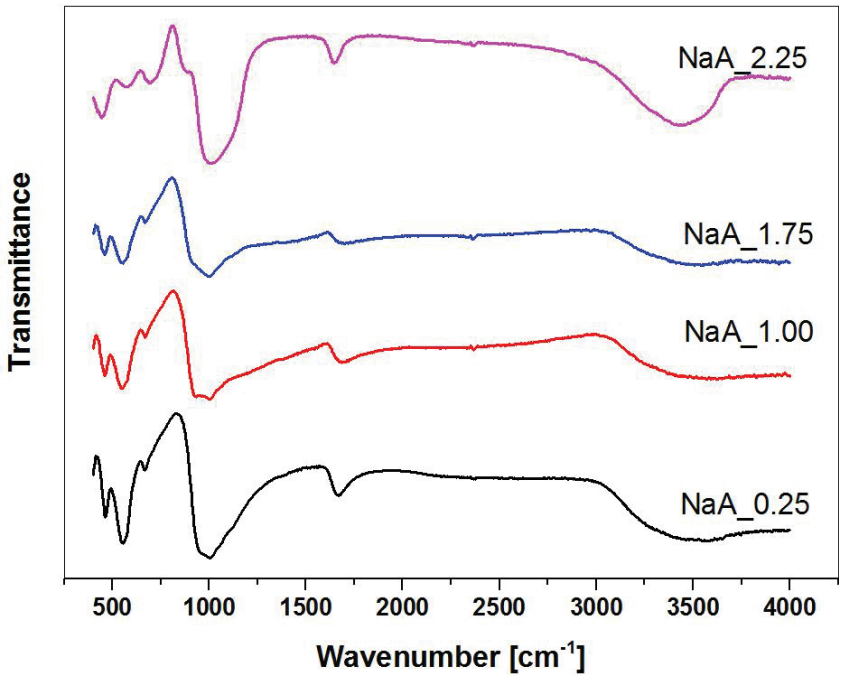

Fig. 4.30 FTIR spectra of zeolite A with different amount of TEA.

Generally, in zeolite, the absorption bands are resulted from the stretching and bending modes of Al and Si in the zeolite framework. From the IR spectra, it can be seen that the bands between 400 and 1300 cm^{-1} are typical for zeolite materials. In Fig. 4.30, the sharp peak at 1000 cm^{-1} is associated with TO_4 tetrahedral (T = Si, Al) asymmetric stretch vibrations. Another sharp band around 460 cm^{-1} can be assigned to the T-O bending vibrations. The bands at about 551 cm^{-1} correspond to the symmetric stretching vibration of 4-membered rings, which is the dominant secondary building unit in the zeolite A structure. Another weak band at 668 cm^{-1} was assigned to T-O-T symmetric stretching. More visible bands were observed between 2000 and 4000 cm^{-1}. The bands at about 1665 cm^{-1} and other broad bands in the range 3700 and 3100 cm^{-1} were assigned to the

bending vibrations of water molecules and the presence of OH^- groups, respectively. The deep bands for water molecules in the zeolite A structure indicate that since the measurements were taken under air conditions, the CO_2 bands (around 2380 cm^{-1}) were inevitable in the spectra. Apparently, there were no typical vibration bands for TEA in all samples, which indicate that the TEA is washed out completely. In other words, the assumption that the decreased lattice parameter is because of the occlusion of TEA in the channels was ruled out.

4.5.3 UV/vis spectra analysis

The XRF result revealed the significant difference in the Si/Al ratio between the zeolite A produced with the low and high TEA concentrations. Therefore, a small amount of $NaAlO_2$ was suspected into the β cages in zeolite A synthesized with low TEA concentrations. UV/vis spectroscopy is usually employed for the investigation of electron transfers between orbitals or bands of atoms, ions, and molecules. Therefore, in this work, this method was employed to study the difference between the two samples.

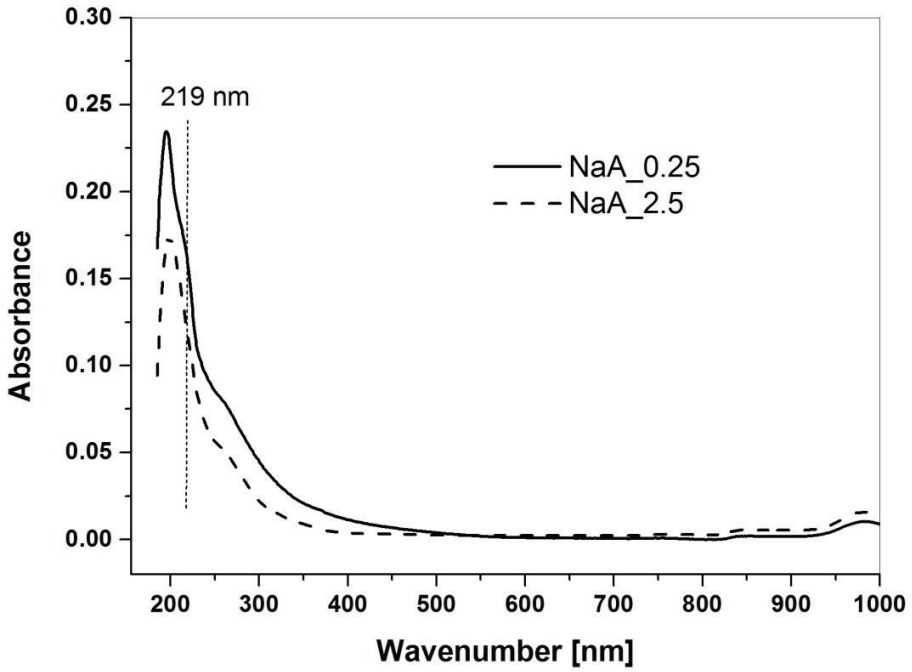

Fig. 4.31 UV-visible absorbance spectrum of different samples.

The UV/vis adsorption spectra of zeolite A from different TEA concentrations are depicted in Fig. 4.31. There are no obvious absorption bands in the visible region (380–800 nm), which indicates that the zeolite A has no optical absorption in that area. The spectrum primarily shows the absorption bands in the violet region (200–380 nm). In the sample NaA_0.25, it is observed that the two obvious adsorption shoulders with the maximum peak are observed at 219 and 295 nm. However, in the sample NaA_2.5, the first shoulder at 219 nm is not easily recognized. Engel *et al.* (1994) reported that the intensity of reflectivity decreased when the amorphous phase was washed out. In other words, those samples with high amorphous material have high intensity of absorbance. Compared with these two samples, it is obvious that sample with low TEA (NaA_0.25) has high intensity of absorbance, which could be an indication for the occluded $NaAlO_2$.

4.5.4 Summary and outlook

In this work, different amounts of TEA were used for the synthesis of zeolite A. The X-ray diffraction patterns of the series of synthetic zeolite A indicate that zeolites were obtained successfully with different amounts of TEA. The chemical compositions derived from X-ray fluorescence analysis showed that the Si/Al ratio increased with the increase in the concentration of TEA. Interestingly, one sample with the addition of 0.25 mol/L TEA has the Si/Al ratio less than 1. TEA was not incorporated in the final products, which is concluded by the FTIR spectroscopy results.

The observation concerning the Si/Al ratio of less than 1 in zeolite A was reported many years ago, and only an assumption that $NaAlO_2$ might be occluded in the sodalite cage was proposed. It is essential to provide the direct evidence. From the previous discussion (crystal structure for K-A and NH_4-A), it was obvious that water molecules also reside in the sodalite cage. Therefore, it would be highly interesting to study the dehydrated zeolite A with other spectra, such as in situ Raman spectroscopy, to verify if it is possible to obtain information about occluded $NaAlO_2$.

Chapter 5 Conclusions and perspectives

In this study, the thermal stability and crystal structure of different cation exchanged zeolite A were investigated. In addition, different spectral methods were employed to study the TEA effects on the synthesis of zeolite A.

5.1 Conclusions

The main focus was on the investigations of different cation exchanged zeolite Na-A in both single crystals and powder samples.

For single crystal, Na^+ ions were directly substituted by monovalent ions (such as K^+ and NH_4^+). Both cation exchanged single crystals were subjected to the static methods. The crystal structure of the different cation exchanged zeolite A was refined in space group $Fm\bar{3}c$ based on data collection at room temperature by the single-crystal X-ray diffraction technique. The thermal stability of different cation exchanged zeolite A was also investigated using powder samples by heating them in air and under vacuum conditions.

(1) The crystal structure of K,Na-A

For K^+ exchanged zeolite A, the microprobe analysis showed that approximately 25% Na^+ ions are not substituted by K^+ ions. After the refinement, two distinct positions are shown for cations and three positions for water molecules. In hydrated K^+ exchanged zeolite A, the most popular position for K^+ is located on the 6-fold axes in *grc* units. This position can be defined as a mixed fully occupied position for K^+ and Na^+. Another position, off the 8-ring window in the *grc* units, generated eight symmetrically equivalent positions. These equivalent positions are too close to each other that simultaneous occupation is not possible. Therefore, in this refinement, this K2 position is constrained to the maximum occupancy of 1/8 because the refinement for this occupancy yielded occupancy values than 1/8. One-third water molecules are located on 6-fold axes in *toc* units.

The other water molecules form a sodalite-cage-like cluster into the *grc* units. However, the possibility that some K^+ ions are located at positions of water molecules cannot completely be excluded.

(2) The crystal structure of NH_4-A

For NH_4^+ exchanged zeolite A, EDX results showed that almost all the Na^+ was replaced by NH_4^+. Considering the possible errors in EDX analysis for determining chemical composition, a mixed occupancy by NH_4^+ and Na^+ cannot be completely ruled out. Zeolite NH_4-A was obtained directly by NH_4^+ exchanged zeolite Na-A. It is reasonable that the distribution of NH_4^+ ions is similar with Na^+ in fully hydrated zeolite Na-A. The distribution of NH_4^+ occurred at two positions. One is on the 6-fold axes. This position is considered to be fully occupied as the free refinement leads to high occupancy than the theoretical maximum occupancy. Another position is on the surface of the 8-ring window, which generates four symmetrical equivalents. All the water molecules were distributed similar to K^+ exchanged zeolite A. Interestingly, the dealumination proceeded in the single crystal zeolite Na-A when it was stored in air at room temperature. After 16 days in air, the lattice parameter *a* of zeolite NH_4-A decreased from 24.5996(3) Å to 24.3378(3) Å, which could be an indirect evidence for a slight collapse of the structure due to the removal of Al from framework. In addition, high electron density was found at the origin position. Refining this position as Al leads the index R1 decreased. The closest neighbors to this origin position are water molecules with a distance of 1.9 Å, which is slightly longer but reasonable to form the sum of the Al and O ionic radii (1.746 Å) (Baur and Ohta, 1982).

(3) The thermal stability of zeolite K-A, NH_4-A and intermediate members

The thermal stability of different cation exchanged zeolite A was investigated in air and under vacuum conditions by using the corresponding powder samples. In order to obtain the pure zeolite K-A and pure zeolite NH_4-A, the exchanged solutions were refreshed several times. The XRF results showed that the Na^+ ions were completely exchanged by K^+ and NH_4^+ ions as two end members. The chemical composition for the intermediate members are $K_{9.6}$-A and $K_{7.8}$-A. Zeolite K-A was stable up to 900°C under both

conditions. Especially under vacuum conditions, the lattice parameter *a* of K-A showed negative thermal expansion after 150°C. Full Rietveld refinement of powder X-ray diffraction patterns was performed using the averaged structure in space group $Pm\bar{3}m$. The results showed that no significant changes occur on the framework T-O distances and O-T-O angles. However, the T-O-T bond angles changed with the increasing temperature, which is considered to be a proper reason for the negative thermal expansion. Pure zeolite NH_4-A is not stable under both atmospheric and vacuum conditions. In air, the samples turned into complete amorphous state at a low temperature of 130°C. Under vacuum conditions, the peaks started to spilt at 50°C, which could be the sign for the formation of zeolite H-A. Partially NH_4^+ exchanged zeolite K-A indicated that zeolite possessing high K^+/NH_4^+ ratio exhibits higher thermal stability. $K_{9.6}$-A was stable up to 900°C regardless of heating conditions. However, $K_{7.8}$-A started losing the crystallinity at 150°C in air and even at a low temperature under vacuum conditions.

In addition, the different heavy atoms exchanged zeolite A were prepared. The lower X-ray diffraction intensity after Ba^{2+} and Sr^{2+} exchange was due to the high absorption coefficient of heavy atoms.

5.2 Future perspectives

This work was mainly focused on the crystal structure and thermal stability of K^+ and NH_4^+ exchanged zeolite A. The structure of hydrated single crystal K-A and NH_4-A were determined in space group $Fm\bar{3}c$. It was found that the dealumination process occurred when NH_4-A stored in air. Further experiments can also be focus on other NH_4^+ exchanged zeolites such as natural zeolites to investigate the dealumination process. Powder sample NH_4-A was unstable even below 130°C in air. It is interesting to study the structure change of zeolite NH_4-A by single-crystal X-ray diffraction upon heating because powder samples provide poor structure information. Additional investigations of other cation exchanged hydrated zeolite A can also be refined in space group $Fm\bar{3}c$. Zeolite K-A exhibited negative thermal expansion during the heating process. Further experiments using other alkalis or heavy atom exchanged zeolite A can be designed to see whether they have the same negative thermal expansion phenomenon or not.

Acknowledgement

Times runs so fast. I have been in Germany for almost five years. The thesis would not be finish without support from my supervisors, colleagues and friends. To all of you, I express my deeply acknowledgement.

First of all, I would like to thank my supervisor Prof. Reinhard X. Fischer to give me the opportunity to start my PhD in his Crystallography group. I appreciated his patiently teaching and discussion in my topic as well as the editing my manuscripts. Also I am grateful for his support to let me attend the international conference in Moscow.

I would like to give my special thanks to Dr. Iris Spieß, Dr. Johannes Birkenstock and Dr. Michael Wendschuh. I can still remember Dr. Iris Spieß show me around the university, the library and mensa when I come to the university on the first day. Thank you to spend a lot of time to discuss my work during my PhD time. Thank Dr. Johannes Birkenstock and Dr. Michael Wendschuh for teaching crystallography knowledge and helping a lot about the instrumental problems.

Great thanks to all my colleagues in crystallography group. Dr. Christoph Vogt, Gabriele Ebert, Thomas Messner, Dr. Michael Fischer, Dr. Manfred Burianek, Dr. Hanna Lührs and my office mate Kristin Hoffmann. All of you not only help me in the scientific work, but also the life in Bremen. I really have a good time with all of you.

I also would like to thank the following people for technical support at various instruments: Julia Butzlaff (SEM, EDX, University of Bremen), Lennart A. Fischer, Karsten Goemann, Sandrin T. Feig (EPMA, University of Tasmania, Hobart, Australia) Andreas Klügel (EPMA, University of Bremen), Johannes Neumann (TG-MS-IR, IFAM of Oldenburg), Bernhard Schnetger (XRF, University of Oldenburg).

I am very thankful to China Scholarship Council for the financial support during my study in Germany. Great thanks to Ocean University of China for providing me this opportunity to apply this financial support.

Last but not the least, I would like to thank all my family members. My parents, thank you for always encourage me when I feel depressed. My husband Debo and my daughter Yufei, thank you for give me a happiness life.

References

A.Bruker, 2009. TOPAS, Version 4.2, Bruker AXS.

Adams, J., Haselden, D., 1983. The structure of dehydrated zeolite 3A (Si/Al= 1.01) by neutron profile refinement. Journal of Solid State Chemistry, 47(2): 123-131.

Agostini Giovanni, Lamberti Carlo, Palin Luca, Milanesio Marco, Danilina Nadiya, Xu Bin, Janousch Markus, A, v.B.J., 2009. In situ XAS and XRPD parametric Rietveld refinement to understand dealumination of Y zeolite catalyst. Journal of the American Chemical Society, 132(2): 667-678.

Alfaro, S., Rodriguez, C., Valenzuela, M., Bosch, P., 2007. Aging time effect on the synthesis of small crystal LTA zeolites in the absence of organic template. Materials Letters, 61(23): 4655-4658.

Armstrong, A., Anderson, P., Edwards, P., 1994. The composition dependence of the structure of potassium-loaded zeolite A: evolution of a potassium superlattice. Journal of Solid State Chemistry, 111(1): 178-189.

Armstrong, J., 1988. Quantitative analysis of silicate and oxide minerals: comparison of Monte Carlo, ZAF and phi-rho-z procedures. Microbeam analysis, 23: 239-246.

Arndt, U.C., RD Deslatters, RD Hubbell, JH Indelicato, P Kessler Jr, EG Lindroth, E, 2006. International tables for crystallography volume C: mathematical, physical and chemical tables. Springer, pp. 230-235.

Bae, D., Zhen, S., Seff, K., 1999. Structure of dehydrated Zn2+-exchanged zeolite X. Overexchange, framework dealumination and reorganization, stoichiometric retention of monomeric tetrahedral aluminate. The Journal of Physical Chemistry B, 103(27): 5631-5636.

Barrer, R., Meier, W., 1958. Structural and ion sieve properties of a synthetic crystalline exchanger. Transactions of the Faraday Society, 54: 1074-1085.

Barri, S.A., Rees, L.V., 1980. Binary and ternary cation exchange in zeolites. Journal of Chromatography A, 201: 21-34.

Barthomeuf, D., 1987. Zeolite acidity dependence on structure and chemical environment. Correlations with catalysis. Materials Chemistry and Physics, 17(1-2): 49-71.

Basaldella, E.I., Tara, J., 1998. Modification of crystallite morphology during synthesis of LTA zeolite using triethanolamine as additive. Materials Letters, 34(3): 119-123.

Baur, W., Ohta, T., 1982. The Si5O16 pentamer in zunyite refined and empirical relations for individual silicon–oxygen bonds. Acta Crystallographica Section B: Structural Crystallography and Crystal Chemistry, 38(2): 390-401.

Baur, W.H., Fischer, R.X., 2010. ZeoBase, a new kind of crystal structure database, International Zeolite Conference Sorrento, Italy.

Bayati, B., Babaluo, A., Karimi, R., 2008. Hydrothermal synthesis of nanostructure NaA zeolite: The effect of synthesis parameters on zeolite seed size and crystallinity. journal of the European ceramic society, 28(14): 2653-2657.

Bennett, J., Blackwell, C., Cox, D., 1983. High-resolution silicon-29 nuclear magnetic resonance and neutron powder diffraction study of Na-A zeolite. Loewenstein's rule vindicated. The Journal of Physical Chemistry, 87(19): 3783-3790.

Beyer, H.K., Jacobs, P.A., Uytterhoeven, J.B., Till, F., 1977. Thermal stability of NH 4-chabazite. Journal of the Chemical Society, Faraday Transactions 1: Physical Chemistry in Condensed Phases, 73: 1111-1118.

Bieniok, A., Hammonds, K.D., 1998. Rigid unit modes and the phase transition and structural distortions of zeolite rho. Microporous and mesoporous materials, 25(1): 193-200.

Birkenstock, J., Fischer, R.X., Messner, T., 2012. BRASS - The Bremen Rietveld Analysis and Structure Suite. Fachbereich Geowissenschaften, Universität Bremen.

Bish, D.L., Carey, J.W., 2000. Coupled X-ray powder diffraction and thermogravimetric analysis of clinoptilolite dehydration behavior. Natural Zeolite for the Third Milennium: Naples, Italy, De Frede Editore: 249-257.

Blackwell, C.S., Pluth, J.J., Smith, J.V., 1985. The silicon/aluminum ratio of single crystals of zeolite A used for crystal structure analysis. The Journal of Physical Chemistry, 89(21): 4420-4422.

Bonaccorsi, L., Proverbio, E., 2008. Influence of process parameters in microwave continuous synthesis of zeolite LTA. Microporous and Mesoporous Materials, 112(1): 481-493.

Bruker, A., 2009. Diffracplus Topas 4.2. Bruker AXS, Karlsruhe.

Carey, T., Tang, C.C., Hriljac, J.A., Anderson, P.A., 2014. Chemical Control of Thermal Expansion in Cation-Exchanged Zeolite A. Chemistry of Materials, 26(4): 1561-1566.

Carmo, M., Gubulin, J., 2002. Ethanol-water separation in the PSA process. Adsorption, 8(3): 235-248.

Charnell, J., 1971. Gel growth of large crystals of sodium A and sodium X zeolites. Journal of Crystal Growth, 8(3): 291-294.

Chen, Z., Li, S., Yan, Y., 2005. Synthesis of template-free zeolite nanocrystals by reverse microemulsion-microwave method. Chemistry of materials, 17(9): 2262-2266.

Chu, P., 1976. The deammoniation reaction of ammonium Y zeolite. Journal of Catalysis, 43(1-3): 346-352.

Chu, P., Dwyer, F.G., 1980. The deammoniation reaction of ammonium X zeolite. Journal of Catalysis, 61(2): 454-460.

Coker, E.N., Rees, L.V.C., 2005. Kinetics of ion exchange in quasi-crystalline aluminosilicate zeolite precursors. Microporous and Mesoporous Materials, 84(1-3): 171-178.

Coker, E.N., Thompson, R.W., Dixon, A.G., Sacco Jr, A., Nam, S.S., Suib, S.L., 1993. Preparation of zeolite X with low levels of iron impurity from reaction mixtures containing triethanolamine. The Journal of Physical Chemistry, 97(24): 6465-6469.

Connolly, J.R., 2012. Introduction to X-ray powder diffraction. EPS400-002, Spring 2012.

Couves, J., Jones, R., Parker, S., Tschaufeser, P., Catlow, C., 1993. Experimental verification of a predicted negative thermal expansivity of crystalline zeolites. Journal of Physics: Condensed Matter, 5(27): L329.

Crupi, V., Majolino, D., Longo, F., Migliardo, P., Venuti, V., 2006. FTIR/ATR study of water encapsulated in Na-A and Mg-exchanged A-zeolites. Vibrational spectroscopy, 42(2): 375-380.

Crutchfield, M., 1978. Organic builders: A review of worldwide efforts to find organic replacements for detergent phosphates. Journal of the American Oil Chemists' Society, 55(1): 58-65.

Dell'Agli, G., Ferone, C., Mascolo, M., Pansini, M., 2000. Thermal transformation of Ba-exchanged A and X zeolites into monoclinic celsian. Solid State Ionics, 127(3): 309-317.

Dondur, V., Rakić, V., Dimitrijević, R., Vučnić, D., 1985. High temperature transformations of NH 4 A zeolite. Thermochimica acta, 93: 753-756.

Dong, M., Gu, X., Zhang, S., Li, H., Jiang, P., 2013. Effects of acidic sites in HA zeolite on the fire performance of polystyrene composite. Industrial & Engineering Chemistry Research, 52(26): 9145-9154.

Dutta, P.K., Jakupca, M., Reddy, K.S.N., Salvati, L., 1995. Controlled growth of microporous crystals nucleated in reverse micelles.

Dutta, P.K., Robins, D., 1991. Synthesis of zeolite A from reactants enclosed in reverse micelles. Langmuir, 7(6): 1048-1050.

Dyballa, M., Obenaus, U., Lang, S., Gehring, B., Traa, Y., Koller, H., Hunger, M., 2015. Brønsted sites and structural stabilization effect of acidic low-silica zeolite A prepared by partial ammonium exchange. Microporous and Mesoporous Materials, 212: 110-116.

El-Rahman, K.A., El-Kamash, A., El-Sourougy, M., Abdel-Moniem, N., 2006. Thermodynamic modeling for the removal of Cs+, Sr2+, Ca2+ and Mg2+ ions from aqueous waste solutions using zeolite A. Journal of radioanalytical and nuclear chemistry, 268(2): 221-230.

Engel, S., Kynast, U., Unger, K., Schüth, F., 1994. Factors affecting the UV-Transparency of Molecular Sieves. Studies in Surface Science and Catalysis, 84: 477-483.

Esmaeili, N., Kazemian, H., Bastani, D., 2011a. Controlled Crystallization of LTA Zeolitic Nanoparticles from a Clear Solution Using Organic Template. Iran. J. Chem. Chem. Eng. Vol, 30(2).

Esmaeili, N., Kazemian, H., Bastani, D., 2011b. Synthesis of nano particles of LTA zeolite by means of microemulsion technique. Iran. J. Chem. Chem. Eng. Mini Review Vol, 30(2).

Feoktistova, N., Ryzhikov, V., 2004. On the variation in the composition of zeolite NaA crystals. Russian chemical bulletin, 53(8): 1625-1629.

Ferone, C., Esposito, S., Pansini, M., 2005. Thermally induced structural and microstructural evolution of barium exchanged zeolite A to celsian. Studies in Surface Science and Catalysis, 155: 249-260.

Ferone, C., Liguori, B., Marocco, A., Anaclerio, S., Pansini, M., Colella, C., 2010. Monoclinic (Ba, Sr)-celsian by thermal treatment of (Ba, Sr)-exchanged zeolite A. Microporous and Mesoporous Materials, 134(1): 65-71.

Fischer, R.X., Baur, W.H., 2006. Zeolite-type crystal structures and their chemistry. Framework Type Codes LTA to RHO. Subvolume D in Landolt-Börnstein, Numerical data and functional relationships in science and technology, New Series, Group IV: Physical Chemistry, Volume 14, Microporous and other framework materials with zeolite-type structures, eds. R.X. Fischer & W.H. Baur, 454pp, Springer-Verlag, Berlin, .

Fischer, R.X., Messner, T., 2010. a new version of the structure drawing program 2010, Universität Bremen, www.brass.uni-bremen.de.

Fischer, R.X., Sehovic, M., Baur, W.H., Paulmann, C., Gesing, T.M., 2012. Crystal structure and morphology of fully hydrated zeolite Na-A. Zeitschrift für Kristallographie Crystalline Materials, 227(7): 438-445.

Flanigen, E.M., Robert, W.B., Stephen, T.W., 2012. Zeolites in industrial separation and catalysis. In: Kulprathipanja, S. (Ed.), Introduction. Wiley-VCH Verlag GmbH & Co. KGaA, pp. 1–26.

Franklin, K.R., Townsend, R.P., 1985a. Multicomponent ion exchange in zeolites. Part 1.—Equilibrium properties of the sodium/calcium/magnesium–zeolite A system. Journal of the Chemical Society, Faraday Transactions 1: Physical Chemistry in Condensed Phases, 81(4): 1071-1086.

Franklin, K.R., Townsend, R.P., 1985b. Multicomponent ion exchange in zeolites. Part 2.—Prediction of exchange equilibria over a range of solution concentrations. Journal of the Chemical Society, Faraday Transactions 1: Physical Chemistry in Condensed Phases, 81(12): 3127-3141.

Gabrovšek, L., 1985. Sodiumtriphosphate Replacement by Builder Systems in Detergents. Studies in Surface Science and Catalysis, 24: 571-578.

Gramlich, V., Meier, W., 1971. The crystal structure of hydrated NaA: A detailed refinement of a pseudosymmetric zeolite structure. Zeitschrift für Kristallographie-Crystalline Materials, 133(1-6): 134-149.

Granato, M.A., Vlugt, T.J., Rodrigues, A.E., 2007. Molecular simulation of propane-propylene binary adsorption equilibrium in zeolite 4A. Industrial & engineering chemistry research, 46(1): 321-328.

Habersberger, K., 1987. Thermoanalytical investigation of zeolites and related compounds. Thermochimica Acta, 110: 337-341.

Hanson, A., Jones, K., Smith, J., 1987. Determination of the SiAl and NaAl ratios of two specimens of zeolite A by proton inelastic scattering. Zeolites, 7(1): 18-20.

Harlick, P.J.E., Tezel, F.H., 2004. An experimental adsorbent screening study for CO2 removal from N2. Microporous and Mesoporous Materials, 76(1-3): 71-79.

Hashemian, S., Hosseini, S.H., Salehifar, H., Salari, K., 2013. Adsorption of Fe(III) from Aqueous Solution by Linde Type-A Zeolite. American Journal of Analytical Chemistry, 04(07): 123-126.

Higgins, F.M., de Leeuw, N.H., Parker, S.C., 2002. Modelling the effect of water on cation exchange in zeolite A. Journal of Materials Chemistry, 12(1): 124-131.

Hui, K., Chao, C., Kot, S., 2005. Removal of mixed heavy metal ions in wastewater by zeolite 4A and residual products from recycled coal fly ash. Journal of Hazardous Materials, 127(1): 89-101.

Ikeda, T., Izumi, F., Kodaira, T., Kamiyama, T., 1998. Structural study of sodium-type zeolite LTA by combination of Rietveld and maximum-entropy methods. Chemistry of materials, 10(12): 3996-4004.

Kerr, G.T., 1969. Chemistry of crystalline aluminosilicates: VII. Thermal decomposition products of ammonium zeolite Y. Journal of Catalysis, 15(2): 200-204.

Khan, A.A., Baur, W.H., 1972. Salt hydrates. VII. The crystal structures of sodium ammonium orthochromate dihydrate and magnesium diammonium bis (hydrogen orthophosphate) tetrahydrate and a discussion of the ammonium ion. Acta Crystallographica Section B: Structural Crystallography and Crystal Chemistry, 28(3): 683-693.

Kosanovic C., Subotic, B., Smit, I., Cizmek, A., Stubicar, M.,Tonejc, Antun., 1997. Study of structural transformations in potassium-exchanged zeolite A induced by thermal and mechanochemical treatments. Journal of materials science, 32(1): 73-78.

Krishna, R., van Baten, J.M., 2013. Influence of adsorption thermodynamics on guest diffusivities in nanoporous crystalline materials. Physical Chemistry Chemical Physics, 15(21): 7994-8016.

Kühl, G., 1973. Structural stability of partially ammonium-exchanged zeolite A. Journal of Catalysis, 29(2): 270-277.

Kühl, G., Schweizer, A., 1975. Structural stability of sodium ammonium zeolite X. Journal of Catalysis, 38(1): 469-476.

Lauriente, D.H., Inoguchi.Y., 2005. The Chemical Economics Handbook-SRI Consulting.

Le Bail, A., 2005. Whole powder pattern decomposition methods and applications: A retrospection. Powder Diffraction, 20(04): 316-326.

Lee, H.S., Cruz, W.V., Seff, K., 1982. Crystal structures of solvated (Cu2+) 2 (OH-) x (NH4+) 8+ xA, x ca. 2, and partially desolvated (CuOH+) 2 (NH4+) 10-A, zeolite A ion-exchanged with copper (II) from ammonia/water solution. The Journal of Physical Chemistry, 86(18): 3562-3569.

Leung, P.C., K. Kevin B., Seff, Karl., Maxwell, IE., 1975. Crystal structures of hydrated and dehydrated potassium-exchanged zeolite A. The Journal of Physical Chemistry, 79(20): 2157-2162.

Liguori, B., Ferone, C., Anaclerio, S., Colella, C., 2008. Monoclinic Sr-celsian by thermal treatment of Sr-exchanged zeolite A, LTA-type framework. Solid State Ionics, 179(40): 2358-2364.

Loewenstein, W., 1954. The distribution of aluminum in the tetrahedra of silicates and aluminates. American Mineralogist, 39(1-2): 92-96.

Lührs, H., Derr, J., Fischer, R.X., 2012. K and Ca exchange behavior of zeolite A. Microporous and Mesoporous Materials, 151: 457-465.

Madarász, J., Krunks, M., Niinistö, L., Pokol, G., 2004. Evolved gas analysis of dichlorobis (thiourea) zinc (II) by coupled TG-FTIR and TG/DTA-MS techniques. Journal of thermal analysis and calorimetry, 78(2): 679-686.

Marocco, A., Liguori, B., Dell'Agli, G., Pansini, M., 2011. Sintering behaviour of celsian based ceramics obtained from the thermal conversion of (Ba, Sr)-exchanged zeolite A. Journal of the European Ceramic Society, 31(11): 1965-1973.

McCusker, L.B., Seff, K., 1981a. Crystal structure of vacuum-dehydrated fully ammonium-exchanged zeolite A. Journal of the American Chemical Society, 103(12): 3441-3446.

McCusker, L.B., Seff, K., 1981b. Crystal structures of hydrated and partially dehydrated fully cadmium (II)-exchanged zeolite A. The Journal of Physical Chemistry, 85(2): 166-174.

MIMURA, H., KANNO, T., 1980. Processing of Radioactive Waste Solution with Zeolites (I): Thermal-Transformations of Na, Cs and Sr Forms of Zeolites.

Moloy, E.C., Davila, L.P., Shackelford, J.F., Navrotsky, A., 2002. High-silica zeolites: a relationship between energetics and internal surface areas. Microporous and mesoporous materials, 54(1): 1-13.

Momma, K., Izumi, F., 2011. VESTA 3 for three-dimensional visualization of crystal, volumetric and morphology data. Journal of Applied Crystallography, 44(6): 1272-1276.

NETZSCH, 2010. NETZSCH Messung. NETZSCH-Gerätebau GmbH, Selb, Germany.

Ohgushi, T., 2007. Relaxation theory for sodium ion in dehydrated Na-A zeolite (LTA) and elucidation of ion movements. The Journal of Physical Chemistry C, 111(12): 4688-4694.

Ohgushi, T., Ishimaru, K., Komarneni, S., 2001. Nepheline and Carnegieite Ceramics from A-Type Zeolites by Microwave Heating. Journal of the American Ceramic Society, 84(2): 321-327.

Ozin, G.A., Kuperman, A., Stein, A., 1989. Advanced zeolite materials science. Advanced Materials, 1(3): 69-86.

Park, J.-Y., Kang, M.-S., Choll, S.-G., Kim, Y., Kim, U.-S., 1994. A Study on the Structure and Thermal Property of Cu2+ and NI-I4+ Ion-Exchanged Zeolite A. Bull. Korean Chem. Soc, 15(5).

Patalinghug, W., Seff, K., 1990. Crystal structure of partially desolvated (NiOH+) 2 (NH4+) 10-A, with some discussion of the fully solvated structure. Journal of Physical Chemistry, 94(19): 7662-7665.

Pelmenschikov, A., Paukshtis, E., Edisherashvili, M., Zhidomirov, G., 1992. On the Loewenstein rule and mechanism of zeolite dealumination. The Journal of Physical Chemistry, 96(17): 7051-7055.

Pluth, J.J., Smith, J.V., 1979. Crystal structure of dehydrated potassium-exchanged Zeolite A. Absence of supposed zero-coordinated potassium. Refinement of silicon, aluminum-ordered superstructure. Journal of Physical Chemistry, 83(6): 741-749.

Pluth, J.J., Smith, J.V., 1982. Crystal structure of dehydrated strontium-exchanged zeolite A. Absence of near-zero-coordinate strontium (2+) ion. Presence of aluminum complex. Journal of the American Chemical Society, 104(25): 6977-6982.

Radosavljevic-Mihajlovic, A.S., Kremenovic, A.S., Dosen, A.M., Andrejic, J.Z., Dondur, V.T., 2015. Thermally induced phase transformation of Pb-exchanged LTA and FAU-framework zeolite to feldspar phases. Microporous and Mesoporous Materials, 201: 210-218.

Reed, T., Breck, D., 1956. Crystalline zeolites. II. Crystal structure of synthetic zeolite, type A. Journal of the American Chemical Society, 78(23): 5972-5977.

Ronald W.T. Wilkins, Abdul Mateen, West, G.W., 1974. The Spectroscopic Study of Oxonium in Minerals. American Minerulogist,, 59: 811-819.

Sathupunya, M., Gulari, E., Wongkasemjit, S., 2003. Na-A (LTA) zeolite synthesis directly from alumatrane and silatrane by sol-gel microwave techniques. Journal of the European Ceramic Society, 23(8): 1293-1303.

Schmitz, W., Kornatowski, J., Finger, G., 1987. Growth of NaA zeolites in the presence of triethanolamine (TEA). The influence of water, TEA and Al contents. Crystal Research and Technology, 22(1): 35-41.

Scott, G., Thompson, R., Dixon, A., Sacco, A., 1990. The role of triethanolamine in zeolite crystallization. Zeolites, 10(1): 44-50.

Seff, K., Mellum, M.D., 1984. The silicon/aluminum ratio and ordering in zeolite A. The Journal of Physical Chemistry, 88(16): 3560-3563.

Seo, S.M., Suh, J.M., Lim, W.T., 2014. Single-Crystal Structure of Fully Dehydrated and Partially Dealuminated Zeolite Y (FAU, Si/Al= 1.56) Mn2+ Exchanged by Flow Method. Journal of Chemical Crystallography, 44(2): 89-97.

Shannon, R.t., 1976. Revised effective ionic radii and systematic studies of interatomic distances in halides and chalcogenides. Acta Crystallographica Section A: Crystal Physics, Diffraction, Theoretical and General Crystallography, 32(5): 751-767.

Sheldrick, G.M., 2007. A short history of SHELX. Acta Crystallographica Section A: Foundations of Crystallography, 64(1): 112-122.

Sheldrick, G.M., 2008. A short history of SHELX. Acta Crystallographica Section A: Foundations of Crystallography, 64(1): 112-122.

Sherry, H.S., 1966. Barium Ion Exchange of the Synthetic Zeolite Linde 4-A. The Journal of Physical Chemistry, 70(4): 1332-1334.

Shu, S., Husain, S., Koros, W.J., 2007. Sonication-assisted dealumination of zeolite A with thionyl chloride. Industrial & engineering chemistry research, 46(3): 767-772.

Slangen, P., Jansen, J., Van Bekkum, H., 1997. The effect of ageing on the microwave synthesis of zeolite NaA. Microporous materials, 9(5): 259-265.

Sleight, A.W., 1998. Negative thermal expansion materials. Current Opinion in Solid State and Materials Science, 3(2): 128-131.

Smith, J., 2000. Tetrahedral Frameworks of Zeolites, Clathrates and Related Materials: Subvolume A. Landolt–Börnstein, New Series I, Group IV: Numerical Data and Functional Relationships in Science and Technology: , ed. W. H. Baur, R. X. Fischer. Vol. A. Berlin: Springer.

Smith, J., Dowell, L., 1968. Revised crystal structure of dehydrated Na-Type A zeolite. Zeitschrift für Kristallographie-Crystalline Materials, 126(1-6): 135-142.

Sun, H., Shen, B., 2012. Effects of organic additives on crystallization process and the adsorption performances of zeolite A. Adsorption, 18(2): 103-111.

Sun, T., Seff, K., 1993. Crystal structure of zeolite A with potassium clusters and continua. The Journal of Physical Chemistry, 97(41): 10756-10760.

Wang, H., Huang, L., Holmberg, B.A., Yan, Y., 2002. Nanostructured zeolite 4A molecular sieving air separation membranes. Chemical Communications(16): 1708-1709.

Weeks, T., Angell, C., Bolton, A., 1975. The thermochemical properties of ammonium exchanged erionite. Journal of Catalysis, 38(1): 461-468.

Yang, J., Lee, C.-H., Chang, J.-W., 1997. Separation of hydrogen mixtures by a two-bed pressure swing adsorption process using zeolite 5A. Industrial & engineering chemistry research, 36(7): 2789-2798.

Yang, X., Albrecht, D., Caro, J., 2006. Revision of Charnell's procedure towards the synthesis of large and uniform crystals of zeolites A and X. Microporous and mesoporous materials, 90(1): 53-61.

Yin, X., Zhu, G., Yang, W., Li, Y., Zhu, G., Xu, R., Sun, J., Qiu, S., Xu, R., 2005. Stainless-Steel-Net-Supported Zeolite NaA Membrane with High Permeance and High Permselectivity of Oxygen over Nitrogen. Advanced Materials, 17(16): 2006-2010.

Zhou, H., Wu, Y., Zhang, W., Wang, J., 2012. Static hydrothermal crystallization of SUZ-4 zeolite in the presence of seed and tetraethylammonium hydroxide. Materials Chemistry and Physics, 134(2): 651-656.

CD Appendix

The CD appendix contains the following contents:

- Digital version of this thesis
- *.cif files for single crystals
    a) *.cif file for single crystal K-A
    b) *.cif file for single crystal dataset NH_4-A_0d
    c) *.cif file for single crystal datasets NH_4-A_16d
- Diffraction data
    a) *.xrdml file for powder sample in air
    b) *.xrdml file for powder sample under vacuum conditions

Manuscripts within this thesis

1. **Li Wang**, Johannes Birkenstock, Iris Spieß, Lennart A. Fischer, Johannes Neumann, Bernhard Schnetger, Werner H. Baur, Reinhard X. Fischer. Thermal behavior and crystal structure of hydrated K^+ exchanged zeolite A **(**to be submitted to " Journal of Physical Chemistry C")

2. **Li Wang**, Johannes Birkenstock, Iris Spieß, Johannes Neumann, Bernhard Schnetger, Werner H. Baur, Reinhard X. Fischer. Thermal behavior and crystal structure of hydrated NH_4^+ exchanged zeolite A. (in preparation).

3. **Li Wang**, Iris Spieß, Reinhard X. Fischer. Spectral studies on the influence of triethanolamine on synthesis zeolite A. (in preparation).

4. **Li Wang**, Iris Spieß, Reinhard X. Fischer. The crystal structure of $Ba^{2+}$and Sr^{2+} exchanged zeolite A. (in preparation).

Conference contributions

Li Wang, Iris Spieß, Hanna Lührs, Werner H. Baur, Reinhard X. Fischer. Synthesis, modification, and characterization of zeolite A and some cation-exchanged forms. 17th International Zeolite Conference. P-1.1-60, July 7-12. 2013, Moscow, Russian.